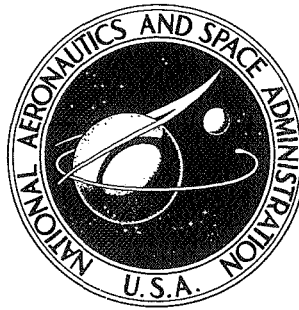


NASA TECHNICAL NOTE



NASA TN D-7630

NASA TN D-7630

CASE FILE  
COPY

SUBSONIC ANNULAR WING THEORY WITH  
APPLICATION TO FLOW ABOUT NACELLES

*by Michael J. Mann*

*Langley Research Center*

*Hampton, Va. 23665*



NATIONAL AERONAUTICS AND SPACE ADMINISTRATION • WASHINGTON, D. C. • SEPTEMBER 1974

1. Report No. NASA TN D-7630	2. Government Accession No.	3. Recipient's Catalog No.	
4. Title and Subtitle SUBSONIC ANNULAR WING THEORY WITH APPLICATION TO FLOW ABOUT NACELLES		5. Report Date September 1974	
		6. Performing Organization Code	
7. Author(s) Michael J. Mann		8. Performing Organization Report No. L-9274	
		10. Work Unit No. 760-64-60-01	
9. Performing Organization Name and Address NASA Langley Research Center Hampton, Va. 23665		11. Contract or Grant No.	
		13. Type of Report and Period Covered Technical Note	
12. Sponsoring Agency Name and Address National Aeronautics and Space Administration Washington, D.C. 20646		14. Sponsoring Agency Code	
		15. Supplementary Notes	
16. Abstract <p>A method has recently been developed for calculating the flow over a subsonic nacelle at zero angle of attack. The method makes use of annular wing theory and boundary-layer theory and has shown good agreement with both experimental data and more complex theoretical solutions. The method permits variation of the mass flow by changing the size of a center body.</p>			
17. Key Words (Suggested by Author(s)) Nacelle design Annular wing Ring wing Propeller shroud		18. Distribution Statement Unclassified - Unlimited  STAR Category 01	
19. Security Classif. (of this report) Unclassified	20. Security Classif. (of this page) Unclassified	21. No. of Pages 91	22. Price* \$4.00

# SUBSONIC ANNULAR WING THEORY WITH APPLICATION TO FLOW ABOUT NACELLES

By Michael J. Mann  
Langley Research Center

## SUMMARY

Jet engine nacelles have generally been designed with the assumption that the intake and nozzle can be treated separately. However, advancements in engine development for subsonic cruise airplanes have tended toward high-bypass-ratio fan engines. This type of engine usually has a short fan nacelle which necessitates analyzing the complete nacelle. These nacelles can be treated as annular wings on which the circulation developed determines both the internal and external flow.

A method has recently been developed for calculating the flow over such a nacelle at zero angle of attack and at subsonic Mach numbers. The method makes use of annular wing theory and boundary-layer theory and has shown good agreement with both experimental data and more complex theoretical solutions. The method permits variation of the mass flow by changing the size of a center body.

## INTRODUCTION

Jet engines have generally been designed with the assumption that the inlet and nozzle can be designed separately. Advancements in engine technology have recently tended toward high-bypass-ratio fan engines with short fan nacelles. For these nacelles, the complete nacelle must be examined. A complete nacelle can be viewed as an annular wing, the thickness and camber of which determine the internal and external flow.

Several methods have been developed for calculating the flow over nacelles or annular wings. The Douglas-Neumann method (ref. 1) has been used to predict accurately the pressures on the surface of a nacelle inlet. Trulin and Iversen (ref. 2), Geissler (ref. 3), and Young (ref. 4) have recently published methods which use surface singularities and show good agreement between theory and experiment for complete nacelles. Geissler's method includes the effects of angle of attack.

Young (ref. 5) also examined the accuracy of a method which distributes the singularities along a mean cylinder of constant diameter. However, Young did not present the details of the theory. Agreement between the theory and experiment is good at low Mach numbers but is inadequate at the higher Mach numbers.

Mascitti (ref. 6) has developed a rapid numerical technique for calculating the subsonic flow over planar and axisymmetric profiles at zero angle of attack. The method solves the exact incompressible potential-flow equations written in terms of the stream function.

Belotserkovskii (ref. 7) and Weissinger (ref. 8) have developed much of the theory of annular wing flow. Their application of the theory has been the determination of overall force and moment characteristics rather than a study of surface pressure distribution. However, much of their theoretical work has been useful in the present study.

Hess (ref. 9) discusses some of the early solutions for axisymmetric flow which made use of vortex rings on the surface. Keith and others (ref. 10), and Grossman and Moretti (ref. 11) have developed numerical methods for solving the exact inviscid flow over two-dimensional and axisymmetric nacelles at subsonic and transonic speeds. Reference 10 uses a stream-tube curvature relaxation technique, and reference 11 uses a time-dependent technique. However, the technique of reference 11 was only successful for subsonic flow. To the author's knowledge, only the present paper and references 3 and 10 have included the effects of the boundary layer.

The purpose of the present study is twofold. First, an inviscid theory, which uses vortex rings to represent the camber and a combination of source rings and vortex rings to represent thickness has been developed. Three-dimensional sources are distributed along the center line to control the mass flow through the wing. This method appears to have some advantage over each of the other methods in terms of either simplicity, a reduction of computer core storage or central processor time requirements, ease of extension to more complex flows, accuracy, or quantities computed. Secondly, an analysis of the importance of including the displacement effect of the boundary layer in the calculations has been made. A boundary-layer iteration procedure has been included in the computer program.

Results of the present theory have been compared with experimental data obtained in tests on four nacelles and good agreement has been found over a range of mass-flow ratios and Mach numbers.

#### SYMBOLS

A	internal-flow cross-sectional area, $m^2$ (ft <sup>2</sup> )
c	wing chord, m (ft)
C <sub>p</sub>	pressure coefficient, $\frac{p - p_\infty}{q_\infty}$

$d$	intake diameter equals highlight diameter less twice inlet lip radius, m (ft)
$D$	average of minimum inner diameter and maximum outer diameter of wing; when subscripted, refers to diameter of wing, m (ft)
$\hat{e}_t, \hat{e}_r, \hat{e}_x$	unit vectors in meridional, r- and x-directions, respectively
$E$	complete elliptic integral of second kind, $\int_0^{\pi/2} \sqrt{1 - k^2 \sin^2 u} \, du$ , dimensionless
$\bar{g}_q(\xi)$	dimensionless correction term for $\gamma_t$ (see eq. (32))
$H$	shape factor, $\delta^*/\theta$
$K$	complete elliptic integral of first kind, $\int_0^{\pi/2} \frac{1}{\sqrt{1 - k^2 \sin^2 u}} \, du$ , dimensionless
$k$	modulus of complete elliptic integrals (see eq. (11)), dimensionless
$k'$	complementary modulus, $\sqrt{1 - k^2}$
$M_\infty$	free-stream Mach number
$m$	mass flow through annular wing, kg/sec (slugs/sec); iteration number or summation index
$N$	number of chordwise divisions for numerical solution
$p$	static pressure, $N/m^2$ (lbf/ft <sup>2</sup> )
$Q(\xi)$	thickness function defined by equation (29), dimensionless
$q(\xi)$	source strength per unit axial distance, m/sec (ft/sec)
$r$	radial coordinate attached to wing, m (ft)
$q_\infty$	free-stream dynamic pressure, $\rho_\infty V_\infty^2 / 2$ , $N/m^2$ (lbf/ft <sup>2</sup> )
$t(\xi)$	wing thickness, $r_{\text{outer}} - r_{\text{inner}}$ , m (ft)

$U_0(\xi - \xi_0, 1)$  dimensionless kernel defined by equation (31) for  $\rho_0 = 1$

$V_q(\xi - \xi_0, 1)$  dimensionless kernel defined by equation (30) for  $\rho_0 = 1$

$V$  total velocity, free stream plus perturbation, m/sec (ft/sec)

$V_\infty$  free-stream velocity, m/sec (ft/sec)

$\left. \begin{array}{l} u(\xi_0, \rho_0) \\ v(\xi_0, \rho_0) \end{array} \right\}$  perturbation velocity components in x- and r-directions, respectively, induced at  $\xi_0, \rho_0$ , m/sec (ft/sec)

$\left. \begin{array}{l} \hat{u}(\xi - \xi_0, \rho_0) \\ \hat{v}(\xi - \xi_0, \rho_0) \end{array} \right\}$  dimensionless perturbation velocity influence functions for x- and r-directions, respectively; these influence functions are for velocity induced at  $\xi_0, \rho_0$  by a ring singularity at  $\xi, \rho = 1$  or by a point singularity at  $\xi, \rho = 0$

$X$  inlet length, m (ft)

$x, y, z, r$  coordinates attached to wing (see fig. 1 and app. A for positive directions), m (ft)

$\alpha_0$  slope of mean camber surface with respect to x-axis (wing centerline), radians

$\alpha_t$  slope of symmetrical thickness profile with respect to x-axis,  $(dt/dx)/2$  radians

$$\beta = \sqrt{1 - M_\infty^2}$$

$\Gamma_0$  dimensionless bound vortex strength of camber solution,  $\gamma_0 \Delta\xi$

$\gamma_0$  dimensionless bound vortex sheet strength of camber solution,  $\gamma_+/\sqrt{V_\infty} \alpha_0$

$\gamma_+$  bound vortex sheet strength of camber solution, m/sec (ft/sec)

$\gamma_t$  vortex sheet strength for thickness, m/sec (ft/sec)

$\gamma$  ratio of specific heats

$\Delta( )$	inner minus outer of ( ); $\Delta\xi =$ dimensionless panel length
$\delta^*$	boundary-layer displacement thickness, m (ft)
$\epsilon$	small positive number
$\theta$	momentum thickness, m (ft)
$\lambda$	aspect ratio, $D/c$
$\mu$	mass-flow ratio (see eq. (41))
$\xi$	dimensionless distance along axis, $\frac{x}{D/2}$
$\xi'$	dummy variable form of $\xi$
$\rho$	dimensionless radius, $\frac{r}{D/2}$ ; gas density, $\text{kg/m}^3$ (slugs/ft <sup>3</sup> )
$v$	dummy variable
$\psi$	digamma function (see app. B)

**Superscripts:**

$( )'$	incompressible quantity except $\xi'$ and $k'$
$(\hat{\quad})$	unit vector; velocity influence function
$(\bar{\quad})$	vector, except $\bar{g}_q(\xi)$
*	critical Mach number condition; boundary-layer displacement thickness

**Subscripts:**

+	dimensional bound vortex sheet strength of camber solution
$\infty$	free stream
b	center body

exp	experimental
h	highlight station (most forward point on inlet lip, $x = c/2$ in fig. 1)
i	location of vortex and source singularities
j	location of point at which velocity is induced
LE	leading edge
m	iteration number (see eq. (44))
max	maximum
min	minimum
o	point at which velocity is induced in $\xi_0, \rho_0$ ; effect due to camber only without angle-of-attack or pitching-motion effects in $\alpha_0, \gamma_0$ , and $\Gamma_0$ ; zeroth order in Fourier expansions in $U_0$ ; also see equation (44)
q	due to source ring of thickness solution
r	radial direction
TE	trailing edge
t	thickness solution; tangential
th	theory
w	wing surface
x	wing axial direction
$\gamma$	due to vortex ring
$\xi_0$	axial location
$\rho_0$	radial location

## THEORETICAL SOLUTION

The subsonic flow over an axisymmetric nacelle or annular wing with a center body of revolution will be determined by use of small perturbation theory. This problem is analogous in many ways to airfoil theory and biplane theory. Linearization of the problem permits computation of the compressibility effects by transforming the wing coordinates  $x$  and  $r$  into an equivalent incompressible wing  $x'$  and  $r'$  by using the Göthert transformation

$$x' = x \quad (1)$$

$$r' = \beta r \quad (2)$$

where  $\beta = \sqrt{1 - M_\infty^2}$ . The incompressible flow over this equivalent wing is then computed, and the compressible perturbation velocities  $u$  and  $v$  in the  $x$ - and  $r$ -directions, respectively, are found by

$$u = u'/\beta^2 \quad (3)$$

$$v = v'/\beta \quad (4)$$

while the free-stream velocity  $V_\infty$  remains unchanged. Compressible flow equations can then be used to determine the pressure distribution. (All primes are dropped from coordinates and velocities from this point on, and these variables are understood to be incompressible, unless otherwise stated.)

Also as a consequence of the linearization of the equations of motion and the boundary conditions, the problem can be broken up into wing camber, wing thickness, and center-body portions. Furthermore, each of these problems can be solved by superimposing elementary singular solutions of Laplace's equation, such as vortexes and sources. The linearized boundary condition on the wing surface at the point  $\xi_0, \rho_0$  is

$$\frac{v(\xi_0, \rho_0)}{V_\infty} = -\left(\frac{dr}{dx}\right)_{\xi_0, \rho_0} \quad (5)$$

where  $dr/dx$  is the local slope of the wing and  $\xi_0$  and  $\rho_0$  are dimensionless  $x$ - and  $r$ -coordinates. The minus sign arises because the positive  $x$ -direction has been chosen to be upstream (fig. 1). This boundary condition is written in two parts, one part for the camber and center body and one part for the thickness

$$\frac{v_{\gamma}(\xi_0, \rho_0)}{V_{\infty}} + \frac{v_b(\xi_0, \rho_0)}{V_{\infty}} = -\alpha_0(\xi_0, \rho_0) \quad (6)$$

$$\frac{v_q(\xi_0, \rho_0)}{V_{\infty}} + \frac{v_{t,\gamma}(\xi_0, \rho_0)}{V_{\infty}} = \mp \alpha_t(\xi_0, \rho_0) \quad (7)$$

where  $\alpha_0$  and  $\alpha_t$  are the slopes of the mean camber line and the symmetrical thickness, respectively. The subscripts  $\gamma$ ,  $b$ ,  $q$ , and  $t,\gamma$  refer to camber vorticity, center body, thickness source, and thickness vorticity, respectively. Two terms arise in the thickness equation because sources alone will not produce a symmetrically thick wing. This point is discussed further when the thickness solution is outlined. When plus and minus signs are used, the upper and lower signs refer to the outer and inner wing surfaces, respectively.

For design purposes it is convenient to separate the problem into its camber and thickness components. Thus, all singularities (except the center body) are placed on a cylinder of constant diameter  $D$  as shown in figure 1 and the boundary conditions are satisfied at control points on this same cylinder (counterpart of the planar wing approximation). A correction for approximating the surface velocities by velocities on this cylinder, which is called the Riegels factor, is discussed subsequently.

The strengths of the singularities are found by solving the boundary conditions given by equations (6) and (7). The solution of these boundary conditions involves evaluating improper integrals. The technique used is simply to replace the integrals by summations, thereby replacing the continuous vortex and source sheets and the source line by distributions of singularities. In the camber solution, proper placement of the vortex

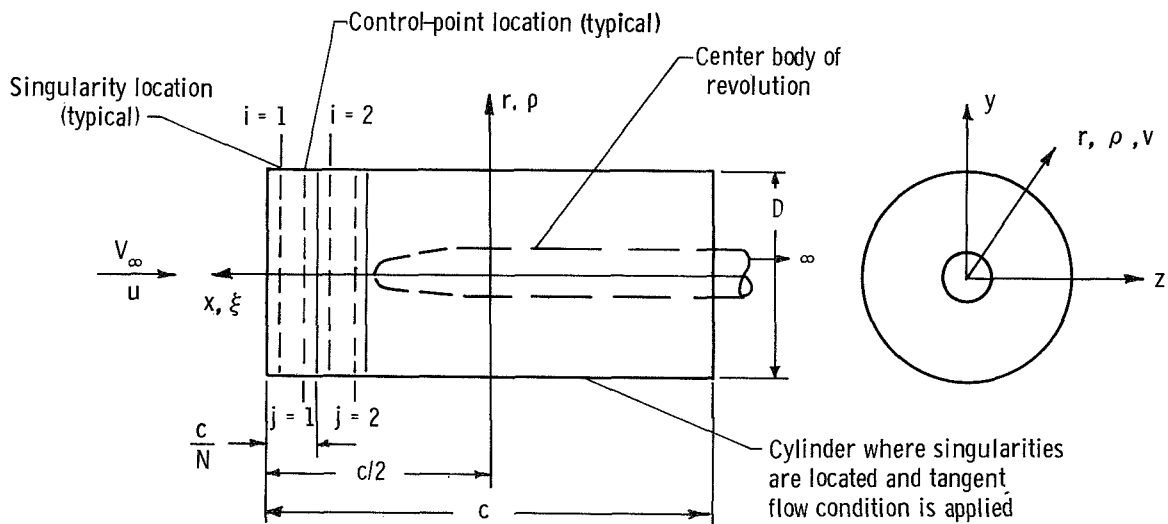


Figure 1.- Coordinates, geometry, and singularity and control-point location.

singularities and control points will satisfy both the principal value of the integral and the Kutta condition (ref. 7, p. 106). The same lattice arrangement is used for the sources as for the vortexes.

Once the velocity expressions are substituted into equations (6) and (7), a set of linear equations results with unknown singularity strengths. The vortex strengths are found by solving these equations by the method of successive orthogonalization. The source strengths for the wing thickness and the center body are proportional to the local body slopes.

In the following sections the major equations are given. The camber—center-body solution, the thickness solution, the complete wing solution, and the boundary-layer calculation are discussed.

### Camber—Center-Body Solution

The flow to be calculated is subsonic flow over an axisymmetric mean camber line at zero angle of attack. Along the center line of this infinitesimally thin wing is mounted a body of revolution. The mass flow inside the camber surface is varied by varying the size of the center body.

In order to obtain a unique solution for the flow over a camber surface, the basic flow conservation equations must be satisfied, boundary conditions on the body and at infinity must be satisfied, and the circulation specified (accomplished by the Kutta condition). As mentioned previously, these conditions can be met by distributing a continuous vortex sheet along a cylinder the length of which is equal to the wing chord. The influence of the center body can be found by use of a source line along the wing axis.

In this study the influence of the wing on the center body is ignored. There are several reasons for ignoring this interference. First, owing to the wide variation in internal structure, such as stings, struts, rakes, and so forth, no attempt was made to simulate any particular internal structural geometry. Secondly, inclusion of the mutual interference would greatly increase the storage requirements of the computer program (see app. A), thereby losing one of the attractive features of this method. Furthermore, the primary objective has been to obtain an accurate solution for the external flow. Thus, a simple body of revolution on the wing axis was selected to represent the internal parts. The size of this body is selected to either match the desired mass flow or match the internal blockage (and compute the mass flow). Both methods have shown good success as is demonstrated in the next section.

The vortex sheet strength is found by first substituting the expressions for the vortex velocities (refs. 7 and 12) and source velocities (refs. 12 and 13) into the boundary condition, equation (6). When this is done, the result is

$$\frac{1}{2\pi} \int_{-1/\lambda}^{1/\lambda} \alpha_o(\xi) \gamma_o(\xi) \hat{v}_\gamma(\xi - \xi_o, 1) d\xi = -\alpha_o(\xi_o) - \int_{\xi_{b,TE}}^{\xi_{b,LE}} \rho_b(\xi) \left( \frac{d\rho_b(\xi)}{d\xi} \right) \hat{v}_b(\xi - \xi_o, 1) d\xi \quad (8)$$

where the influence functions are defined by

$$\hat{v}_\gamma(\xi - \xi_o, \rho_o) = -\frac{(\xi - \xi_o)k}{4\rho_o^{3/2}} \left( \frac{2 - k^2}{1 - k^2} E - 2K \right) \quad (9)$$

$$\hat{v}_b(\xi - \xi_o, \rho_o) = \frac{\rho_o}{2 \left[ (\xi - \xi_o)^2 + \rho_o^2 \right]^{3/2}} \quad (10)$$

and  $K$  and  $E$  are complete elliptic integrals of the first and second kinds with modulus

$$k^2 = \frac{4\rho_o}{(\xi - \xi_o)^2 + (1 + \rho_o)^2} \quad (11)$$

The variables  $\xi$  and  $\rho$  are the dimensionless x- and r-locations of singularities ( $\rho = 1$ ), and  $\xi_o, \rho_o$  is the point at which the velocity is calculated ( $\rho_o = 1$ ). The variable  $\lambda$  is the wing aspect ratio;  $\gamma_o(\xi)$  is the vortex strength and is related to the usual definition of vortex sheet strength by

$$\gamma_+ = V_\infty \alpha_o \gamma_o$$

where  $\gamma_+$  is proportional to  $\Delta p / \rho V_\infty$ .

The subscript  $o$  on  $\gamma_o$  and  $\alpha_o$  is used in reference 7 to indicate camber effects without angle of attack or pitching motion. For the sake of consistency this notation is retained. When angle-of-attack effects are included, the vortex sheet is no longer of constant strength around its circumference and a trailing vortex system must also be included (ref. 7). The camber effect alone will give a nonzero radial force; however, owing to symmetry the net lift is zero.

Equation (8) is solved numerically by replacing the continuous vortex sheet by  $N$  equally spaced vortex rings. The source line along the center-body axis is replaced by three-dimensional point sources at the same axial locations as the vortex rings.<sup>1</sup> The

---

<sup>1</sup>Center-body length can be less than the wing chord  $c$ . The case of a semi-infinite center body can be simulated by a constant body radius to downstream infinity because the local source strength is zero where  $d\rho_b/d\xi = 0$ .

singularity location is  $i$  and the control-point location is  $j$ . When the quantity  $\gamma_o d\xi$  is replaced by

$$\Gamma_{oi} = \gamma_{oi} \Delta\xi$$

equation (8) becomes

$$\sum_{i=1}^N \alpha_{oi} \Gamma_{oi} \hat{v}_\gamma(\xi_i - \xi_{oj}, 1) = -2\pi \left[ \alpha_{oj} + \sum_{i=1}^N \rho_{bi} \left( \frac{d\rho_b}{d\xi} \right)_i \hat{v}_b(\xi_i - \xi_{oj}, 1) \Delta\xi \right] \quad (12)$$

Because the vortex rings and control points are located on a constant-diameter right circular cylinder of diameter  $D$ , then  $\rho_i = \rho_{oj} = 1$  in equation (12).<sup>2</sup> Each circular panel has a chord length of  $c/N$ . The vortex ring is located at one-fourth of this length from the panel leading edge and the control point is located at three-fourths of this length from the panel leading edge (fig. 1).

As previously mentioned, the influence of the wing on the body is neglected. Thus the body source strengths are given by the body slopes and everything on the right-hand side of equation (12) is known. Equation (12) is then a set of  $N$  simultaneous linear equations with  $N$  unknown vortex strengths  $\Gamma_{oi}$  (see definition of CAM in app. A for discussion of case when  $\alpha_o = 0$ ).

The set of equations resulting from equation (12) was solved for the unknown vortex strengths  $\Gamma_{oi}$  by the successive orthogonalization procedure outlined in reference 1. This procedure gave the same results as an alternate matrix inversion technique but has a great advantage on computer storage requirements. The method of reference 1 requires storage for a single  $N$ -dimensional array, the elements of which are  $\hat{v}_\gamma(\xi_i - \xi_{oj}, 1) \alpha_{oi}$  as opposed to other matrix techniques which require  $N$ - by  $N$ -array storage.

Once the vortex and source strengths are computed, the perturbation velocities can be found at each location  $\xi_{oj}$  on the cylinder  $\rho_{oj} = 1$  by use of the following expressions

$$\frac{u_\gamma(\xi_{oj}, 1)}{V_\infty} = \sum_{i=1}^N \frac{\alpha_{oi} \Gamma_{oi}}{2\pi} \hat{u}_\gamma(\xi_i - \xi_{oj}, 1) \pm \frac{\alpha_{oj} \Gamma_{oj}}{2 \Delta\xi} \quad (13)$$

$$\frac{v_\gamma(\xi_{oj}, 1)}{V_\infty} = \sum_{i=1}^N \frac{\alpha_{oi} \Gamma_{oi}}{2\pi} \hat{v}_\gamma(\xi_i - \xi_{oj}, 1) \quad (14)$$

---

<sup>2</sup>The radius  $\rho$  of a singularity ring always has a value of 1 in this paper; however, the radius of the point at which the velocity is computed  $\rho_o$  varies between 0 and 1 in the mass-flow computation but has a value of 1 elsewhere.

$$\frac{u_b(\xi_{0j}, 1)}{V_\infty} = \sum_{i=1}^N \rho_{bi} \left( \frac{d\rho_b}{d\xi} \right)_i \hat{u}_b(\xi_i - \xi_{0j}, 1) \Delta\xi \quad (15)$$

$$\frac{v_b(\xi_{0j}, 1)}{V_\infty} = \sum_{i=1}^N \rho_{bi} \left( \frac{d\rho_b}{d\xi} \right)_i \hat{v}_b(\xi_i - \xi_{0j}, 1) \Delta\xi \quad (16)$$

where the influence functions are

$$\hat{u}_\gamma(\xi_i - \xi_{0j}, 1) = \frac{k}{2}(E - K) \quad (17)$$

$$\hat{v}_\gamma(\xi_i - \xi_{0j}, 1) = -(\xi_i - \xi_{0j}) \frac{k}{4} \left( \frac{2 - k^2}{1 - k^2} E - 2K \right) \quad (18)$$

$$\hat{u}_b(\xi_i - \xi_{0j}, 1) = \frac{\xi_i - \xi_{0j}}{2 \left[ (\xi_i - \xi_{0j})^2 + 1 \right]^{3/2}} \quad (19)$$

$$\hat{v}_b(\xi_i - \xi_{0j}, 1) = \frac{1}{2 \left[ (\xi_i - \xi_{0j})^2 + 1 \right]^{3/2}} \quad (20)$$

For points off the cylinder<sup>3</sup>  $\rho_{0j} = 1$  (necessary when computing mass flow), equations (13) to (16) apply with the  $\pm$  term dropped in equation (13) and using the influence functions

$$\hat{u}_\gamma(\xi_i - \xi_{0j}, \rho_{0j}) = \frac{k}{4\sqrt{\rho_{0j}}} \left[ \left( \frac{2 - k^2}{1 - k^2} - \frac{1}{\rho_{0j}} \frac{k^2}{1 - k^2} \right) E - 2K \right] \quad (21)$$

$$\hat{u}_b(\xi_i - \xi_{0j}, \rho_{0j}) = \frac{\xi_i - \xi_{0j}}{2 \left[ (\xi_i - \xi_{0j})^2 + \rho_{0j} \right]^{3/2}} \quad (22)$$

---

<sup>3</sup>The variables  $\xi$  and  $\rho$  locate a singularity, and  $\xi_0, \rho_0$  is the point at which the velocity is calculated. When going from integrals and continuous distributions to summations and discrete distributions, it is necessary to indicate these quantities by  $\xi_i, \rho_i$  and  $\xi_{0j}, \rho_{0j}$ , respectively. When  $\rho_{0j} = 1$ , the location  $\xi_{0j}, \rho_{0j}$  is a control point; but when  $\rho_{0j} \neq 1$ , then  $\xi_{0j}, \rho_{0j}$  is meant to indicate any arbitrary point.

$\hat{v}_\gamma(\xi_i - \xi_{oj}, \rho_{oj})$  and  $\hat{v}_b(\xi_i - \xi_{oj}, \rho_{oj})$  as given in equations (9) and (10). Equation (13) is derived in appendix B by using the influence function in equation (21).

A linear interpolation of the  $\Gamma_{oi}$  was used to find the  $\Gamma_{oj}$ . A check of the  $\Gamma_{oi}$  distributions showed that the distribution approaches zero at the trailing edge, thereby satisfying the Kutta condition. Note that the pressure distribution over the camber surface depends on three quantities: camber surface slopes, aspect ratio, and mass flow (controlled by the size of the center body).

### Thickness Solution

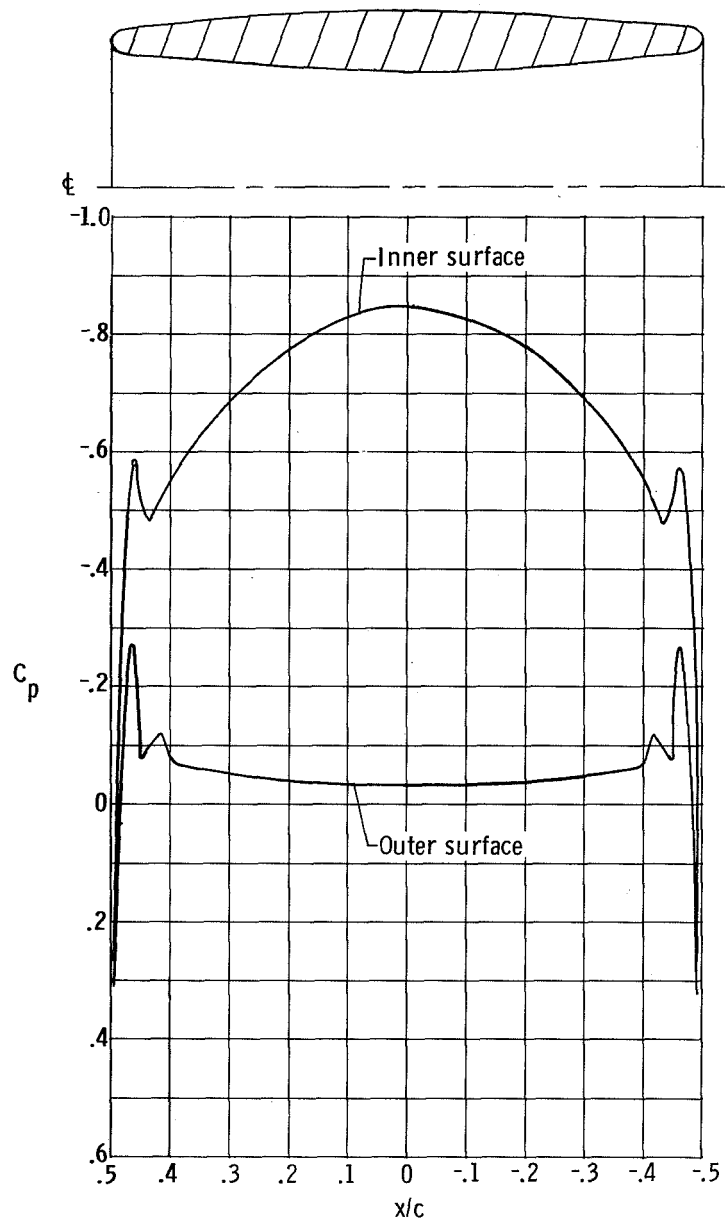
The flow to be calculated in this case is the subsonic flow over an annular wing with a symmetrical airfoil section at zero angle of attack. The flow must satisfy the same basic equations and conditions as the camber solution. The tangent flow condition is now equation (7).

In the case of planar problems, thickness can be accounted for by a distribution of sources on a plane. Such a distribution has the necessary symmetry property and discontinuous change of sign in the vertical velocity for the planar wing thickness. However, if two planar source sheets are placed in close proximity to form a biplane, the interference between the two sets of source distributions will cause a mutual induction of camber. The vertical velocity at some point on either sheet will no longer depend solely on the local source strength but will also depend on the complete source distribution of the other sheet. This interference problem also exists for an annular wing. The induced camber effects can be canceled by a vortex distribution, the strength of which is adjusted to just cancel the interference effects on the wing. Then the total source and vortex radial velocity will have the necessary discontinuous property across the singularity sheet.

Note that, because of the interference effects, an annular wing with thickness only at zero angle of attack has a negative radial force; that is, it tends to collapse. The internal flow area reduction due to thickness accelerates the flow much more than the same flow area reduction externally. Figure 2 shows the pressure distributions for an annular wing with thickness only and the same wing with enough camber to make the inside diameter constant. The radial force changes sign when geometric camber is added, and with the proper amount of geometric camber the inner and outer pressures can be equalized.

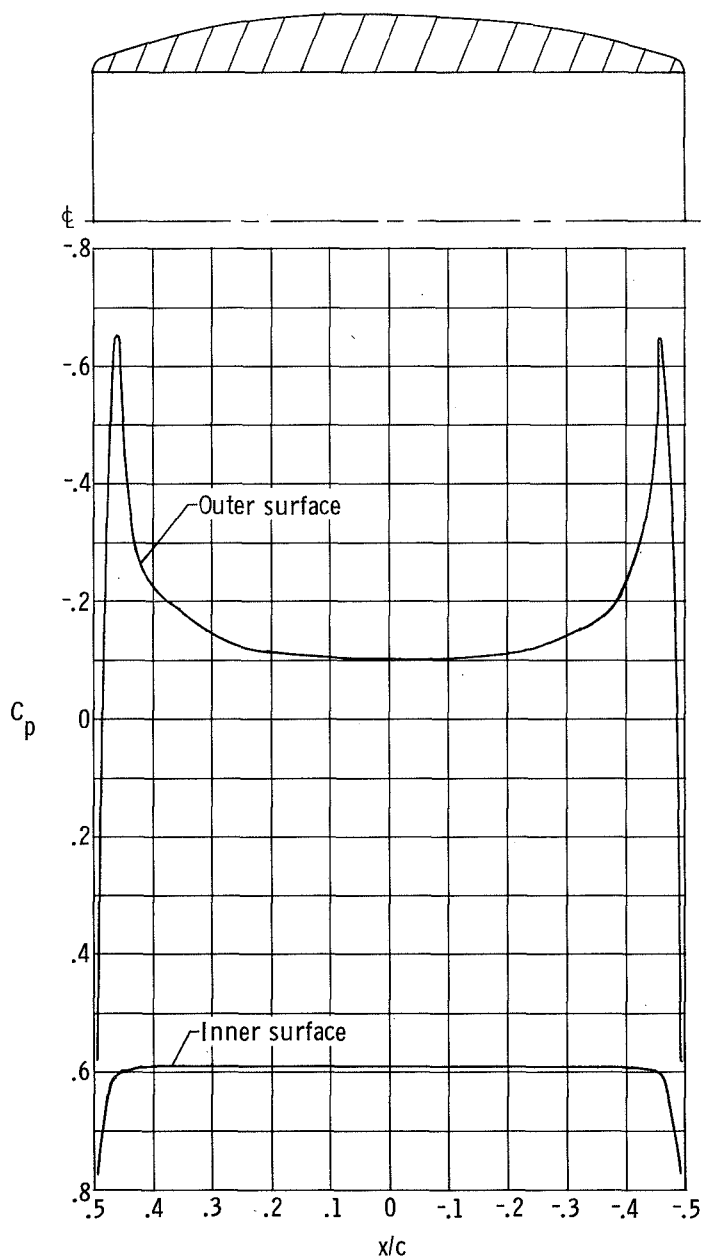
Because the annular wing with thickness only has the effect of camber in its flow, namely a nonzero radial force, it would be convenient to refer to this effect as an aerodynamic camber. Then the variations of the mean camber line from the chord could be referred to as geometric camber.

The radial velocity induced at  $\xi_0$  and  $\rho_0 = 1$  by a continuous distribution of source rings of diameter  $D$  (radius  $\rho = 1$ ) over an axial length of  $c$  is (see app. B)



(a) 4.3-percent thickness and zero camber;  $\mu = 0.87$ .

Figure 2.- Pressure distribution on an annular wing without and with camber at  $M_\infty = 0.50$ .



(b) 4.3-percent thickness and constant inside diameter;  $\mu = 0.70$ .

Figure 2.- Concluded.

$$\frac{v_q(\xi_0, 1)}{V_\infty} = \pm \frac{q(\xi_0)}{2V_\infty} - \int_{-\frac{1}{\lambda}}^{\frac{1}{\lambda}} \frac{1}{4\pi V_\infty} \hat{v}_q(\xi - \xi_0, 1) d\xi \quad (23)$$

where  $q(\xi)$  is the source strength at  $\xi$  and the influence function  $\hat{v}_q(\xi - \xi_0, 1)$  is related to the vortex influence function for the velocity  $u$  by

$$\hat{v}_q(\xi - \xi_0, 1) = 2\hat{v}_\gamma(\xi - \xi_0, 1) \quad (24)$$

The integral term in equation (23) is the induced camber due to interference effects. This integral can be canceled by a vortex distribution the strength of which is determined by

$$\begin{aligned} \frac{v_{t,\gamma}(\xi_0, 1)}{V_\infty} &= \frac{1}{2\pi} \int_{-\frac{1}{\lambda}}^{\frac{1}{\lambda}} \frac{\gamma_t(\xi)}{V_\infty} \hat{v}_{t,\gamma}(\xi - \xi_0, 1) d\xi \\ &= \int_{-\frac{1}{\lambda}}^{\frac{1}{\lambda}} \frac{1}{4\pi V_\infty} \frac{q(\xi)}{V_\infty} \hat{v}_q(\xi - \xi_0, 1) d\xi \end{aligned} \quad (25)$$

where  $\gamma_t(\xi)$  has the dimensions of  $\gamma_+$ , and  $\hat{v}_{t,\gamma}$  is computed by using equation (18). When this is done, equation (23) can be written as

$$\frac{v_q(\xi_0, 1)}{V_\infty} + \frac{v_{t,\gamma}(\xi_0, 1)}{V_\infty} = \pm \frac{q(\xi_0)}{2V_\infty} \quad (26)$$

The flow constructed in this way will satisfy the required boundary condition in equation (7). Thus from equations (7) and (26) the source strength is determined by

$$q(\xi_0) = -2V_\infty \alpha_t(\xi_0) \quad (27)$$

where the boundary condition is being satisfied at points  $(\xi_0, \rho_0 = 1)$ .

The solution of equation (25) for the unknown vortex strength is the same type of numerical problem found in the camber solution. An alternate method of finding  $\gamma_t(\xi)$  has been outlined by Weissinger (ref. 8). By examination of the boundary conditions for a vortex flow, the vortex strength necessary to cancel the integral of equation (23) is determined by

$$\frac{1}{2} \int_{-\frac{1}{\lambda}}^{\frac{1}{\lambda}} Q(\xi) V_q(\xi - \xi_0, 1) d\xi = - \int_{-\frac{1}{\lambda}}^{\frac{1}{\lambda}} \frac{\bar{g}_q(\xi)}{\lambda(\xi - \xi_0)} d\xi + \frac{1}{\lambda} \int_{-\frac{1}{\lambda}}^{\frac{1}{\lambda}} \bar{g}_q(\xi) U_0(\xi - \xi_0, 1) d\xi \quad (28)$$

where

$$Q(\xi) = \lambda \int_{-\frac{1}{\lambda}}^{\xi} \frac{q(\xi')}{V_\infty} d\xi' = 2 \frac{t(\xi)}{c} \quad (29)$$

$$V_q(\xi - \xi_0, 1) = \frac{\sqrt{1 - k^2}}{2} \frac{(\xi - \xi_0)}{|\xi - \xi_0|} \left[ 2(1 + k^2)E - (2 + k^2)K \right] \quad (30)$$

$$U_0(\xi - \xi_0, 1) = \frac{1}{\xi - \xi_0} \left\{ \frac{1}{k} \left[ (k^2 - 2)E + 2(1 - k^2)K \right] + 1 \right\} \quad (31)$$

and  $t(\xi)$  is the wing thickness and  $\bar{g}_q(\xi)$  is related to the vortex strength by

$$\frac{\gamma_t(\xi)}{V_\infty} = - \frac{1}{2\lambda} Q(\xi) - \frac{1}{\lambda^2} \bar{g}_q(\xi) \quad (32)$$

(The symbol  $-\gamma_t(\xi)/V_\infty$  is called  $g_q(\xi)$  in ref. 8.) The kernel functions  $V_q$  and  $U_0$  are continuous and antisymmetrical. The solutions of equations (25) and (28) for  $\gamma_t(\xi)$  should require about the same computing time; equation (28) was chosen for this study. In numerical form, equations (28) and (29) yield

$$\sum_{i=1}^N \frac{t_i}{c} V_q(\xi_i - \xi_{0j}, 1) \Delta\xi = \sum_{i=1}^N \left[ U_0(\xi_i - \xi_{0j}, 1) - \frac{1}{\xi_i - \xi_{0j}} \right] \frac{\bar{g}_{qi}}{\lambda} \Delta\xi \quad (33)$$

The source and vortex-ring locations  $(\xi_i, \rho_i = 1)$  and control-point locations  $(\xi_{0j}, \rho_{0j} = 1)$  are the same as in the camber solution. The same method of solution of linear equations discussed previously was used for equation (33).

Once the source and vortex strengths are computed, the perturbation velocities can be computed at any point  $(\xi_{0j}, \rho_{0j})$ . Equations (13) and (14) give the vortex velocities  $u_{t,\gamma}$  and  $v_{t,\gamma}$  when  $\alpha_{oi} \Gamma_{oi}$  is replaced by  $(\gamma_{ti}/V_\infty) \Delta\xi$  and similarly for  $\alpha_{oj} \Gamma_{oj}$ . Recall that for points off the cylinder  $\rho_{oj} = 1$ , the  $\pm$  term in equation (13) must be dropped. The source velocities at points on the cylinder  $\rho_{oj} = 1$  are computed from (refs. 8 and 12)

$$\frac{u_q(\xi_{oj}, 1)}{V_\infty} = \sum_{i=1}^N \frac{\alpha_{ti} \Delta \xi}{2\pi} \hat{u}_q(\xi_i - \xi_{oj}, 1) \quad (34)$$

$$\frac{v_q(\xi_{oj}, 1)}{V_\infty} = \sum_{i=1}^N \frac{\alpha_{ti} \Delta \xi}{2\pi} \hat{v}_q(\xi_i - \xi_{oj}, 1) \mp \alpha_{tj} \quad (35)$$

where the influence function  $\hat{v}_q$  is given by equation (24) and  $\hat{u}_q$  is

$$\hat{u}_q(\xi_i - \xi_{oj}, 1) = \frac{-2kE}{\xi_i - \xi_{oj}} \quad (36)$$

Equation (35) can be obtained from equations (23) and (27). For points off the cylinder defined by  $\rho_{oj} = 1$  (necessary when computing the mass flow), equations (34) and (35) apply with the term  $\mp \alpha_{tj}$  in equation (35) dropped and by using the influence functions

$$\hat{u}_q(\xi_i - \xi_{oj}, \rho_{oj}) = \frac{-4(\xi_i - \xi_{oj})E}{\sqrt{(\xi_i - \xi_{oj})^2 + (1 + \rho_{oj})^2} \left[ (\xi_i - \xi_{oj})^2 + (1 - \rho_{oj})^2 \right]} \quad (37)$$

$$\hat{v}_q(\xi_i - \xi_{oj}, \rho_{oj}) = \left[ \frac{2}{\rho_{oj} \sqrt{(\xi_i - \xi_{oj})^2 + (1 + \rho_{oj})^2}} \right] \times \left\{ \left[ 1 - \frac{2\rho_{oj}(\rho_{oj} - 1)}{\left[ (\xi_i - \xi_{oj})^2 + (1 - \rho_{oj})^2 \right]} \right] E - K \right\} \quad (38)$$

Note that the thickness solution depends on two quantities: thickness distribution  $t(\xi)$  and aspect ratio.

### Pressure Distribution and Mass Flow

Once the singularity strengths are determined, the velocities due to camber, center body, and thickness can be added to give the total surface velocity and pressure distribution. The internal flow velocities can be integrated over a surface perpendicular to the center line at some  $\xi$ -location to calculate the mass flow through the annular wing.

In regions of high body curvature, such as the nose, approximation of the surface velocity by the velocity on a constant-diameter cylinder is not satisfactory. A correction for this approximation called the Riegels factor, is shown by Weber (ref. 14) to improve the calculated velocities in the nose region of a two-dimensional airfoil.

The Riegels factor can be developed from geometry as follows. By writing the equation for the wing surface<sup>4</sup> as

$$f(x,r) = r - r_w(x) = 0$$

the unit tangential vector in the meridional direction is

$$\hat{e}_t = \frac{\hat{e}_x + \frac{dr_w}{dx} \hat{e}_r}{\sqrt{1 + \left(\frac{dr_w}{dx}\right)^2}}$$

where  $\hat{e}_x$  and  $\hat{e}_r$  are unit vectors in the x- and r-directions, respectively. Writing the total compressible surface velocity as

$$\bar{V} = (V_\infty + u) \hat{e}_x + v \hat{e}_r$$

the total tangential surface velocity is

$$V_t = \bar{V} \cdot \hat{e}_t = \frac{(V_\infty + u) + v \frac{dr_w}{dx}}{\sqrt{1 + \left(\frac{dr_w}{dx}\right)^2}}$$

Consistent with linear theory the total surface velocity is approximated by

$$V = \frac{(V_\infty + u)_{\rho=1}}{\sqrt{1 + \left(\frac{dr_w}{dx}\right)^2}} \quad (39)$$

The quantity in the denominator is the Riegels factor. Equation (39) shows that the total velocity on the wing surface is found by computing the total x-velocity on the cylinder  $\rho = 1$  and multiplying this result by the Riegels factor.

---

<sup>4</sup>All velocities from now on are compressible and coordinates are for the actual (untransformed) geometric shape.

The surface pressure distribution is computed by making compressibility and Riegels factor corrections to the incompressible velocities and calculating the pressure from

$$C_p = \frac{2}{\gamma M_\infty^2} \left\{ \left[ 1 + \frac{\gamma - 1}{2} M_\infty^2 \left( 1 - \frac{V^2}{V_\infty^2} \right) \right]^{\frac{\gamma}{\gamma - 1}} - 1 \right\} \quad (40)$$

where  $\gamma$  is the ratio of specific heats.

The mass flow is computed in the form of a ratio

$$\mu \equiv \frac{m}{\rho_\infty A_h V_\infty} = \left( \frac{\rho_{\xi_0}}{\rho_\infty} \right) \left( \frac{A_{\xi_0}}{A_h} \right) \left( \frac{V_{\xi_0}}{V_\infty} \right) \quad (41)$$

where  $m$  is the mass flow through the annular wing,  $V_{\xi_0}$  is the total x-velocity at some  $\xi_0$  location, and  $A_h$  is a reference area based on the highlight diameter (diameter at  $x = c/2$  in fig. 1). The area  $A_{\xi_0}$  is the internal cross-sectional area of the wing at  $\xi_0$  less the local center-body cross-sectional area. The velocity ratio is computed by dividing the flow area into small annuli and calculating the mass flow through each annulus and summing the result as follows (assuming density constant over the cross section)

$$\frac{V_{\xi_0}}{V_\infty} = \sum_j \frac{V(\xi_0, \rho_{0j})}{V_\infty} \frac{A(\xi_0, \rho_{0j})}{A_{\xi_0}} \quad (42)$$

The  $V(\xi_0, \rho_{0j})$  are the total x-velocities computed at a fixed  $\xi_0$  and the particular  $\rho_{0j}$  location. The annulus area  $A(\xi_0, \rho_{0j})$  is at the  $\xi_0, \rho_{0j}$  location. The density ratio is calculated from the one-dimensional relation

$$\frac{\rho_{\xi_0}}{\rho_\infty} = \left[ 1 + \frac{\gamma - 1}{2} M_\infty^2 \left( 1 - \frac{V_{\xi_0}^2}{V_\infty^2} \right) \right]^{\frac{1}{\gamma - 1}} \quad (43)$$

### Boundary-Layer Solution

The boundary layer was approximated by a turbulent boundary layer over the entire chord length. The incompressible turbulent boundary-layer method of Truckenbrodt (ref. 15) was used. John B. Peterson, Jr., of NASA Langley Research Center developed the necessary equations for computing the boundary layer and programed these equations for the boundary-layer subroutine used in this study.

The inviscid velocity distribution at the trailing edge is greatly in error since a stagnation point is computed there. Hence, the velocity was extrapolated to the trailing edge (ref. 16). A procedure similar to that used in reference 17 was employed. In each case an estimate was made of the point beyond which the inviscid velocity became unreasonable because of the trailing-edge stagnation point. Then a least-square-curve fit of the velocities was made between that point (97-percent-chord station) and the 80- or 90-percent-chord station. This least-square-curve fit was then used to recompute the velocities between the 80- or 90-percent station and the trailing edge. The outer surface was computed first so that the Nth value of the recomputed outer surface velocity (value closest to trailing edge) could also be included in the inner surface curve fit. A linear-curve fit was used on the outer surface and a parabolic fit on the inner surface. This procedure produced smooth and reasonable velocities for the boundary-layer calculation. It was determined that uncertainties in this method gave 2-percent or less error in  $\mu$ . The figures to be presented indicate the range in which the curve fit was made.

It should be clearly understood, however, that this trailing-edge procedure is simply an approximate scheme in place of calculating the true effect of the correct wake. (For a nonzero trailing-edge thickness the total source strength is nonzero, and therefore some wake is simulated.) It may be possible to simulate the correct wake effect by use of a wake annular thickness distribution which has just enough geometric camber to cancel the  $\Delta C_p$  due to thickness, thereby making the inner and outer pressures equal.

In order to obtain convergence of the boundary-layer displacement thickness, it was necessary to modify the wing coordinates, on the mth iteration, with the following effective displacement thickness

$$\delta^* = \frac{\delta_0^* + 2\delta_1^* + \dots + (m+1)\delta_m^*}{1 + 2 + \dots + (m+1)} \quad (44)$$

where  $\delta_0^*$  is based on velocities computed by using the actual wing geometry. On the first iteration the wing coordinates were modified by  $\delta_0^*/2$ , rather than  $\delta_0^*$  as indicated in equation (44). When separation occurred during the iteration process (shape factor  $H \geq 2.4$ ), the shape factor was limited to 2.55 to permit convergence.

### Computer Program

The complete computer program is described in appendix A. Input and output quantities and the program listing are included. One output quantity is the critical Mach number, which is determined by an approximate method of von Kármán (ref. 18). The printed value of the critical Mach number is valid only when  $M_\infty$  is low enough for the flow to be assumed incompressible.

The number of chordwise divisions  $N$  was 150. For the nacelles of this study the magnitude of the leading-edge suction peak had reached a stationary value by this value of  $N$ . For the mass-flow computation the radial increments were  $r_{\text{inner}}/170$ . Since the velocity generally had a very small variation across the flow area (substantiating the usual one-dimensional-flow assumption), these radial increments were more than sufficient.

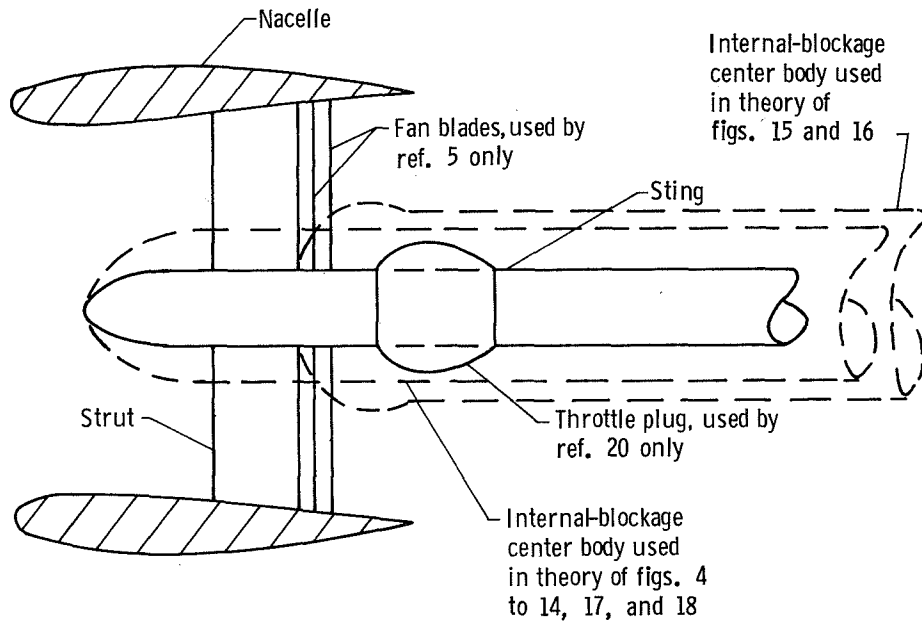
Calculations on a CDC-6600 computer required 2 minutes for an inviscid calculation and 4 minutes for a viscous calculation. Each additional iteration on the viscous calculation required about 2 minutes. This time could be reduced by use of a cosine distribution of singularities which would increase the singularity density in regions of strong pressure gradients and reduce the density in the center of the body. Such a distribution of vortexes will produce the same downwash at points midway between the vortexes as a continuous distribution of vorticity (app. B of ref. 19).

## COMPARISON OF THEORY AND EXPERIMENT

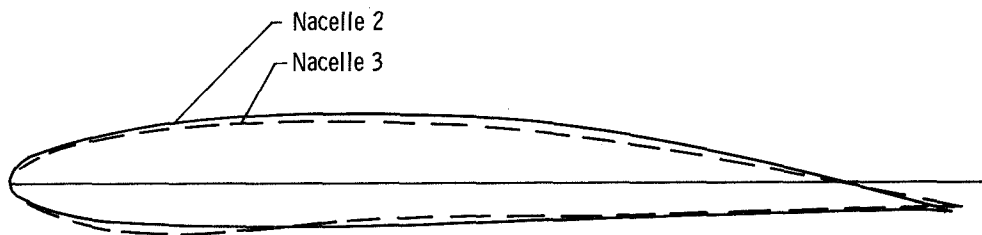
Calculations were compared with experimental data obtained in two wind tunnels (refs. 5 and 20) to provide a check on the present theory. The comparison with the tests of reference 5 is discussed first. These tests covered a range of subsonic Mach numbers at primarily zero angle of attack. Figure 3(a) shows a sketch of the experimental setup and its relation to the theoretical model used to represent it. The mass flow in the experiment was controlled by the insertion of stationary sets of fan blades. The blockage of the sting, struts, and fan blades was represented in the theory by the blockage of a center body. In the experiment, the highest mass flow was obtained without a set of blades installed. In this condition the experimental setup was more faithfully modeled by the theory than with sets of blades installed, and the best agreement between measured and calculated internal pressures would be expected. This expected result was achieved as will be discussed.

The pressure distribution and mass flow are not sensitive to variations in the diameter  $D$  of the vortex and source rings (see fig. 1). The value of  $D$  used in this study was the average of the minimum inside diameter and the maximum outside diameter of the wing.

Nacelles 2 and 3 of reference 5 were selected for the present study (fig. 3(b)). These nacelles were designed to have prescribed external pressure distributions and internal contraction ratios. Comparisons between theory and experiment were made for three Mach numbers and several mass-flow ratios. The exact sting leading edge and nose shape were not given. Thus the nose of the center body in the theoretical model was placed at approximately the position of the sting leading edge and the shape was arbitrarily selected to be that of a NASA supercritical body of revolution (ref. 21). At the maximum diameter



(a) Relation of experimental setup to theoretical model. (Not to scale.)



(b) Profile shapes for nacelles 2 and 3.

Figure 3.- Geometry of experimental setup and theoretical model.

station of the center body, a constant-diameter cylinder was attached and extended downstream. As seen in figure 3(a), the constant diameter portion of the center body extended to infinity for the high-mass-flow cases of figures 4 to 14. However, for the low-mass-flow cases of figures 15 and 16 the center body was expanded at the approximate location of the fan blades. The necessity of this expansion for the low-mass-flow cases is discussed subsequently.

The quoted accuracy of the measured mass flows in reference 5 is 1.5 percent based on boundary layer and instrument errors. However, Young also states that the presence of the fan blades tended to separate the flow. Hence, for the lower mass flows tested, larger errors in the mass-flow ratio  $\mu$  may be present. Errors in  $\mu$  would be reflected in a lack of agreement of measured and calculated pressures, especially on the inner surface and at the leading-edge suction peak.

In the experiments the transition bands were applied from 6.25 to 10.4 percent of the chord. Therefore in the theory the boundary layer was approximated by a turbulent boundary layer over the entire chord length, as discussed previously. The Reynolds number based on chord length was fixed at the experimental value of  $2 \times 10^6$ .

In all the pressure-distribution curves shown herein, with the exception of figure 2(a), the upper and lower curves correspond to the outer and inner surfaces, respectively.

A comparison of the theory and experiment is presented in figures 4 to 12. Mach numbers of 0.3, 0.5, and 0.7 were examined. In selecting the center-body diameter, two approaches are available. First, if the desired mass flow is known, the procedure is simply to vary the body size until the desired mass flow is achieved. Only a few trial solutions are necessary to establish a curve of mass flow versus maximum body radius from which the maximum body radius can be selected to yield the desired mass flow. The second approach is to match the internal blockage area between the experimental geometry and a body of revolution and calculate the mass flow. Figures 4 to 7 used the first approach, and figures 8 to 11 used the second. Each figure gives the number of iterations on the boundary layer and the chordwise range from which velocities were used to obtain the least-square-curve fits. The iteration was continued until the maximum change in  $\delta^*$  on either surface was less than 2 percent of the maximum  $\delta^*$  for the respective surfaces. Good agreement is obtained between measured and calculated pressures when the boundary layer is included.

Note that figures 6, 7, 10, and 11 have slightly supercritical flow as shown by the value of the critical pressure coefficient  $C_p^*$ . A weak shock seems to occur near the leading edge. However, aft of this region agreement is good.

Insight into the effect of the boundary layer on the mass flow is provided by examining figures 8 to 11. These figures indicate that for a fixed geometry, the presence of the boundary layer increases the mass flow, contrary to what might at first be expected. Recall the case of a two-dimensional airfoil where the boundary layer causes an effective decrease in angle of attack; that is, the boundary layer reduces the lift and therefore the area under the curve of  $C_p$  versus  $\xi$  (ref. 17). As seen from figures 8 to 11, the boundary layer has the same effect on an annular wing, only in this case the radial force is being lowered. As this happens, the leading-edge stagnation point moves more toward

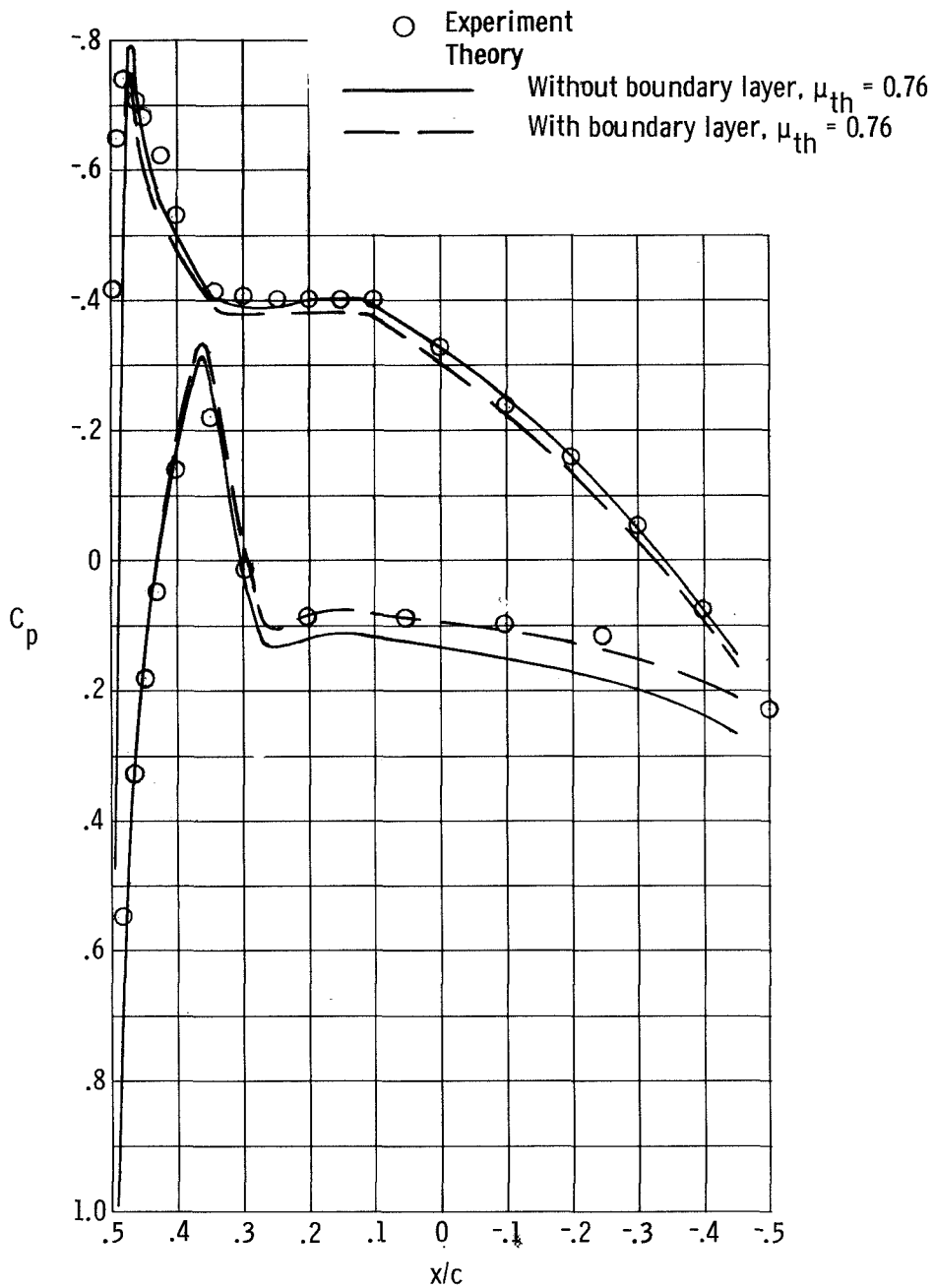


Figure 4.- Pressure distribution on nacelle 3;  $M_\infty = 0.3$ ;  $\mu_{th} = \mu_{exp} = 0.76$ .  
 Boundary layer: Six iterations; least square 90- to 97-percent c.

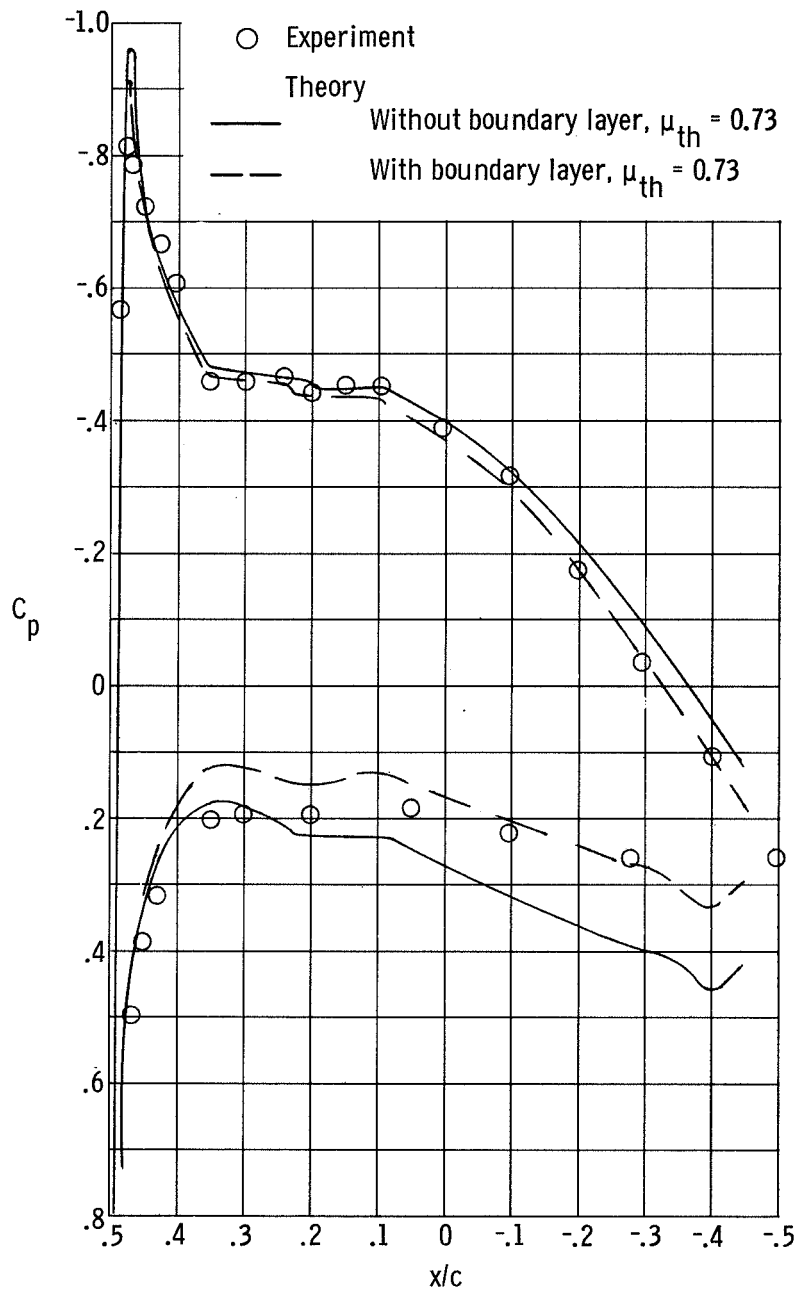


Figure 5.- Pressure distribution on nacelle 2;  $M_\infty = 0.5$ ;  $\mu_{th} = \mu_{exp} = 0.73$ .  
 Boundary layer: Six iterations; least square 90- to 97-percent c.

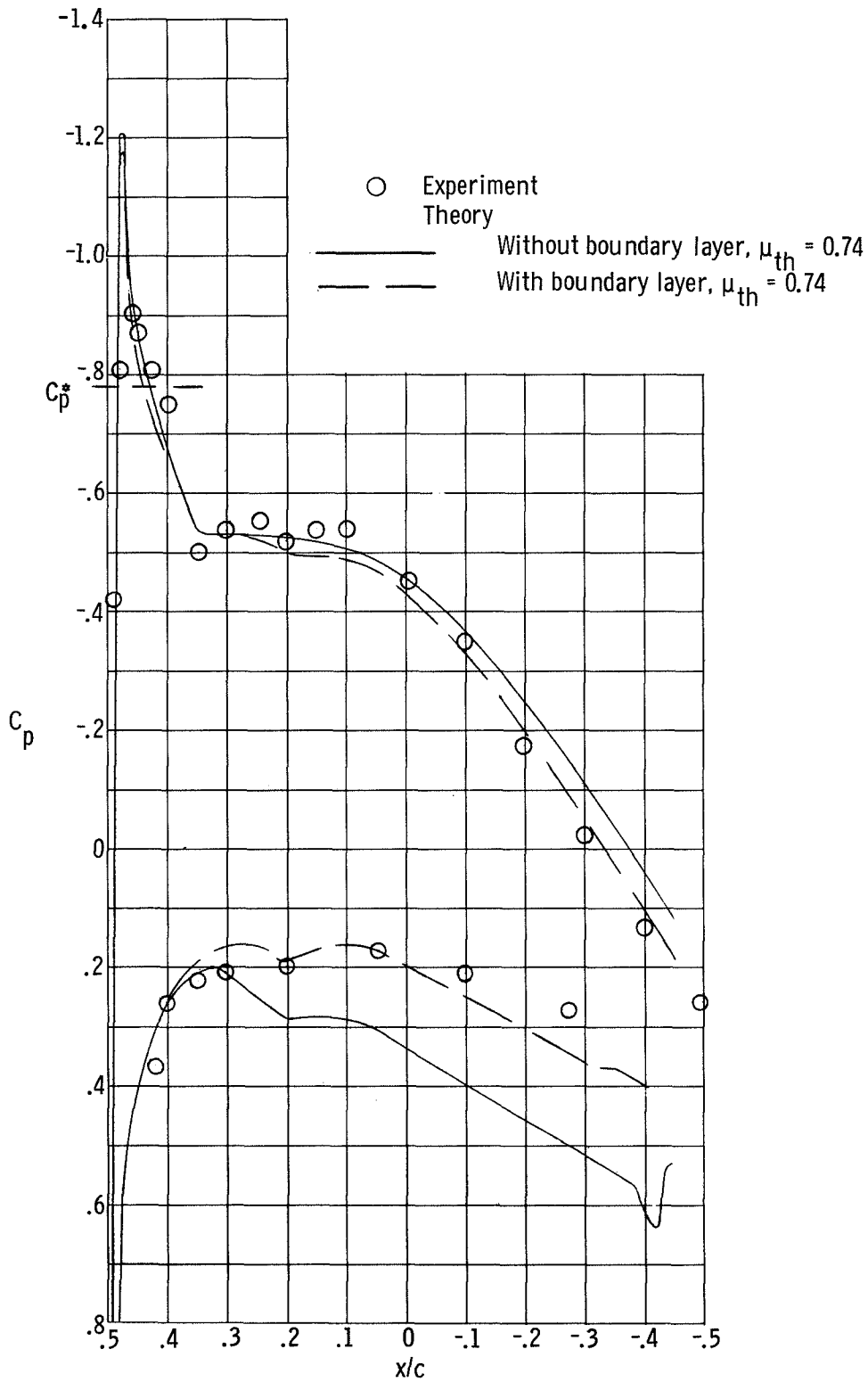


Figure 6.- Pressure distribution on nacelle 2;  $M_\infty = 0.7$ ;  $\mu_{th} = \mu_{exp} = 0.74$ .  
 Boundary layer: Five iterations; least square 80- to 97-percent  $c$ .

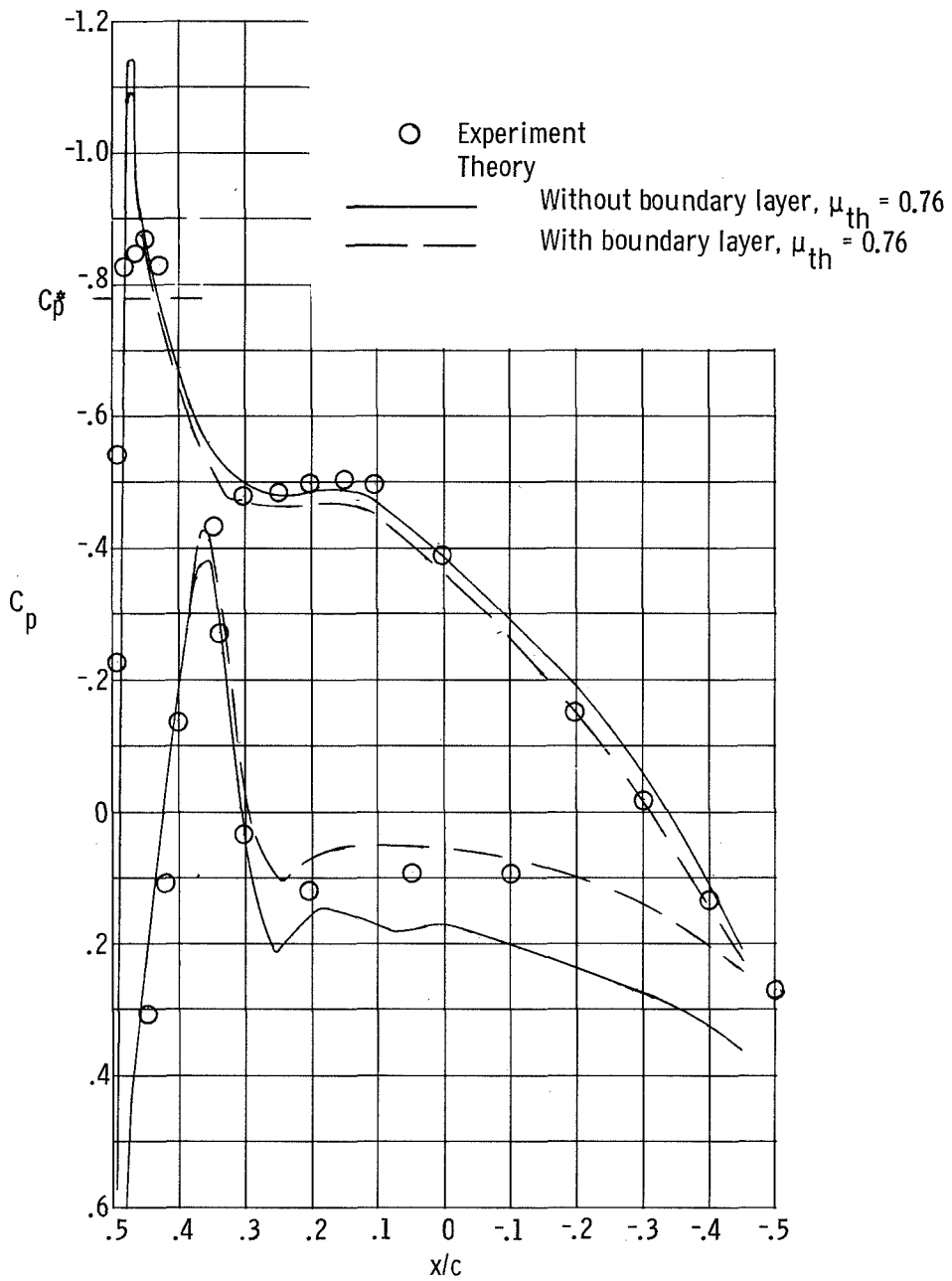


Figure 7.- Pressure distribution on nacelle 3;  $M_\infty = 0.7$ ;  $\mu_{th} = \mu_{exp} = 0.76$ .  
 Boundary layer: Five iterations; least square 80- to 97-percent c.

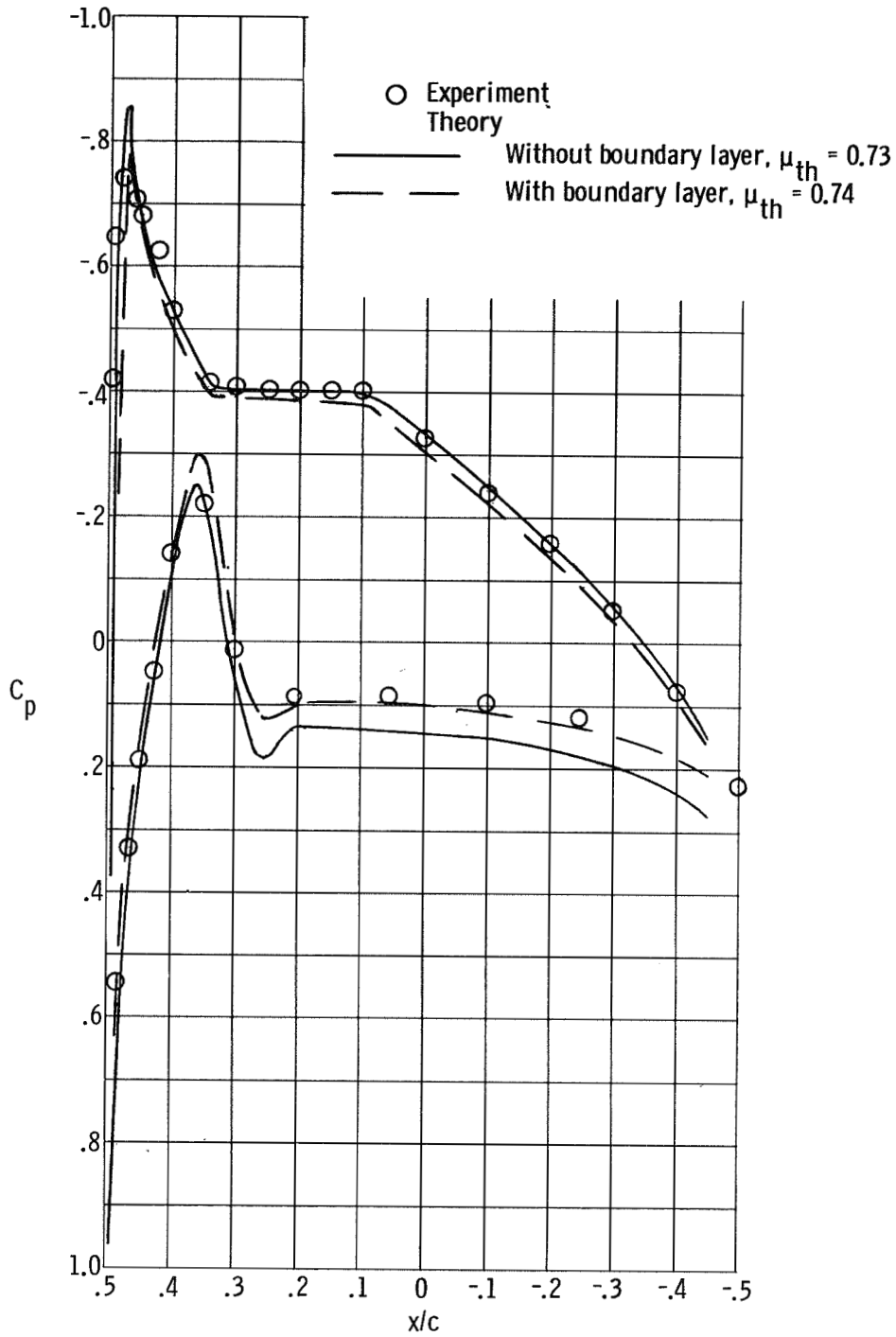


Figure 8.- Pressure distribution on nacelle 3;  $M_\infty = 0.3$ ;  $(r_b/c)_{max} = 12.79$  percent;  $\mu_{exp} = 0.76$ . Boundary layer: Six iterations; least square 90- to 97-percent c.

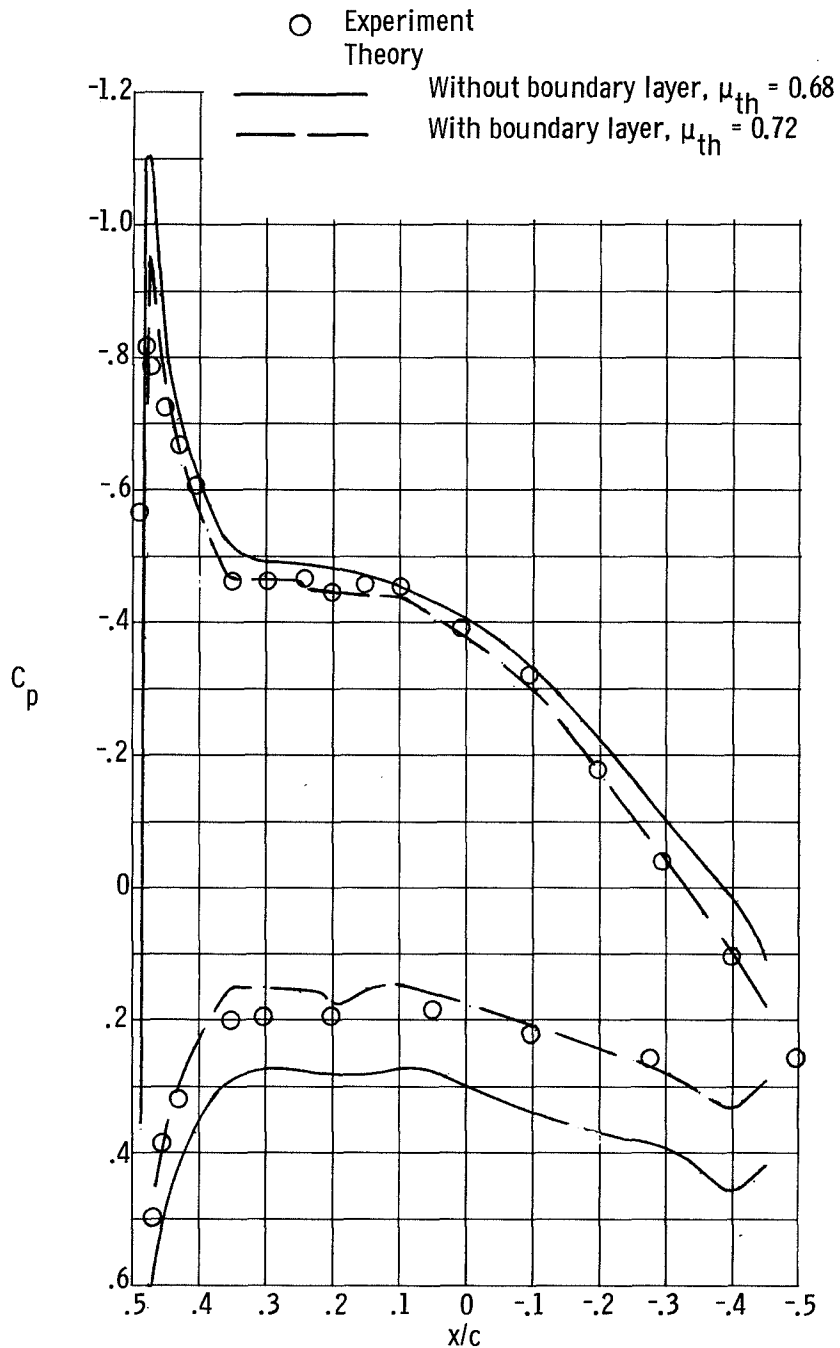


Figure 9.- Pressure distribution on nacelle 2;  $M_{\infty} = 0.5$ ;  $\left(r_b/c\right)_{max} = 12.61$  percent;  $\mu_{exp} = 0.73$ . Boundary layer: Six iterations; least square 90- to 97-percent c.

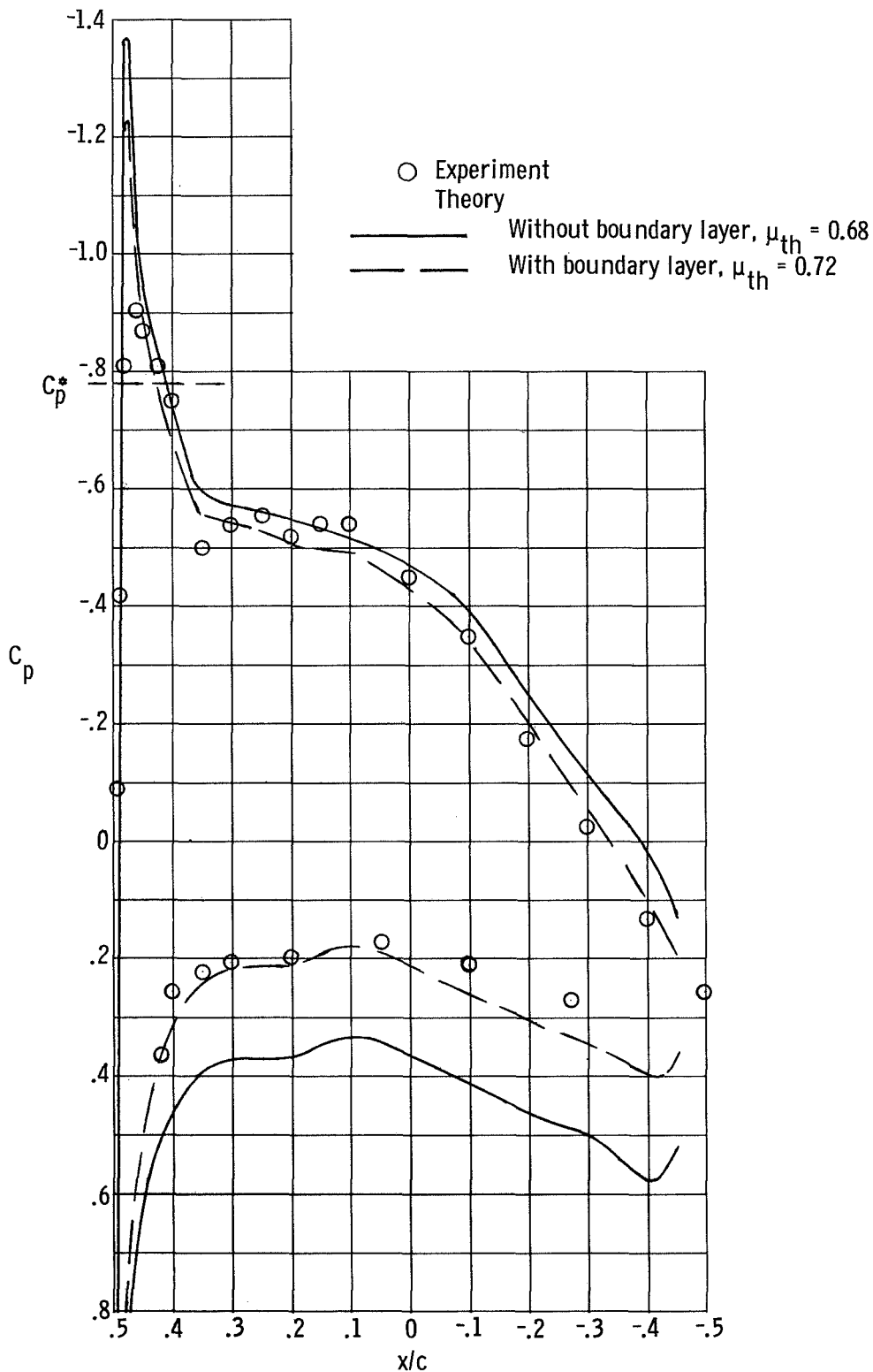


Figure 10.- Pressure distribution on nacelle 2;  $M_\infty = 0.7$ ;  $(r_b/c)_{max} = 12.61$  percent;  $\mu_{exp} = 0.74$ . Boundary layer: Five iterations, least square 80- to 97-percent  $c$ .

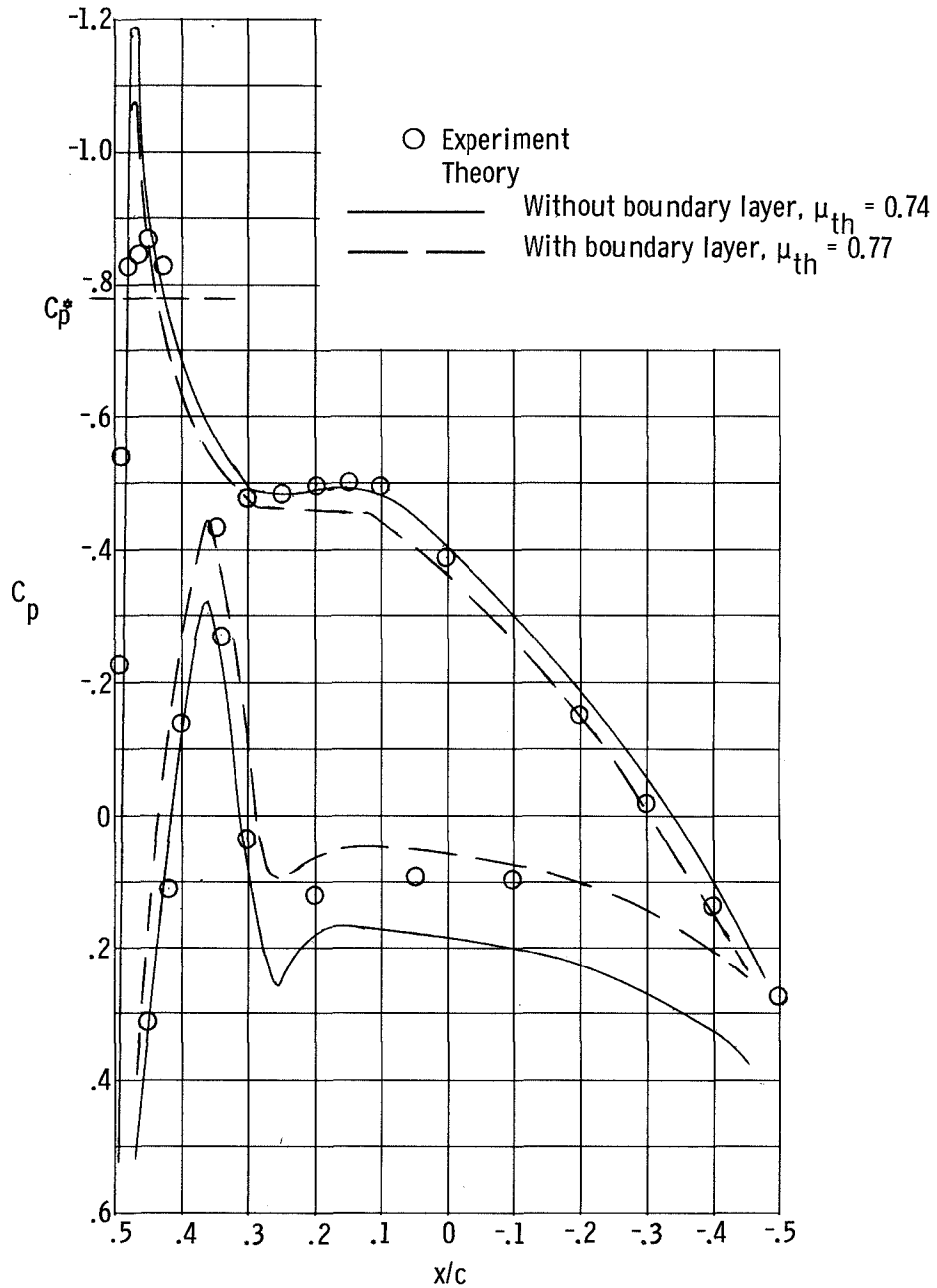


Figure 11.- Pressure distribution on nacelle 3;  $M_\infty = 0.7$ ;  $(r_b/c)_{max} = 12.79$  percent;  $\mu_{exp} = 0.76$ . Boundary layer: Five iterations; least square 80- to 97-percent  $c$ .

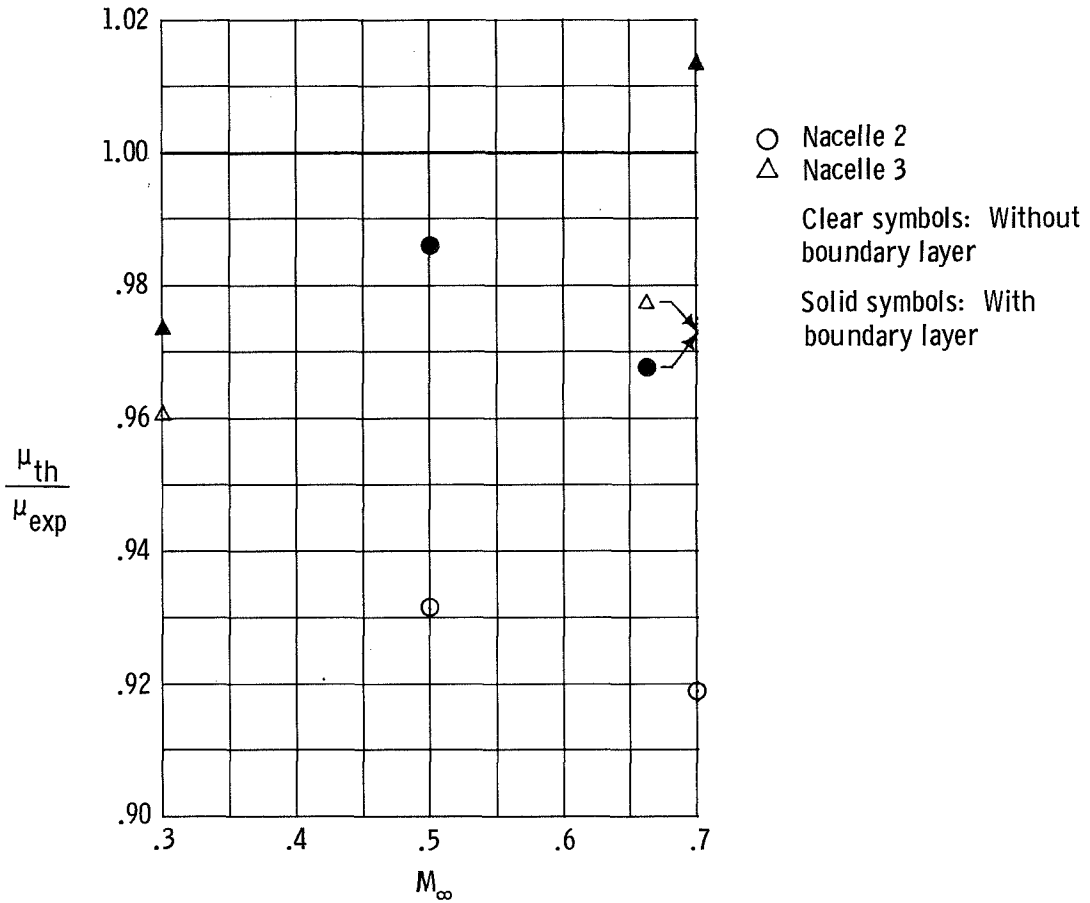
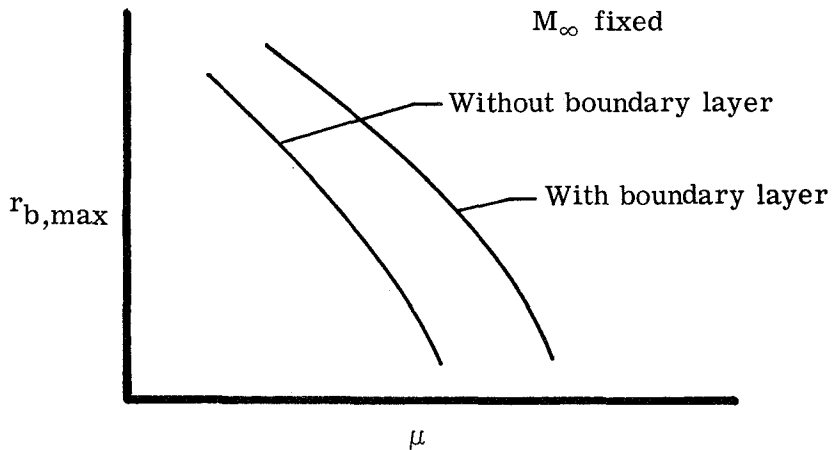


Figure 12.- Summary of calculated mass-flow ratios for cases where internal blockage was estimated, including effect of boundary layer.

the outer surface. Thus far ahead of the body the capture streamline for the internal mass flow is at a larger radius and more flow is swallowed by the wing. A summary of the effect of the boundary layer on the mass flow is shown in the following sketch:



Both methods of selecting the center-body size show good results and neither seems superior to the other. The center-body size used in figures 8 to 11 was estimated from information given in reference 5. The accuracy with which the mass flow was calculated is summarized in figure 12 which shows that inclusion of the boundary layer in the calculations improved this accuracy.

Figures 13 and 14 compare the present theory with the methods of references 5 and 10 for the flow condition of figure 4. Figure 13 is without the boundary layer and figure 14 is with it. All methods are seen to give very close to the same results; therefore, the use of surface singularities gives essentially the same result in this case as the present method, which uses singularities placed on a mean diameter cylinder.

When comparing different theoretical solutions of the flow over a nacelle, caution must be exercised to ensure that the mass flow from each solution is the same. Because the mass flow is a function of the circulation, different methods of approximating the Kutta condition can result in different mass flows on the same geometry.

The experiments of figures 4 to 11 were run without fan blades present (highest mass-flow runs). When fan blades were present, it was found that the straight center-body model used previously was not sufficient to calculate accurately the internal nacelle surface pressures. Hence the center body was modified to approximate the experimental sting up to the fan-blade location, which was estimated to be at about the 75-percent-chord location (the exact sting diameter and fan-blade location were not given in ref. 5). In this region the fan blade blockage was simulated by expanding the center body into an ellipsoid with a circular cross section (see fig. 3(a)). The ellipse in the  $x-r$  plane had a semi-minor axis of about 13 percent of the chord and a semimajor axis ( $r$ -direction), which was adjusted to give the experimental mass flow. Where the ellipsoid intersected the plane of the nozzle exit, a constant-diameter cylinder was extended to infinity. Figures 15 and 16 show the results of using this model for two low-mass-flow cases. The external pressure distributions are well predicted in spite of the discrepancies on the internal surface. Furthermore a fairly reasonable estimate of the internal pressure distribution is obtained. In figure 16 some large experimental errors may occur in  $\mu$  because of internal-flow separation as mentioned previously. This would explain the discrepancy at the leading-edge suction peak.

Calculations were also compared with experimental data obtained from reference 20. The investigation of reference 20 was made on several NACA 1-series inlet contours tested over a range of subsonic and transonic Mach numbers, mass-flow ratios, and angles of attack. The thickness ratio  $(t/c)_{\max}$  of the two nacelles of reference 20 selected for the present study was much smaller than the thickness ratio of nacelles 2 and 3 (2 percent compared with 11 percent). As shown in figure 3(a), the nacelles were sting supported with a throttle plug at the rear of the model for controlling the mass flow (the strut arrangement

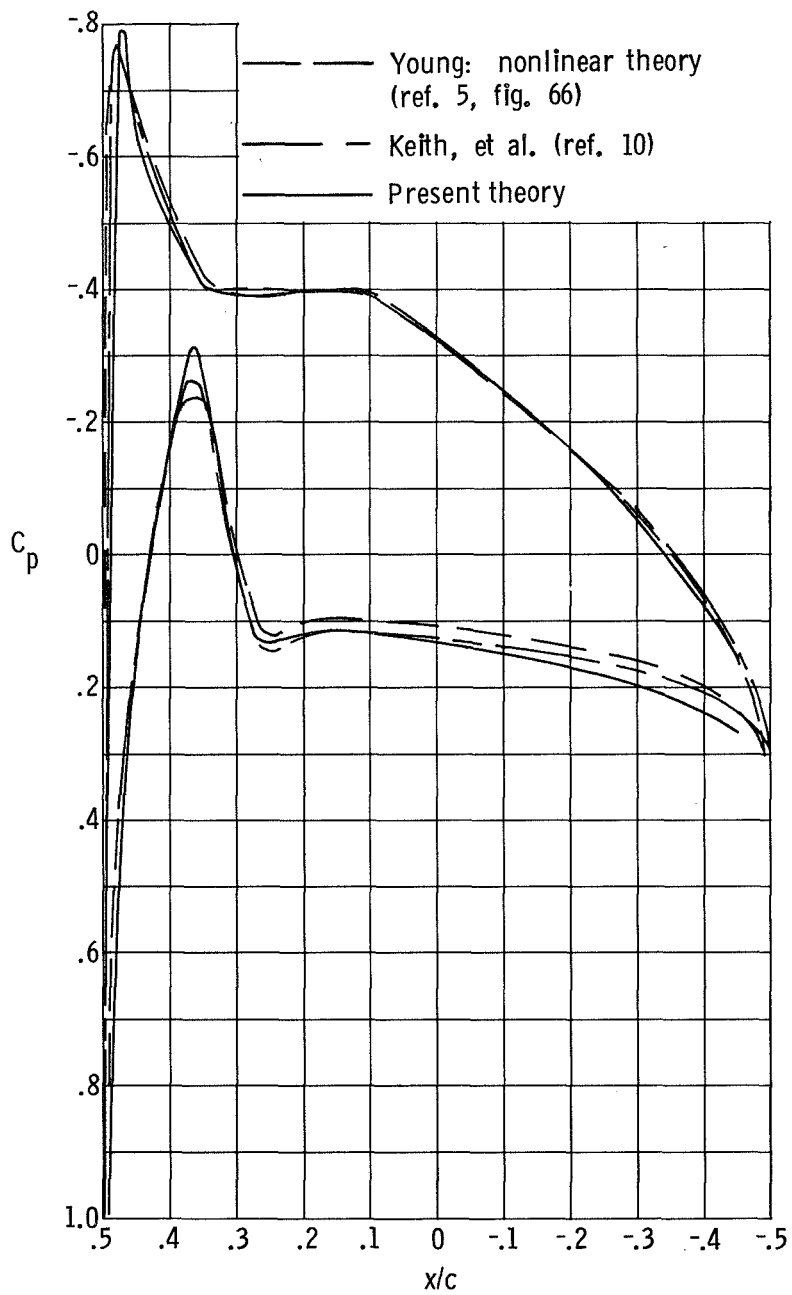


Figure 13.- Pressure distribution on nacelle 3;  $M_\infty = 0.3$ ;  
 $\mu_{th} = 0.76$ . All theories without boundary layer.

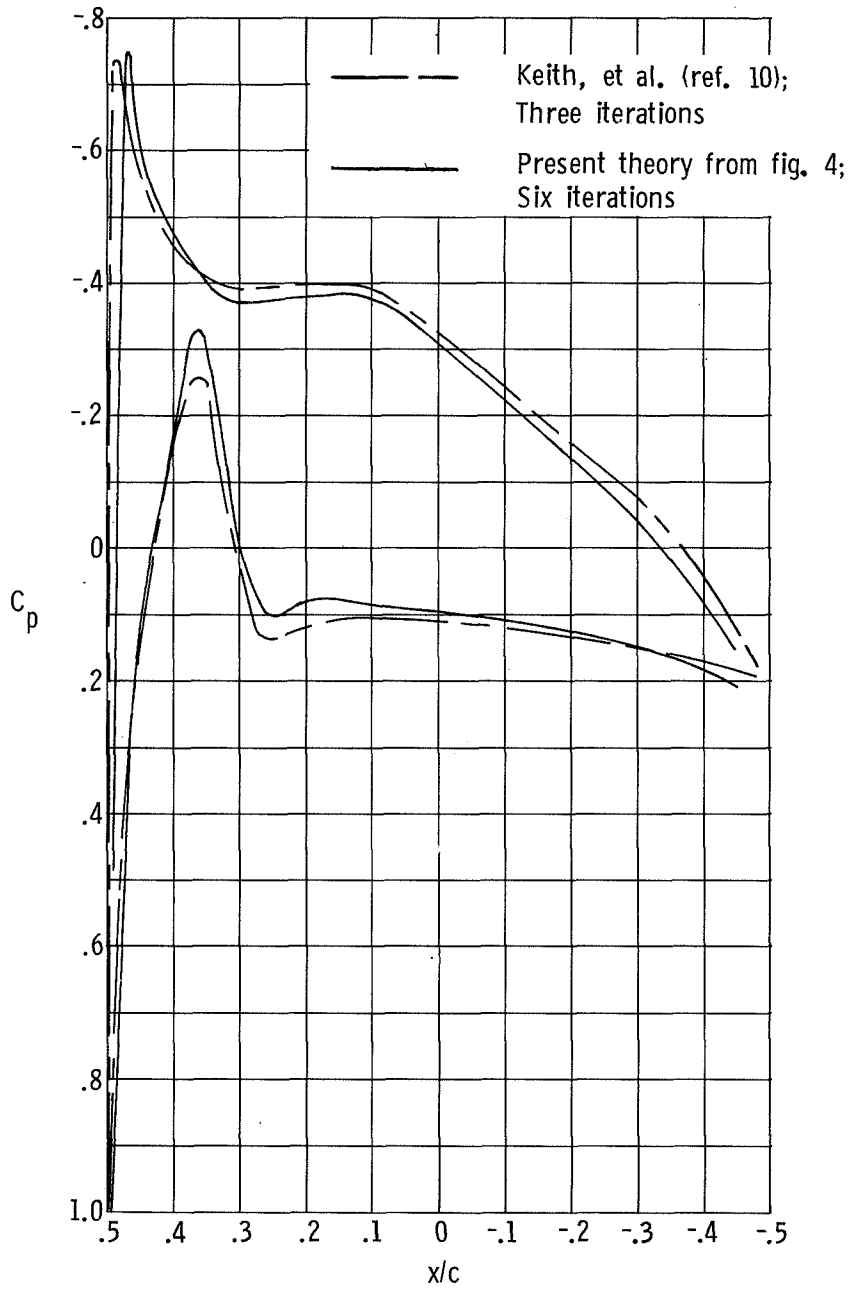


Figure 14.- Pressure distribution on nacelle 3;  $M_\infty = 0.3$ ;  $\mu_{th} = 0.76$ . Both theories with boundary layer.

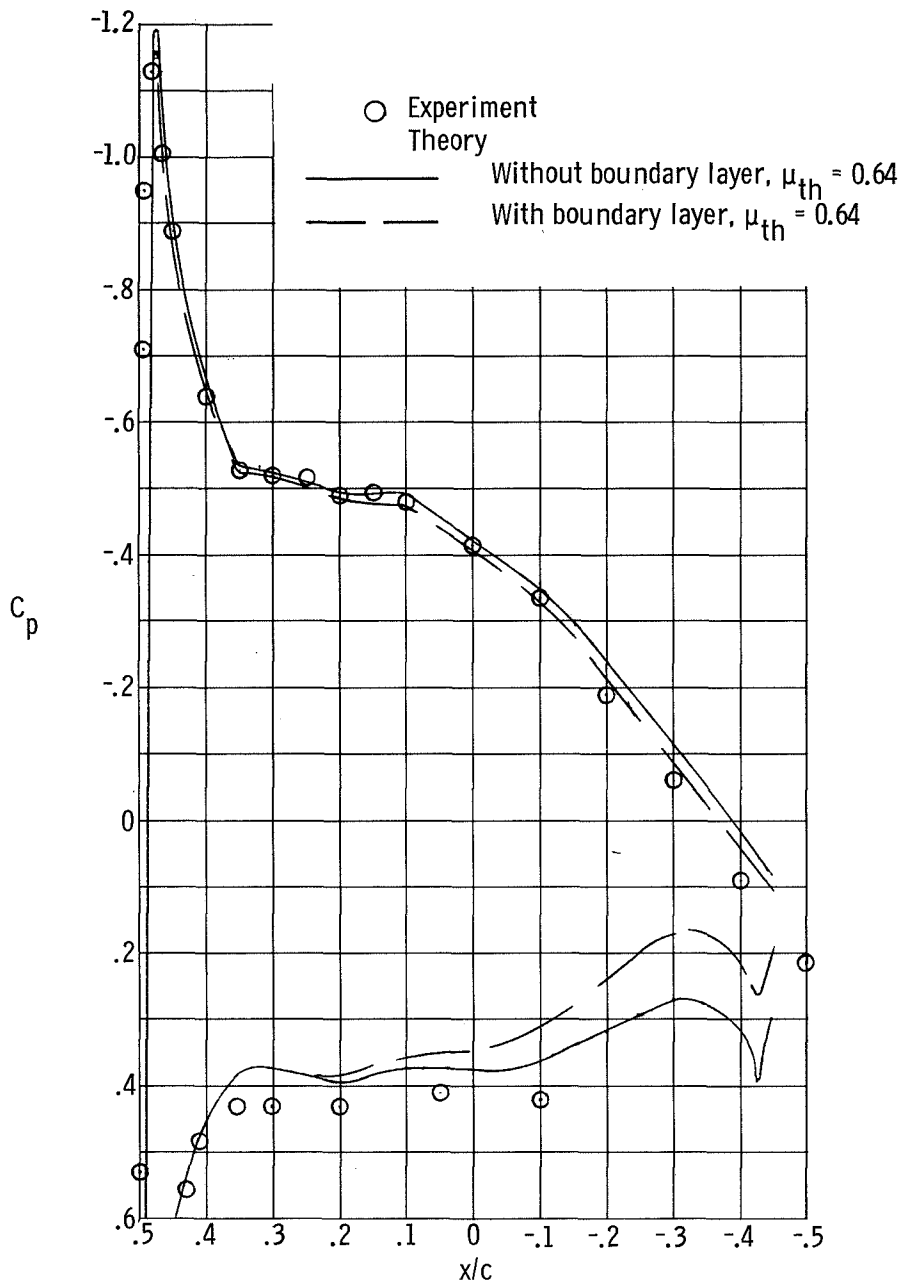


Figure 15.- Pressure distribution on nacelle 2;  $M_\infty = 0.5$ ;  $\mu_{th} = \mu_{exp} = 0.64$ .  
 Boundary layer: Five iterations; least square 90- to 97-percent c.

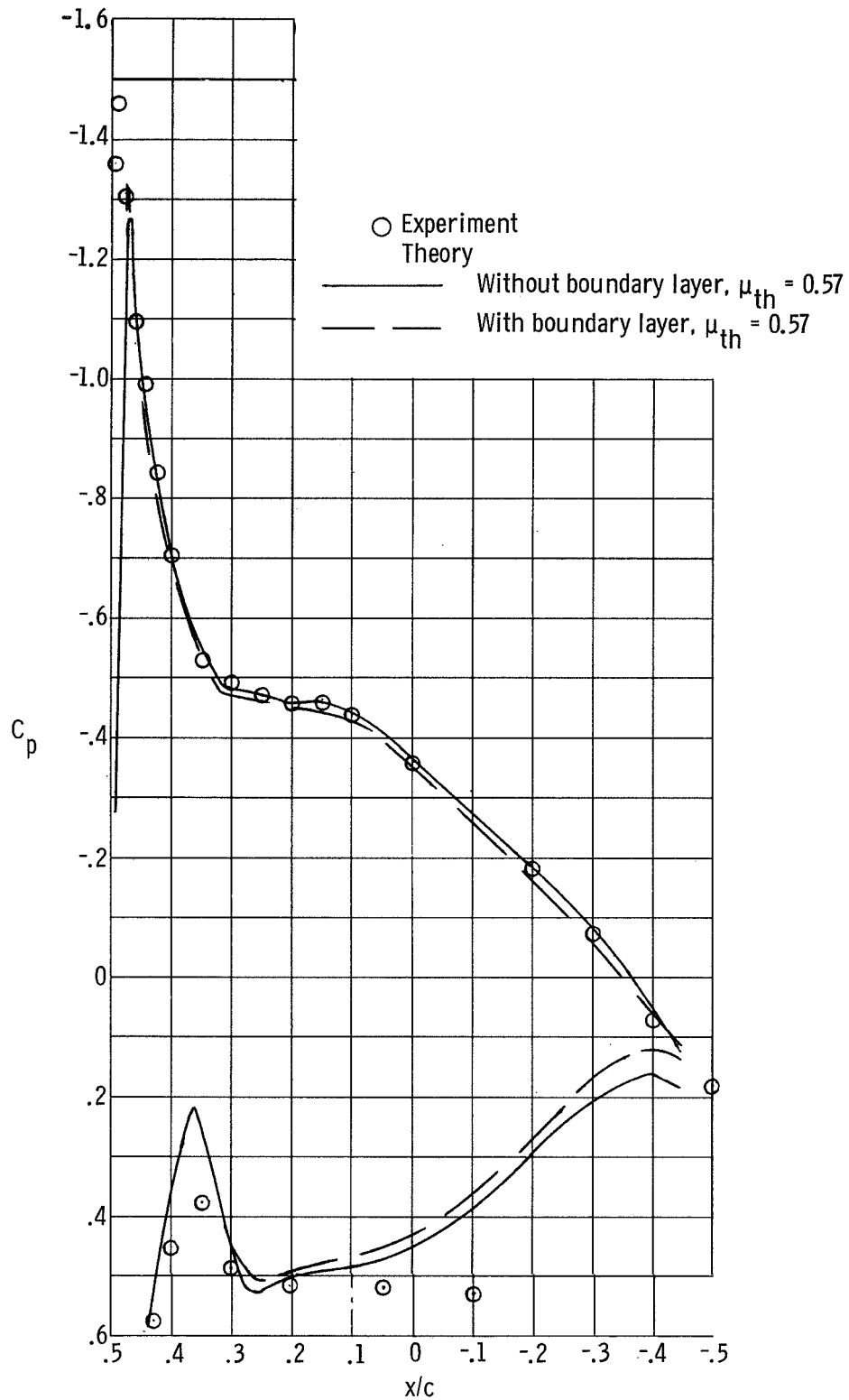


Figure 16.- Pressure distribution on nacelle 3;  $M_\infty = 0.30$ ;  $\mu_{th} = \mu_{exp} = 0.57$ .  
 Boundary layer: Five iterations; least square 90- to 97-percent c.

differed from that of fig. 3(a) in that fore and aft sets of struts were used). The plug was moved forward and backward to vary the mass flow. As previously, the blockage of the sting, struts, and plug was represented in the theory by the blockage of a center body. High-mass-flow ratios were selected for study to minimize the effect of the plug on the afterbody pressures.

The models of reference 20 consisted of the same afterbody attached to various inlets. The inlets had NACA 1-series outer profiles and various inner profiles depending upon the contraction ratio. The two inlets selected for the present study were the NACA 1-81-100 with a contraction ratio of 1.012 and the NACA 1-85-100 with a contraction ratio of 1.009. The numbers in the NACA designation indicate first the series, then  $d/D_{\max}$  in percent, and finally  $X/D_{\max}$  in percent. The quantity  $d$  is the highlight diameter less twice the inlet lip radius;  $X$  is the inlet length; and  $D_{\max}$  is the inlet (and nacelle, in this case) maximum diameter.

The nose of the center body in the theoretical model was again placed at the position of the sting leading edge and had the same shape as used previously. (See fig. 3(a).)

The tests of reference 20 were conducted without artificial boundary-layer transition. A limited amount of data obtained with a transition band located 2.54 cm aft of the lip (the maximum nacelle diameter was 45.72 cm) showed no difference in pressure when compared with free transition data. Thus, it again seemed reasonable to assume a turbulent boundary layer over the entire chord length for the viscous calculations. The Reynolds number was a function of Mach number. For  $M_{\infty}$  of 0.40 and 0.80 the Reynolds number was  $7.437 \times 10^4/\text{cm}$  and  $1.159 \times 10^5/\text{cm}$ , respectively.

The comparison between theory and experiment is shown in figures 17 and 18 for  $M_{\infty}$  of 0.80 and 0.40. The theoretical center-body size was selected to give the mass-flow ratio measured in the experiment. The data on the inner surface and the data labeled "other" were obtained from the author of reference 20. The data points labeled "other" are an average of measurements made at that  $x/c$  location on the sting, mass-flow rake, and inner surface (these measurements were not separately available). Good agreement was obtained on the outer surface for both cases when the boundary layer was included. The very large adverse pressure gradient on the inner surface of the inlet in figure 17 occurs at the higher Mach numbers. The boundary-layer calculation indicated flow separation in this region. Thus, the boundary layer on the outer surface did not converge to any better than a maximum change in  $\delta^*$  of 12 percent of the maximum  $\delta^*$ . This lack of convergence was due to erroneous changes in the thickness and camber caused primarily by incorrect values of  $\delta^*$  on the inner surface. Hence, flow separation and a possible influence of the mass-flow plug on the measured pressures at the trailing edge could explain the discrepancies between the theory and experiment in figure 17.

In figure 18 the boundary layer converged on both surfaces to a maximum change in  $\delta^*$  of less than 0.2 percent of the maximum  $\delta^*$  for the respective surfaces. The

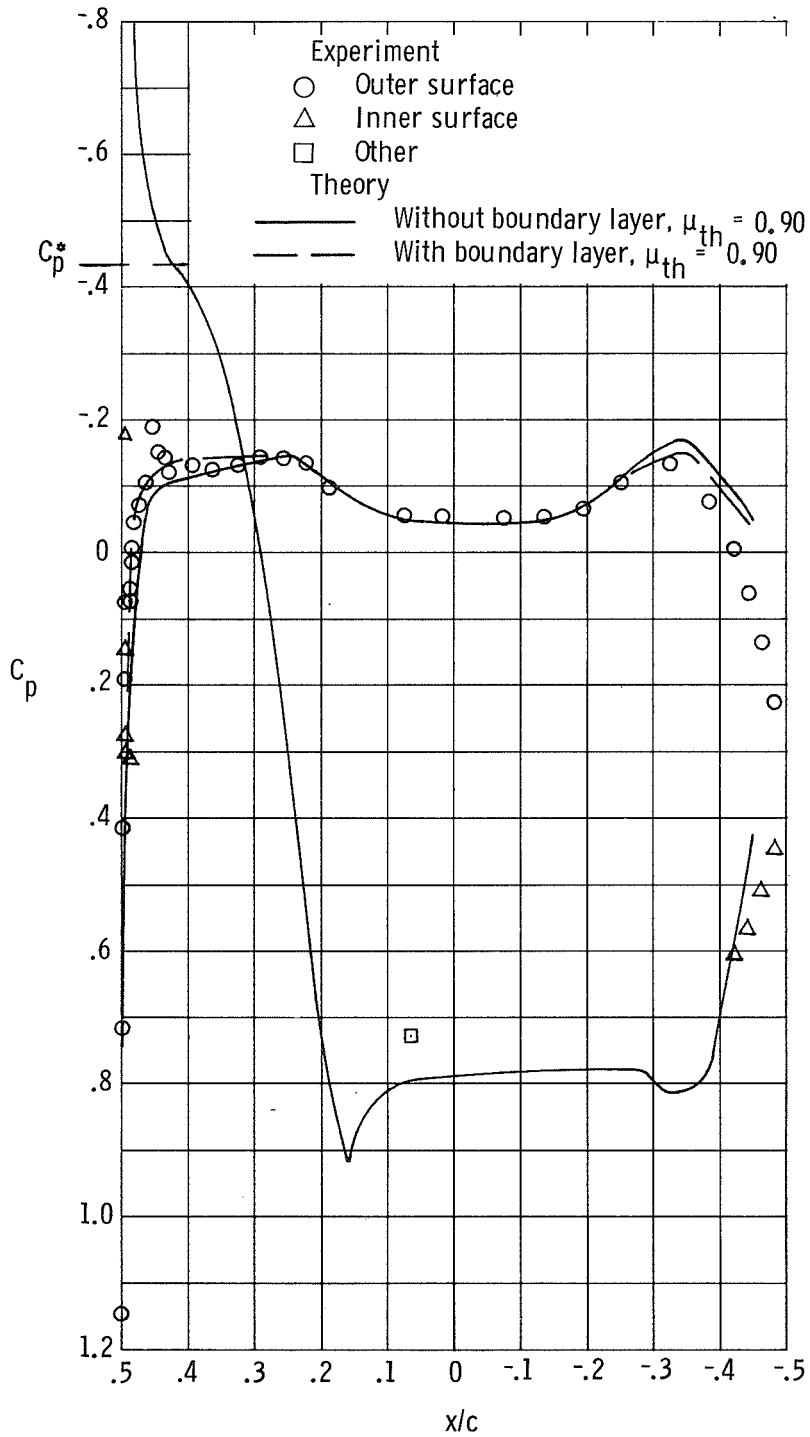


Figure 17.- Pressure distribution on NACA nacelle 1-81-100; contraction ratio, 1.012;  $M_\infty = 0.80$ ;  $\mu_{th} = \mu_{exp} = 0.901$ . Boundary layer: Three iterations; least square 90- to 97-percent  $c$ .

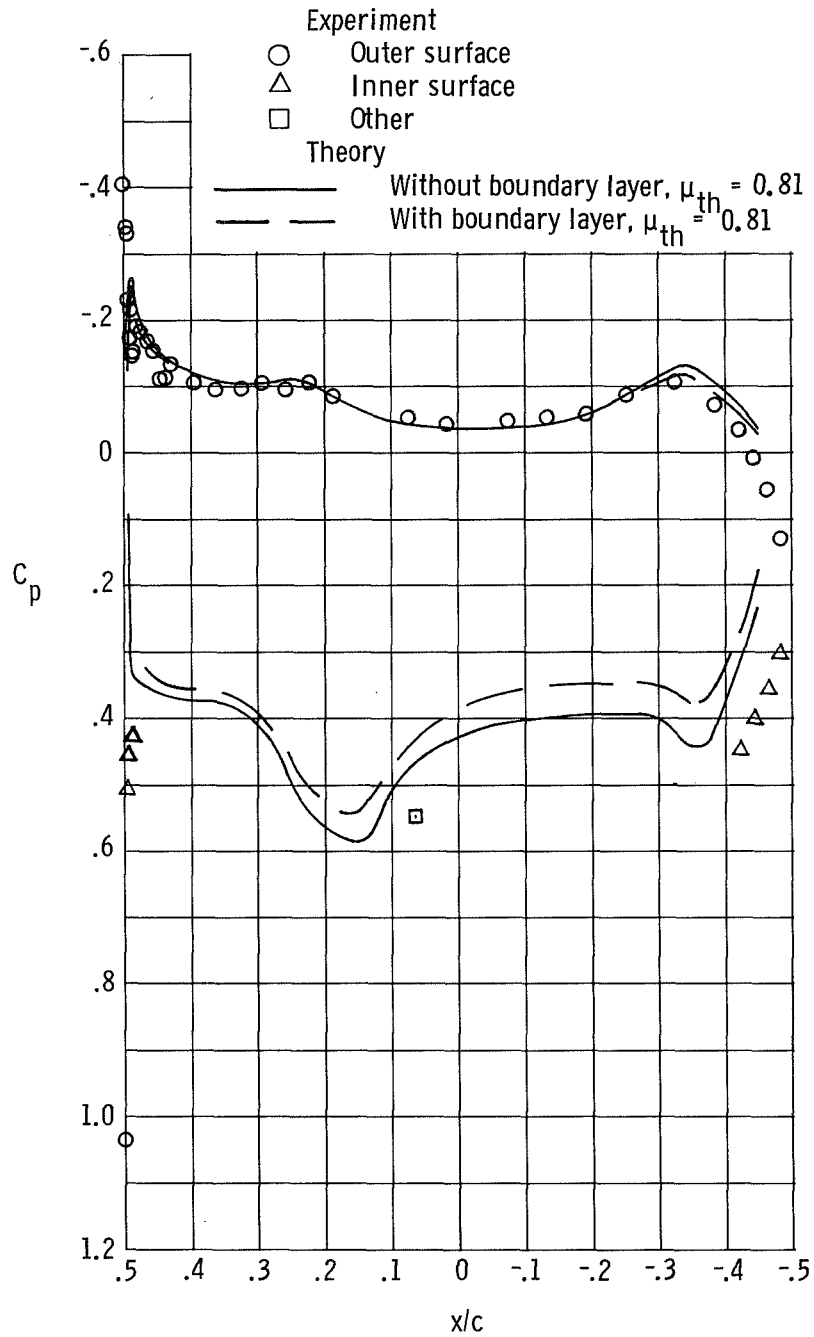


Figure 18.- Pressure distribution on NACA nacelle 1-85-100; contraction ratio, 1.009;  $M_\infty = 0.40$ ;  $\mu_{th} = \mu_{exp} = 0.815$ . Boundary layer: Six iterations; least square 90- to 97-percent  $c$ .

discrepancy at the leading-edge suction point could be due to inaccuracies in the leading-edge shape. The pressure in this region is very sensitive to slight errors in the manufacture. The inner surface pressures are approximately predicted by the theory. The calculated velocities in this region are somewhat higher than the actual velocities because the center-body radius used in the theory was larger than the sting radius.

Finally, figure 19 shows the accuracy of calculating the critical Mach number on nacelle 2 by using von Kármán's method (ref. 18). The free-stream Mach number must be low enough to assume incompressible flow. The critical conditions are based on the external pressure distribution. The curve labeled "Minimum  $C_p$ " is from the leading-edge suction peak. The intersection of this curve and the curve for  $C_p^*$  gives a critical Mach number for nacelle 2 of 0.632. The method of von Kármán yields a critical Mach number of 0.658.

In the case of a propulsive device the addition of energy to the internal flow will have an effect on the pressure distribution over the nacelle. Energy addition is treated in references 10 and 22. Shollenberger (ref. 22) has made a theoretical and experimental study of a two-dimensional propulsive lifting system. The external pressure distribution was found to have a relatively weak dependence on the intensity of energy addition to the internal flow; however, the inner surface pressure distribution was strongly affected. The theoretical formulation of the present study could be extended to include energy addition by use of a method similar to that of reference 22.

## CONCLUSIONS

A method analogous to classical airfoil theory has been developed for computing the pressure distribution on an annular wing with a center body at zero angle of attack and subsonic speeds. The following conclusions are drawn:

1. For the geometries investigated, this method was found to give essentially the same results as a method using a surface distribution of singularities and a stream-tube method.
2. Comparison of the results with experimental data for a range of flow conditions and thickness ratios showed that when the boundary-layer displacement effects are included in the calculations, the pressure distribution and mass flow can be calculated with good accuracy. An accurate prediction is dependent on the existence of attached flow and a fairly accurate modeling of the internal-blockage geometry.

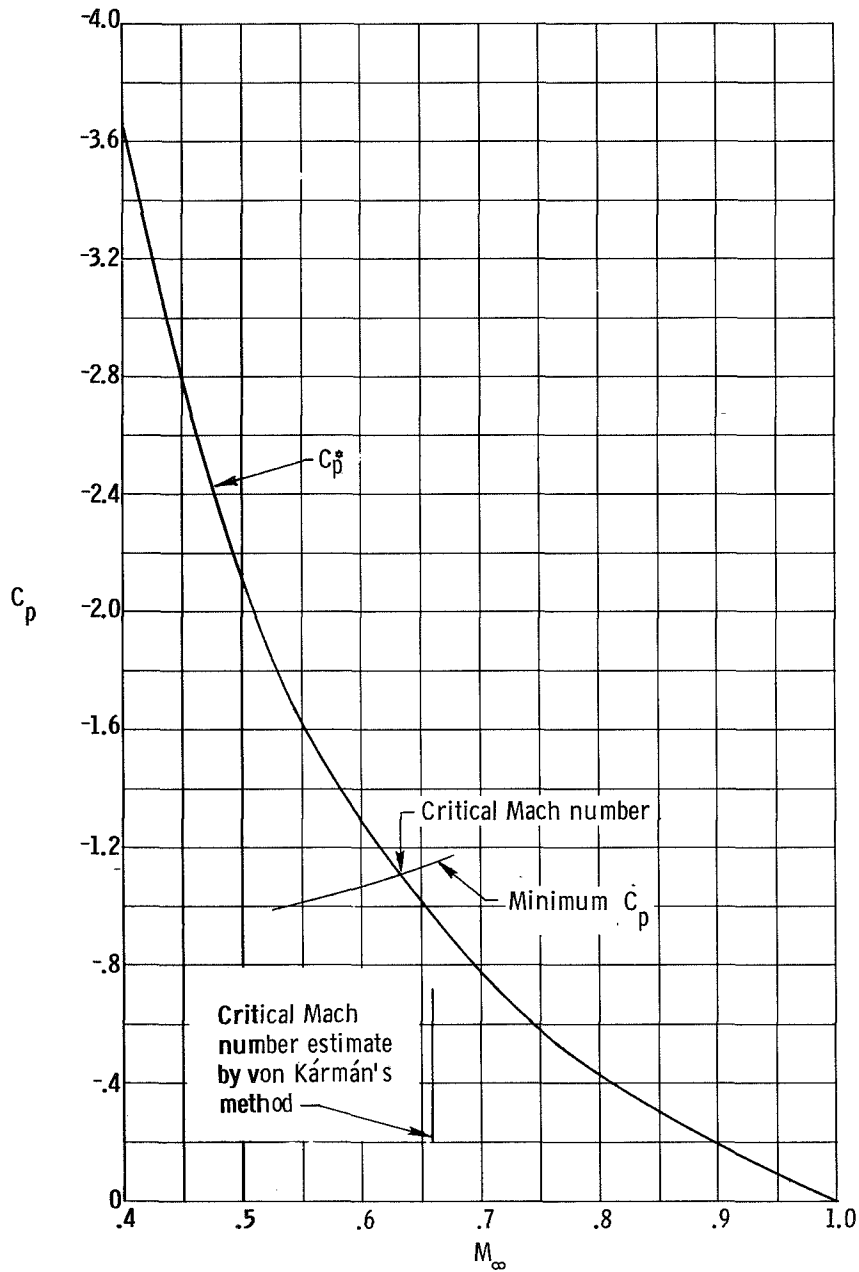


Figure 19.- Critical Mach number for nacelle 2 with  $(r_b/c)_{\max} = 3.354$  percent.

3. For cases in which the internal blockage was not accurately modeled or flow separation may have been present, the inner pressures were not accurately calculated. However, the outer pressures were still calculated to a fairly good degree of accuracy. If internal flow separation occurs, the experimentally measured mass flow will be in error, and this error must be accounted for when comparing experimental and theoretical results.

4. When calculating the boundary-layer thickness, the inviscid velocities were extrapolated to the trailing edge. A more accurate calculation would include the effect of the wake.

5. The method requires modest computer running times and storage and can be generalized to include such effects as lift and internal energy addition.

Langley Research Center,  
National Aeronautics and Space Administration,  
Hampton, Va., May 9, 1974.

## APPENDIX A

### COMPUTER PROGRAM

#### Input Variables

The input data format is the Namelist method used by the Control Data series 6600 computer system at the Langley Research Center. The input variables are listed in this appendix and the input format can easily be modified to any other format. The body radius and wing inner and outer coordinates are each listed in sequential order to correspond with the x-values listed. The x-values are input from the leading edge to the trailing edge. The first quantities in the arrays X, RB, RI, and RO are X(1), RB(1), RI(1), and RO(1), respectively. The positive direction for a radius is shown in figure 1; however x is measured from the leading edge, positive downstream. Any length units can be used so long as the same units are used for all variables. Meters are indicated, however, for dimensional quantities.

The program uses 1.4 for  $\gamma$ , the ratio of specific heats; however, a gas which has a value of  $\gamma$  different from 1.4 can be treated by changing  $\gamma$  in the pressure-coefficient equations and the mass-flow equation. Incompressible cases can be run by simply inputting zero for the free-stream Mach number. Special cases, such as camber with zero thickness or thickness with zero camber, can be treated by simply inputting the correct outer and inner surface coordinates. Some limitations are discussed. (See CAM.) For no center body, input all values of RB equal to 0 or set SCALE equal to 0 (both RB and SCALE must be input).

AIAM  $A_h/A_{\min} = (D_h/D_{\min})^2$

C wing chord, m

CAM use 1. when there is camber; use 0. when desire all  $\Gamma_0 = 0$ , which is an inviscid thickness-only case with no center body. Note that zero geometric camber (all  $\alpha_0 = 0$ ) is just a special case of equation (6). However, because of the method of defining the vortex strengths,  $v_\gamma/V_\infty$  would become indeterminate if  $\alpha_0 = 0$ . Thus the form of the equation for  $v_\gamma/V_\infty$  will not permit use of equation (6) (as given by eqs. (8) or (12)) to account for the center-body interference for zero camber. Therefore a geometry which has a center body but no geometric camber (all  $\alpha_0 = 0$ ) cannot be treated by this computer program. Likewise, if portions of a cambered wing have a mean camber line with zero slope, a very small slope must be used in these regions. These limitations could be removed by replacing  $\alpha_0\gamma_0$  by  $\gamma_+/V_\infty$  in the vortex equations (see definition of  $\gamma_0$ ).

APPENDIX A – Continued

DMAX	maximum wing outside diameter, m
DMIN	minimum wing inside diameter, m
FINI	use 1. for the last data set and 0. for preceding data sets when more than one set in input; one data set is shown in sample input
ITMAX	number of times boundary layer is computed; potential flow is computed ITMAX + 1 times; use 0. for inviscid solution
M	free-stream Mach number
N	number of wing panels in chordwise direction (same N used in text, see pages 10 and 17); maximum value is 170
NN	number of x-stations where quantities in arrays X, RI, RO, and RB are input; maximum value is 170
NRHO	number of annuli internal flow area is divided into to compute mass flow; maximum value is 170
RB	array of center-body radii; for $X \leq X_{BN}$ , use .0 for values of RB, m
RI	array of inner wing radii, m
RO	array of outer wing radii, m
SCALE	scale factor to expand or shrink elements of RB so as to vary mass flow; SCALE is ratio of desired body radius to input body radius
UNRREF	Reynolds number per meter
X	array of x-stations where arrays RI, RO, and RB are input, m
XBN	x-station of center-body nose, m

APPENDIX A - Continued

XAFT, } Between the x/c values of XFOR and XAFT, a linear least-square-curve  
 XFOR } fit is applied to outer surface velocities. Then the outer surface velocities  
 are recomputed from XFOR to the trailing edge with this curve fit. Similarly, a parabolic least-square-curve fit is applied to the inner surface velocities between XFOR and XAFT and the Nth value of recomputed outer surface velocity. Then the inner surface velocities are recomputed from XFOR to the trailing edge with this curve fit.

Sample Input

The input for the viscous calculation of figure 4 is shown below. If more than one case is to be run, the complete data set must be repeated by using the proper values for FINI. The last card is identification information and uses format (6A10).

```
$GEOM N=150, NN=55, M=.30, C=4.4101, DMIN=3.9395, DMAX=5., NRHO=170,
XFOR=.90, XAFT=.97,
SCALE=3.125,
ITMAX=6,
AIAM=1.2580,
FINI=1., CAM=1.,
XBN=.8,
UNRREF=453500.,
X= 0.0000, .0250, .0450, .0700, .0882, .1200, .1500, .1764, .2646,
    .3528, .4410, .5292, .6174, .7056, .7938, .8000, .8057, .8114,
    .8171, .8228, .8820, .9702, 1.0584, 1.1466, 1.2348, 1.3230, 1.4112,
    1.4994, 1.5876, 1.6758, 1.7640, 1.8522, 1.9404, 2.0286, 2.1168, 2.2051,
    2.2933, 2.4256, 2.5138, 2.6020, 2.7343, 2.8666, 2.9548, 3.0871, 3.2194,
    3.3517, 3.5281, 3.6604, 3.7927, 3.9691, 4.1014, 4.1896, 4.2778, 4.3660,
    4.4101,
RI= 2.2093, 2.1758, 2.1467, 2.1170, 2.1019, 2.0822, 2.0694, 2.0603, 2.0307,
    2.0073, 1.9888, 1.9760, 1.9698, 1.9711, 1.9773, 1.9782, 1.9787, 1.9792,
    1.9797, 1.9802, 1.9852, 1.9927, 1.9985, 2.0016, 2.0038, 2.0056, 2.0073,
    2.0095, 2.0117, 2.0140, 2.0162, 2.0184, 2.0206, 2.0228, 2.0246, 2.0268,
    2.0290, 2.0321, 2.0338, 2.0360, 2.0396, 2.0427, 2.0449, 2.0480, 2.0511,
    2.0542, 2.0586, 2.0617, 2.0648, 2.0683, 2.0710, 2.0723, 2.0736, 2.0749,
    2.0749,
RO= 2.2093, 2.2428, 2.2717, 2.3010, 2.3153, 2.3344, 2.3459, 2.3537, 2.3811,
    2.4019, 2.4174, 2.4302, 2.4412, 2.4509, 2.4602, 2.4611, 2.4616, 2.4621,
    2.4626, 2.4631, 2.4682, 2.4757, 2.4823, 2.4876, 2.4920, 2.4956, 2.4982,
    2.4995, 2.5000, 2.4991, 2.4969, 2.4934, 2.4889, 2.4832, 2.4761, 2.4686,
    2.4602, 2.4456, 2.4355, 2.4240, 2.4054, 2.3855, 2.3714, 2.3493, 2.3263,
    2.3020, 2.2671, 2.2389, 2.2106, 2.1730, 2.1443, 2.1257, 2.1067, 2.0877,
    2.0785,
RB= 0.0000, 0.0000, 0.0000, 0.0000, 0.0000, 0.0000, 0.0000, 0.0000, 0.0000,
    0.0000, 0.0000, 0.0000, 0.0000, 0.0000, 0.0000, 0.0000, 0.0193, .0263,
    .0315, .0358, .0620, .0840, .0980, .1080, .1160, .1230, .1290,
    .1345, .1390, .1415, .1450, .1460, .1480, .1495, .1498, .1500,
    .1500, .1500, .1500, .1500, .1500, .1500, .1500, .1500, .1500,
    .1500, .1500, .1500, .1500, .1500, .1500, .1500, .1500, .1500,
    .1500,
$
YOUNGS COWL 3
```

## APPENDIX A – Continued

### Output Variables

Most of the input quantities are printed and identified with the symbols of the preceding section. Other quantities have the meanings listed in this section. In the output for the wing surface solution, all perturbation velocities, including center-body velocities are for the equivalent incompressible flow and are on the wing surface ( $\rho_0 = 1$ ). In the mass-flow computation output the perturbation velocities and the RAD are also for the equivalent incompressible flow. The pressure coefficients, total velocities, terms of equation (42), MFC and MU are for the compressible flow. Other output sections are either labeled as to compressibility or the nature is obvious (for example, GQ, etc. are obviously for the incompressible flow). The coordinate system of figure 1 is used except in the case of the center-body slopes as noted in the following list. Output which follows the boundary layer output is for the wing shape modified with the final  $\delta^*$  distribution.

ALPHO  $\alpha_0$  at  $\xi_1$ , rad

ALPHOO  $\alpha_0$  at  $\xi_{0j}$  in first listing, rad;  $-2\pi\left(\alpha_{0j} + \frac{v_{bj}}{V_\infty}\right)$  in second listing

ALPHQBB left-hand side of equation (33) at  $\xi_{0j}$

ALPT  $\alpha_t$  at  $\xi_1$ , rad

ALPTH  $\alpha_t$  at  $\xi_{0j}$ , rad

CPO  $C_p$  on wing outer surface

CPI  $C_p$  on wing inner surface

CPBA  $C_p$  on center body (only approximate because the source strength does not correspond to the input center-body shape owing to neglect of wing interference on the center body)

CPBI isolated center body  $C_p$ ; this  $C_p$  would be theoretically correct if the wing were absent

DDEL  $\delta_m^* - \delta_{m-1}^*$ , m

DELI  $\delta^*$  from equation (44) on wing inner surface, m

DELO  $\delta^*$  from equation (44) on wing outer surface, m

APPENDIX A - Continued

DELST	$\delta_m^*$ , m
DRDX	$dr/dx$ of center body at $\xi_i$ , with $x$ positive downstream
DRDXH	$dr/dx$ of center body at $\xi_{oj}$ , with $x$ positive downstream
GAM	$\Gamma_{oi}$
GQ	$\gamma_t/V_\infty$ at $\xi_i$
GQB	$\bar{g}_q$ at $\xi_i$
H	shape factor, $\delta^*/\theta$
I	$i$
IT	number of times boundary layer has been computed; IT - 1 equals iteration number
J	$j$
LAM	$\lambda$ on equivalent incompressible wing
MCR	critical Mach number
MFC	$m/\rho_\infty A_{\min} V_\infty$ where $A_{\min} = \pi D_{\min}^2/4$
MU	$\mu$
RAD	radii of annuli in mass-flow computation, m
RIN	RI - DELI (input values of RI used), m
ROUT	RO + DELO (input values of RO used), m
RHOO	$\rho_{oj}$
RHOO-BODY	$\rho_b$ at $\xi_{oj}$

APPENDIX A – Continued

TEMP10	quantity under summation sign of equation (42) at a given value of $\rho_{0j}$
THE	$\theta$ , m
UOURO	$V/V_\infty$ on wing outer surface at X-stations, used to compute boundary layer
UOURI	$V/V_\infty$ on wing inner surface at X-stations, used to compute boundary layer; for $x/c < 0.02$ , UOURI is set equal to UOURO(1) to obtain more reasonable values
VTO	$(V/V_\infty)^2$ on outer surface of wing
VTI	$(V/V_\infty)^2$ on inner surface of wing first time printed; $[(V_\infty + u)/V_\infty]^2$ at $\rho_{0j}$ second time printed (square of velocity term under summation sign in eq. (42))
VIVIN	summation of equation (42) evaluated from $j = 1$ to the value of $J$ listed for any given value of VIVIN. The summation progresses from wing inner surface toward center line, or center body if one is present, at fixed axial location. This sum is evaluated at $\xi_0 = 0$ (midchord) presently but this station can be changed by changing card numbers T170, T320, T650, and T870 in program MASFLOW. The last value of VIVIN equals VI/VIN.
VI/VIN	$V_{\xi_0}/V_\infty$ of equation (42)
WX1JUOO	$u_\gamma/V_\infty$ at $\xi_{0j}$ on wing outer surface ( $\rho_{0j} = 1$ )
WX1JUOI	$u_\gamma/V_\infty$ at $\xi_{0j}$ on wing inner surface ( $\rho_{0j} = 1$ )
WX1JUO	summation in equation (13); for points where $\rho_{0j} \neq 1$ (required for computing mass flow), this quantity is $u_\gamma/V_\infty$ at $\xi_{0j}, \rho_{0j}$
WR1JUO	$v_\gamma/V_\infty$ at $\xi_{0j}, \rho_{0j}$
WX1QJUO	$u_{t,\gamma}/V_\infty$ at $\xi_{0j}$ on wing outer surface ( $\rho_{0j} = 1$ )
WX1QJUI	$u_{t,\gamma}/V_\infty$ at $\xi_{0j}$ on wing inner surface ( $\rho_{0j} = 1$ )
WX1QJU	same as WX1JUO only with respect to $u_{t,\gamma}/V_\infty$

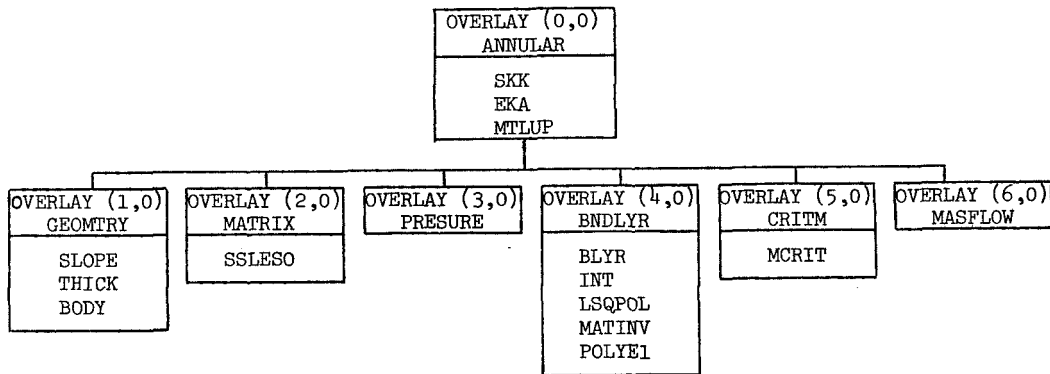
APPENDIX A - Continued

- WR1QJU  $v_{t,\gamma}/V_\infty$  at  $\xi_{0j}, \rho_{0j}$
- WXQJU  $u_q/V_\infty$  at  $\xi_{0j}, \rho_{0j}$
- WRQJUO  $v_q/V_\infty$  at  $\xi_{0j}$  on wing outer surface ( $\rho_{0j} = 1$ )
- WRQJUI  $v_q/V_\infty$  at  $\xi_{0j}$  on wing inner surface ( $\rho_{0j} = 1$ )
- WRQJU summation in equation (35); for points where  $\rho_{0j} \neq 1$  (required for mass flow), this quantity is  $v_q/V_\infty$  at  $\xi_{0j}, \rho_{0j}$
- WXBQJU  $u_b/V_\infty$  at  $\xi_{0j}, \rho_{0j}$
- WRBQJU  $v_b/V_\infty$  at  $\xi_{0j}, \rho_{0j}$
- XI  $\xi_i$
- XIO  $\xi_{0j}$
- XOJ/C  $x_{0j}/c$  (x of fig. 1)

Program Structure and Listing

This program is written in FORTRAN IV, Version 2.3 for the Control Data series 6600 computer system with the run compiler and execution routines operating under SCOPE 3.0. The program requires 65,000<sub>8</sub> words of storage.

The program operates in the OVERLAY mode. The main overlay program is called ANNULAR and has six primary overlay programs - GEOMETRY, MATRIX, PRESURE, BNDLYR, CRITM, and MASFLOW. The overlay structure and subprogram arrangement are shown in the following sketch:



## APPENDIX A – Continued

The function `LOCF(A)` used by subroutine `MTLUP` is a library function which returns the address of argument `A`. No listing is provided for `LOCF`.

Numerous comment cards have been inserted in the main overlay to assist the user in understanding the flow of the computations. The purpose of each overlay and subprogram is described by comment cards at the beginning of the overlay or subprogram.

APPENDIX A - Continued

	OVERLAY(RING,0,0)	A 10
	PROGRAM ANNULAR(INPUT,OUTPUT,TAPE5=INPUT,TAPE6=OUTPUT,TAPE10)	A 20
C		A 30
C		A 40
C	PROGRAM ANNULAR EMPLOYS ANNULAR WING THEORY TO COMPUTE THE	A 50
C	SUBSONIC FLOW OVER NACELLES INCLUDING THE COMPRESSIBILITY EFFECTS	A 60
C	AND VISCOUS EFFECTS	A 70
C		A 80
C		A 90
C	ANY ERRORS OR PROBLEMS ENCOUNTERED IN USING THE PROGRAM SHOULD BE	A 100
C	DIRECTED TO DR. MICHAEL J. MANN AT NASA LANGLEY. AREA CODE 804-827	A 110
C	-3711.	A 120
C		A 130
C		A 140
C	A CARD DECK AND DOCUMENTATION FOR THE PROGRAM ARE AVAILABLE FROM	A 150
C	COSMIC, UNIVERSITY OF GEORGIA, ATHENS, GEORGIA, 30601.	A 160
C		A 170
C		A 180
C	THIS PROGRAM IS WRITTEN IN CDC FORTRAN IV, VERSION 2.3, TO RUN ON	A 190
C	CDC 6600 SERIES COMPUTERS WITH THE SCOPE 3.0 OPERATING SYSTEM AND	A 200
C	LIBRARY TAPE.	A 210
C		A 220
C		A 230
	COMMON /CORD/ X(170),R(170),C,RAVG,NN,N,DMIN,T(170),RB(170),XBN	A 240
	COMMON /ONE/ ROUT(170),RIN(170),M,DMAX,XI(170),XIO(170),ALPHO(170)	A 250
	1,ALPHOO(170,1),XBL(170),ALPT(170),ALPTH(170),DRDX(170),DRDXH(170),	A 260
	2LAM,IT,ITMAX	A 270
	COMMON /TWO/ IP,CAM,GAM(170),GQ(170),ALPOO(170,1)	A 280
	COMMON /THREE/ VOUT(170),VIN(170)	A 290
	COMMON /FOUR/ XOVC(170),RO(170),RI(170),DELO(170),DELI(170),WLS(40	A 300
	1),DOLDO(170),DOLDI(170),UNRREF,SAM,XFOR,XAFT	A 310
	COMMON /FIVE/ CPO(170),MCR	A 320
	COMMON /SIX/ NRHO,RAD(170),VIVIN,RXX,RBXI	A 330
	DIMENSION IDENT(6)	A 340
	REAL LAM,KSQ,M,MFC,MCR,JOHN,MU	A 350
C		A 360
C	INPUT	A 370
C		A 380
	NAMelist /GEOM/ N,NN,M,C,DMIN,DMAX,X,RO,RI,FINI,CAM,NRHO,RB,XBN,SC	A 390
	IALE,UNRREF,ITMAX,AIAM,XFOR,XAFT	A 400
10	READ (5,GEOM)	A 410
	READ (5,100) IDENT	A 420
	WRITE (6,80)	A 430
	WRITE (6,100) IDENT	A 440
	WRITE (6,90) C,DMIN,DMAX,NRHO,UNRREF,ITMAX,N,M,AIAM,XFOR,XAFT,(X(I	A 450
	1),RO(I),RI(I),RB(I),I=1,NN)	A 460
	DO 20 I=1,40	A 470
	WLS(I)=1.	A 480
20	CONTINUE	A 490
	DO 30 I=1,NN	A 500
	XOVC(I)=X(I)/C	A 510
	ROUT(I)=RO(I)	A 520
	RIN(I)=RI(I)	A 530
	DELO(I)=0.	A 540
	DELI(I)=0.	A 550
	DOLDI(I)=0.	A 560
	DOLDO(I)=0.	A 570
30	CONTINUE	A 580
C		A 590
C	SCALE CENTER BODY	A 600

APPENDIX A - Continued

C		A 610
	DO 40 I=1,NN	A 620
	RB(I)=RB(I)*SCALE	A 630
40	CONTINUE	A 640
	WRITE (6,120) SCALE,(X(I),RB(I),I=1,NN)	A 650
C		A 660
C	COMPUTE EQUIVALENT INCOMPRESSIBLE CENTER BODY	A 670
C		A 680
	DO 50 I=1,NN	A 690
	RB(I)=RB(I)*SQRT(1.-M**2)	A 700
50	CONTINUE	A 710
	IP=-1	A 720
	SAM=0.	A 730
	IT=1	A 740
C		A 750
C	COMPUTE NACELLE MEAN CAMBER AND THICKNESS AND EQUIVALENT	A 760
C	INCOMPRESSIBLE SHAPE - THEN COMPUTE NACELLE CAMBER AND THICKNESS	A 770
C	SLOPES AND CENTER BODY SLOPES	A 780
C		A 790
60	CONTINUE	A 800
	CALL OVERLAY (4HRING,1,0,6HRECALL)	A 810
C		A 820
C	COMPUTE CAMBER AND THICKNESS VORTEX STRENGTHS - GAM(I) AND GQ(I)	A 830
C		A 840
	CALL OVERLAY (4HRING,2,0,6HRECALL)	A 850
C		A 860
C	COMPUTE NACELLE AND CENTER BODY SURFACE PRESSURES	A 870
C		A 880
	CALL OVERLAY (4HRING,3,0,6HRECALL)	A 890
C		A 900
C	TEST FOR INVISCID ONLY SOLN OR END OF BOUNDARY LAYER ITERATION	A 910
C		A 920
	IF (IT.GT.ITMAX) GO TO 70	A 930
C		A 940
C	EXTRAPOLATE FOR TRAILING EDGE VELOCITIES AND COMPUTE BOUNDARY	A 950
C	LAYER. MODIFY NACELLE COORDINATES FOR DISPLACEMENT THICKNESS.	A 960
C		A 970
	CALL OVERLAY (4HRING,4,0,6HRECALL)	A 980
	GO TO 60	A 990
70	CONTINUE	A1000
C		A1010
C	CRITICAL MACH NUMBER	A1020
C		A1030
	CALL OVERLAY (4HRING,5,0,6HRECALL)	A1040
C		A1050
C	COMPUTE VI/VIN BY NACELLE INTERNAL MASS FLOW INTEGRATION	A1060
C		A1070
	CALL OVERLAY (4HRING,6,0,6HRECALL)	A1080
C		A1090
C	CALCULATE MFC	A1100
C		A1110
	MFC=((RXX**2-RBXI**2)/((DMIN/2.)**2))*VIVIN*((1.+(.2*(M**2)*(1.-VI	A1120
	IVIN**2)))**2.5)	A1130
	MU=MFC/AIAM	A1140
	WRITE (6,110) MCR,VIVIN,MFC,MU	A1150
C		A1160
C	CHECK TO SEE IF THERE IS ANOTHER CASE	A1170
C		A1180
	IF (FINI.EQ.0.) GO TO 10	A1190
	STOP	A1200

APPENDIX A - Continued

C		A1210
C		A1220
80	FORMAT (1H1)	A1230
90	FORMAT (//16X,14HINPUT GEOMETRY//4X,2HC=,F9.3,4X,5HDMIN=,F9.3,4X,5	A1240
	1HDMAX=,F9.3,4X,5HNRHO=,I9/4X,7HUNRREF=,E11.4,4X,6HITMAX=,I3,4X,2HN	A1250
	2=,I3,4X,2HM=,F9.4,4X,5HAIAM=,F9.4,4X,5HXFOR=,F9.4,4X,5HXAFT=,F9.4/	A1260
	3/9X,1HX,8X,2HRO,8X,2HRI,8X,2HRB//(4F10.4))	A1270
100	FORMAT (5A10)	A1280
110	FORMAT (1H0,4X,4HMCR=,F9.4,4X,7HVI/VIN=,F9.4,4X,4HMFC=,F9.4,4X,3H	A1290
	1U=,F9.4//4X,56HMCR IS CORRECT ONLY IF M IS LOW ENOUGH FOR INCOMP A	A1300
	2SSUMP)	A1310
120	FORMAT (1H1/2X,29HCENTER BODY EXPANDED BY SCALE,5X,6HSCALE=,F10.4/	A1320
	1//9X,1HX,8X,2HRB//(2F10.4))	A1330
	END	A1340-

APPENDIX A – Continued

	FUNCTION SKK (Z)	B 10
C		B 20
C	FUNCTION SKK COMPUTES THE COMPLETE ELLIPTICAL INTEGRAL OF THE	B 30
C	FIRST KIND K(K)	B 40
C		B 50
C	S. WAGNER, NASA AMES RESEARCH CENTER, MOFFETT FIELD CALIF. 94035	B 60
C		B 70
C	REFERENCE C. HASTINGS, APPROXIMATIONS FOR DIGITAL COMPUTERS, P.172	B 80
C		B 90
C	INPUT Z = K**2	B 100
C		B 110
	IF (Z) 10,20,30	B 120
10	WRITE (6,60) Z	B 130
	STOP	B 140
20	SKK=1.570796326794896	B 150
	RETURN	B 160
30	E=1.0-Z	B 170
	IF (E) 10,40,50	B 180
40	WRITE (6,70) Z	B 190
	STOP	B 200
50	SKK=((E*.1451196212E-01+.3742563713E-01)*E+.3590092383E-01)*E+.96	B 210
	166344259E-01)*E+1.38629436112-(((E*.441787012E-02+.3328355346E-01	B 220
	2)*E+.6880248576E-01)*E+.12498593597)*E+.5)*ALOG(E)	B 230
	RETURN	B 240
C		B 250
C		B 260
60	FORMAT (1H1,10X,21HFUNCTION SKK K**2 = ,E16.9)	B 270
70	FORMAT (1H1,10X,7HK**2 = ,E16.9,13HK(K) INFINITE)	B 280
	END	B 290-

APPENDIX A – Continued

	FUNCTION EKA (Z)	C 10
C		C 20
C	FUNCTION EKA COMPUTES THE COMPLETE ELLIPTICAL INTEGRAL OF THE	C 30
C	SECOND KIND E(K)	C 40
C		C 50
C	S. WAGNER, NASA AMES RESEARCH CENTER, MOFFETT FIELD CALIF. 94035	C 60
C		C 70
C	REFERENCE C. HASTINGS, APPROXIMATIONS FOR DIGITAL COMPUTERS, P.175	C 80
C		C 90
C	INPUT Z = K**2	C 100
C		C 110
	IF (Z) 10,20,30	C 120
10	WRITE (6,60) Z	C 130
	STOP	C 140
20	EKA=1.570796326794896	C 150
	RETURN	C 160
30	E=1.0-Z	C 170
	IF (E) 10,40,50	C 180
40	EKA=1.0	C 190
	RETURN	C 200
50	EKA=1.+(((.1736506451E-01*E+.4757383546E-01)*E+.6260601220E-01)*E+	C 210
	1.44325141463)*E-(((.526449639E-02*E+.4069697526E-01)*E+.9200180037	C 220
	2E-01)*E+.24998368310)*E*ALOG(E)	C 230
	RETURN	C 240
C		C 250
C		C 260
60	FORMAT (1H1,10X,21HFUNCTION EKA K**2 = ,E16.9)	C 270
	END	C 280-



APPENDIX A - Continued

```

IF ((I+IN).GE.N) GO TO 90          D 610
I=I+IN                             D 620
IF ((VARI(I)-X)*(VARI(I+1)-X)) 100,100,80 D 630
C                                  D 640
C  EXTRAPOLATION                   D 650
C                                  D 660
90  EX=.T.                         D 670
100 IF (M.EQ.2) GO TO 120          D 680
C                                  D 690
C  FIRST ORDER                     D 700
C                                  D 710
      DO 110 NT=1,NTAB             D 720
110  Y(NT)=(VARD(I,NT)*(VARI(I+1)-X)-VARD(I+1,NT)*(VARI(I)-X))/(VARI(I+
      11)-VARI(I))                 D 730
      IF (EX) I=I+IN               D 740
      RETURN                       D 750
C                                  D 760
C                                  D 770
C  SECOND ORDER                    D 780
C                                  D 790
120  IF (N.EQ.2) GO TO 10          D 800
      IF (I.EQ.(N-1)) GO TO 140    D 810
      IF (I.EQ.1) GO TO 130        D 820
C                                  D 830
C  PICK THIRD POINT                D 840
C                                  D 850
      SK=VARI(I+1)-VARI(I)         D 860
      IF ((SK*(X-VARI(I-1))).LT.(SK*(VARI(I+2)-X))) GO TO 140 D 870
130  L=I                           D 880
      GO TO 150                    D 890
140  L=I-1                          D 900
150  V(1)=VARI(L)-X                 D 910
      V(2)=VARI(L+1)-X             D 920
      V(3)=VARI(L+2)-X             D 930
      DO 160 NT=1,NTAB             D 940
      YY(1)=(VARD(L,NT)*V(2)-VARD(L+1,NT)*V(1))/(VARI(L+1)-VARI(L)) D 950
      YY(2)=(VARD(L+1,NT)*V(3)-VARD(L+2,NT)*V(2))/(VARI(L+2)-VARI(L+1)) D 960
160  Y(NT)=(YY(1)*V(3)-YY(2)*V(1))/(VARI(L+2)-VARI(L))           D 970
      IF (EX) I=I+IN               D 980
      RETURN                       D 990
C                                  D1000
C  ZERO ORDER                      D1010
C                                  D1020
170  DO 180 NT=1,NTAB             D1030
180  Y(NT)=VARD(1,NT)              D1040
      RETURN                       D1050
C                                  D1060
C                                  D1070
190  FORMAT (1H1,49H TABLE BELOW OUT OF ORDER FOR MTLUP AT POSITION ,I D1080
      15,/31H X TABLE IS STORED IN LOCATION ,06,/(8G15.8))       D1090
      END                          D1100-

```

APPENDIX A - Continued

```

OVERLAY(RING,1,0) E 10
PROGRAM GEOMTRY E 20
C E 30
C THIS OVERLAY COMPUTES NACELLE MEAN CAMBER RADII AND THICKNESS E 40
C FOR THE EQUIVALENT INCOMPRESSIBLE SHAPE. THEN THE SLOPES ARE E 50
C COMPUTED ON THE EQUIVALENT NACELLE CAMBER AND THICKNESS SHAPES E 51
C AND ON THE EQUIVALENT CENTER BODY. E 52
C E 60
COMMON /CORD/ X(170),R(170),C,RAVG,NN,N,DMIN,T(170),RB(170),XRN E 70
COMMON /ONE/ ROUT(170),RIN(170),M,DMAX,XI(170),XIO(170),ALPHO(170) E 80
1,ALPHOO(170,1),XBL(170),ALPT(170),ALPTH(170),DRDX(170),DRDXH(170), E 90
2LAM,IT,ITMAX E 100
RFAL LAM,M E 110
C E 111
C COMPUTE NACELLE MEAN CAMBER RADII AND THICKNESS AND E 112
C COMPUTE NACELLE EQUIVALENT INCOMPRESSIBLE BODY E 113
C E 114
DO 10 I=1,NN E 120
R(I)=(ROUT(I)+RIN(I))/2. E 130
T(I)=ROUT(I)-RIN(I) E 140
10 CONTINUE E 150
DO 20 I=1,NN E 160
R(I)=R(I)*SQRT(1.-M**2) E 170
T(I)=T(I)*SQRT(1.-M**2) E 180
20 CONTINUE E 190
DMAX=DMAX*SQRT(1.-M**2) E 200
DMIN=DMIN*SQRT(1.-M**2) E 210
RAVG=(DMIN+DMAX)/4. E 220
C E 230
C COMPUTE NACELLE CAMBER AND THICKNESS SLOPES AND CENTER BODY SLOPES E 240
C E 250
CALL SLOPE (XI,XIO,ALPHO,ALPHOO) E 260
DO 30 J=1,N E 270
XRL(J)=(C/2.)-(XIO(J)*RAVG) E 280
30 CONTINUE E 290
CALL THICK (ALPT,ALPTH) E 300
CALL BODY (DRDX,DRDXH) E 310
LAM=(DMAX+DMIN)/(2.*C) E 320
IF (IT.LE.ITMAX) GO TO 40 E 330
WRITE (6,50) LAM,(ALPHO(I),ALPHOO(I,1),XI(I),XIO(I),ALPT(I),ALPTH( E 340
I),DRDX(I),DRDXH(I),I,I=1,N) E 350
40 CONTINUE E 360
RETURN E 370
C E 380
C E 390
50 FORMAT (1H1,25X,42HGEOMETRY ON EQUIVALENT INCOMPRESSIBLE BODY//7X, E 400
14HLAM=,F9.4//5X,5HALPHO,4X,6HALPHOO,8X,2HXI,7X,3HXIO,6X,4HALPT,5X, E 410
25HALPTH,6X,4HDRDX,5X,5HDRDXH,4X,6HI OR J//(8F10.5,I10)) E 420
END E 430-

```

APPENDIX A - Continued

	SUBROUTINE SLOPE (XI,XIO,ALPHO,ALPHOO)	F 10
C		F 20
C	THIS SUBROUTINE COMPUTES XI(I), XIO(J), ALPHO(I), ALPHOO(J)	F 30
C		F 40
C	THE XI AND XIO ARE FOR NACELLE AND CENTER BODY .	F 50
C	THE SLOPES ARE NACELLE CAMBER SLOPES.	F 60
C		F 70
	COMMON /CORD/ X(170),R(170),C,RAVG,NN,N,DMIN	F 80
	DIMENSION ALPHO(170), ALPHOO(170,1), XI(170), XIO(170)	F 90
	IP=-1	F 100
	XXX=-.25*(C/N)	F 110
	XX=(C/N)*.75	F 120
	DO 30 I=1,N	F 130
	IF (I.EQ.1) GO TO 10	F 140
	CALL MTLUP (XXX,RXI1,2,NN,170,1,IP,X,R)	F 150
	CALL MTLUP (XX,RXI,2,NN,170,1,IP,X,R)	F 160
	TEMP4=(RXI1-RXI)/(C/N)	F 170
	GO TO 20	F 180
10	PIP=0.	F 190
	POP=(C/N)*.5	F 200
	CALL MTLUP (PIP,RXI1,2,NN,170,1,IP,X,R)	F 210
	CALL MTLUP (POP,RXI,2,NN,170,1,IP,X,R)	F 220
	TEMP4=(RXI1-RXI)/((C/N)*.5)	F 230
20	CONTINUE	F 240
	ALPHO(I)=ATAN(TEMP4)	F 250
	XXX=XXX+(C/N)	F 260
	XX=XX+(C/N)	F 270
30	CONTINUE	F 280
	DO 50 I=1,N	F 290
	IF (I.EQ.N) GO TO 40	F 300
	ALPHOO(I,1)=(ALPHO(I)+ALPHO(I+1))*0.5	F 310
	GO TO 50	F 320
40	ALPHOO(I,1)=ALPHO(I)+(.5*(ALPHO(I)-ALPHO(I-1)))	F 330
50	CONTINUE	F 340
	TEMP5=.5*C/RAVG	F 350
	TEMP6=(C/N)/RAVG	F 360
	DO 70 I=1,N	F 370
	IF (I.EQ.1) GO TO 60	F 380
	XI(I)=XI(I-1)-TEMP6	F 390
	XIO(I)=XIO(I-1)-TEMP6	F 400
	GO TO 70	F 410
60	XI(I)=TEMP5-(.25*TEMP6)	F 420
	XIO(I)=TEMP5-(.75*TEMP6)	F 430
70	CONTINUE	F 440
	RETURN	F 450
	END	F 460-

APPENDIX A - Continued

	SUBROUTINE THICK (ALPT,ALPTH)	G 10
C		G 20
C	THIS SUBROUTINE COMPUTES NACELLE THICKNESS SLOPES.	G 30
C		G 40
	COMMON /CORD/ X(170),R(170),C,RAVG,NN,N,DMIN,T(170)	G 50
	DIMENSION ALPT(170), ALPTH(170)	G 60
	IP=-1	G 70
	XXX=-.25*(C/N)	G 80
	XX=(C/N)*.75	G 90
	DO 30 I=1,N	G 100
	IF (I.EQ.1) GO TO 10	G 110
	CALL MTLUP (XXX,TXI1,2,NN,170,1,IP,X,T)	G 120
	CALL MTLUP (XX,TXI,2,NN,170,1,IP,X,T)	G 130
	TEMP4=((TXI1-TXI)/2.)/(C/N)	G 140
	GO TO 20	G 150
10	X14=(C/N)*.5	G 160
	CALL MTLUP (X14,TXI,2,NN,170,1,IP,X,T)	G 170
	TEMP4=((0.-TXI)/2.)/((C/N)*.5)	G 180
20	CONTINUE	G 190
	ALPT(I)=ATAN(TEMP4)	G 200
	XXX=XXX+(C/N)	G 210
	XX=XX+(C/N)	G 220
30	CONTINUE	G 230
	DO 50 I=1,N	G 240
	IF (I.EQ.N) GO TO 40	G 250
	ALPTH(I)=(ALPT(I)+ALPT(I+1))*0.5	G 260
	GO TO 50	G 270
40	ALPTH(I)=ALPT(I)+(.5*(ALPT(I)-ALPT(I-1)))	G 280
50	CONTINUE	G 290
	RETURN	G 300
	END	G 310-

APPENDIX A – Continued

	SUBROUTINE BODY (DRDX,DRDXH)	H 10
C		H 20
C	THIS SUBROUTINE COMPUTES CENTER BODY SLOPES.	H 30
C		H 40
	COMMON /CORD/ X(170),R(170),C,RAVG,NN,N,DMIN,T(170),RB(170),XBN	H 50
	DIMENSION DRDX(170), DRDXH(170)	H 60
	IP=-1	H 70
	XXX=-.25*(C/N)	H 80
	XX=(C/N)*.75	H 90
	DO 30 I=1,N	H 100
	IF (I.EQ.1) GO TO 10	H 110
	CALL MTLUP (XXX,RBXI1,2,NN,170,1,IP,X,RB)	H 120
	IF (XXX.LE.XBN) RBXI1=0.	H 130
	CALL MTLUP (XX,RBXI,2,NN,170,1,IP,X,RB)	H 140
	IF (XX.LE.XBN) RBXI=0.	H 150
	DRDX(I)=(RBXI-RBXI1)/(C/N)	H 160
	GO TO 20	H 170
10	X14=(C/N)*.5	H 180
	CALL MTLUP (X14,RBXI,2,NN,170,1,IP,X,RB)	H 190
	IF (X14.LE.XBN) RBXI=0.	H 200
	DRDX(I)=RBXI/((C/N)*.5)	H 210
20	XXX=XXX+(C/N)	H 220
	XX=XX+(C/N)	H 230
30	CONTINUE	H 240
	DO 50 I=1,N	H 250
	IF (I.EQ.N) GO TO 40	H 260
	DRDXH(I)=(DRDX(I)+DRDX(I+1))/2.	H 270
	GO TO 50	H 280
40	DRDXH(I)=DRDX(I)+(.5*(DRDX(I)-DRDX(I-1)))	H 290
50	CONTINUE	H 300
	IF (DRDXH(1).NE.0.) GO TO 80	H 310
	DO 60 I=2,N	H 320
	IF (DRDXH(I).NE.0.) GO TO 70	H 330
60	CONTINUE	H 340
70	DRDXH(I)=0.	H 350
80	CONTINUE	H 360
	RETURN	H 370
	END	H 380-

APPENDIX A - Continued

```

OVERLAY(RING,2,0) I 10
PROGRAM MATRIX I 20
C I 30
C THIS OVERLAY COMPUTES NACELLE CAMBER AND THICKNESS VORTEX I 40
C STRENGTHS - GAM(I) AND GQ(I) I 41
C I 50
COMMON /CORD/ X(170),R(170),C,RAVG,NN,N,DMIN,T(170),RB(170),XBN I 60
COMMON /ONE/ ROUT(170),RIN(170),M,DMAX,XI(170),XIO(170),ALPHO(170) I 70
1,ALPHOO(170,1),XBL(170),ALPT(170),ALPTH(170),DRDX(170),DRDXH(170), I 80
2LAM,IT,ITMAX I 90
COMMON /TWO/ IP,CAM,GAM(170),GQ(170),ALPOO(170,1) I 100
REAL KSQ,LAM,M I 110
DIMENSION WA(170), WY(170), GQB(170), ANS(170), ALPHQBB(170,1), RH I 120
100(170) I 130
C I 131
C COMPUTE SECOND ALPHOO WHICH IS PRINTED - DO 20 I 132
C I 133
DO 20 J=1,N I 140
WRBQJU=0. I 150
RHOO(J)=1. I 160
XX=(C/N)*.25 I 170
DO 10 I=1,N I 180
CALL MTLUP (XX,RBXI,2,NN,170,1,IP,X,RB) I 190
IF (XX.LE.XBN) RBXI=0. I 200
DELXI=XI(I)-XIO(J) I 210
TEMP11=RHOO(J)/(2.*((DELXI**2+RHOO(J)**2)**1.5)) I 220
WRBQJU=WRBQJU+TEMP11*(RBXI/RAVG)*DRDX(I)*(XI(1)-XI(2)) I 230
XX=XX+(C/N) I 240
10 CONTINUE I 250
ALPOO(J,1)=ALPHOO(J,1) I 260
ALPHOO(J,1)=-2.*3.14159*(ALPHOO(J,1)+WRBQJU) I 270
20 CONTINUE I 280
C I 290
C SOLVE MATRIX EQUATION FOR THE GAM(I) MATRIX I 300
C I 310
IF (CAM.EQ.0.) GO TO 50 I 320
REWIND 10 I 330
DO 40 J=1,N I 340
DO 30 I=1,N I 350
DELXI=XI(I)-XIO(J) I 360
KSQ=4./(DELXI**2+4.) I 370
EK=EKA(KSQ) I 380
SK=SKK(KSQ) I 390
30 WA(I)=(((1.-DELXI*SQRT(KSQ))/4.)*(((2.-KSQ)/(1.-KSQ))*EKA(KSQ)) I 400
1-(2.*SKK(KSQ))*ALPHO(I) I 410
WRITE (10) (WA(IT),IT=1,N),ALPHOO(J,1) I 420
40 CONTINUE I 430
CALL SSLES0 (N,1,GAM) I 440
REWIND 10 I 450
GO TO 70 I 460
50 DO 60 I=1,N I 470
GAM(I)=0. I 480
60 CONTINUE I 490
70 CONTINUE I 500
C I 510
C COMPUTE ALPHQBB - DO 80 I 520
C I 530
DO 80 J=1,N I 540
ALPHQBB(J,1)=0. I 550
XX=C/N*.25 I 560

```

APPENDIX A - Continued

```

DO 80 I=1,N I 570
DELXI=XI(I)-XIO(J) I 580
KSQ=4./(DELXI**2+4.) I 590
EK=EKA(KSQ) I 600
SK=SKK(KSQ) I 610
CALL MTLUP (XX, TX, 2, NN, 170, 1, IP, X, T) I 620
ALPHQBB(J,1)=ALPHQBB(J,1)+((TX/C)*(((SQRT(1.-KSQ))/2.)*(-DELXI/ABS I 630
1(DELXI))*((KSQ+2.)*SK)-(2.*(KSQ+1.)*EK)))*(XI(1)-XI(2))) I 640
XX=XX+(C/N) I 650
CONTINUE I 660
80 C I 670
C SOLVE MATRIX EQUATION FOR GQB(I) MATRIX I 680
C I 690
REWIND 10 I 700
DO 100 J=1,N I 710
DO 90 I=1,N I 720
DELXI=XI(I)-XIO(J) I 730
KSQ=4./(DELXI**2+4.) I 740
EK=EKA(KSQ) I 750
SK=SKK(KSQ) I 760
90 WY(I)=(((KSQ-2.)*EK+2.*(1.-KSQ)*SK)/SQRT(KSQ))*((XI(1)-XI(2))/DELX I 770
1I)*(1./LAM) I 780
WRITE (10) (WY(IT), IT=1,N), ALPHQBB(J,1) I 790
100 CONTINUE I 800
CALL SSLES0 (N,1,GQB) I 810
C I 820
C COMPUTE GQ I 830
C I 840
XX=C/N*.25 I 850
DO 110 I=1,N I 860
CALL MTLUP (XX, TX, 2, NN, 170, 1, IP, X, T) I 870
GQ(I)=((TX/C)/LAM)+(((C/(2.*RAVG))**2)*GQB(I)) I 880
GQ(I)=-GQ(I) I 890
XX=XX+(C/N) I 900
110 CONTINUE I 910
IF (IT.LE.ITMAX) GO TO 130 I 920
PRINT 140 I 930
DO 120 I=1,N I 940
WRITE (6,150) I,GAM(I),GQ(I),GQB(I),ALPHQBB(I,1),ALPH00(I,1) I 950
120 CONTINUE I 960
130 CONTINUE I 970
RETURN I 980
C I 990
C I1000
140 FORMAT (1H1,11X,1HI,9X,3HGAM,11X,2HGQ,10X,3HGQB,6X,7HALPHQBB,7X,6H I1010
1ALPH00) I1020
150 FORMAT (9X,I3,2X,E12.5,4(2X,E11.4)) I1030
END I1040-

```

APPENDIX A - Continued

```

SUBROUTINE SSLES0 (NT,NCFLG,ANS)                                J  10
C                                                                J  20
C THIS SUBROUTINE SOLVES SIMULTANEOUS LINEAR EQUATIONS BY     J  30
C SUCCESSIVE ORTHOGONALIZATION **.                             J  40
C                                                                J  50
C IF MATRIX ORDER IS = N, AND NUMBER OF RIGHT-HAND SIDES = M, THEN J  60
C THE AMOUNT OF CORE THAT MUST BE AVAILABLE FOR EACH ARRAY IS -- J  70
C  $R = N+M$ ,  $RV = N+M-1$ ,  $CV = N-1$ ,  $V = J(J+1)$  WHERE J IS THE INTEGER J  80
C PORTION OF  $(N+M)/2$                                           J  90
C                                                                J 100
C DIMENSIONS BASED ON THE VALUES  $N+M \leq 283$ , MAX N IS 281   J 110
C                                                                J 120
C DIMENSION RV(170), R(170), CV(170), V(8100), ANS(NT)       J 130
C REWIND 10                                                    J 140
C N1=NT+NCFLG                                                 J 150
C J=N1-1                                                       J 160
C                                                                J 170
C READ (10)                                                    J 180
C                                                                J 190
C READ (10) (R(I),I=1,N1)                                     J 200
C DO 10 I=1,J                                                 J 210
10 V(I)=-R(I+1)/R(I)                                          J 220
C IN=1                                                         J 230
C                                                                J 240
C READ (10)                                                    J 250
C                                                                J 260
20 READ (10) (R(I),I=1,N1)                                     J 270
C I2=0                                                         J 280
C DO 40 I=1,J                                                 J 290
C RV(I)=0.                                                     J 300
C DO 30 II=1,IN                                               J 310
C I2=I2+1                                                      J 320
30 RV(I)=RV(I)+R(II)*V(I2)                                    J 330
C N2=I+IN                                                       J 340
40 RV(I)=RV(I)+R(N2)                                          J 350
C I2=IN+1                                                       J 360
C NN=J*IN+1                                                    J 370
C KK=J*I2                                                        J 380
C J=J-1                                                         J 390
C DO 60 I=1,J                                                 J 400
C DO 50 II=1,IN                                               J 410
C NN=NN-1                                                       J 420
C KK=KK-1                                                       J 430
50 V(KK)=V(NN)                                                J 440
60 KK=KK-1                                                      J 450
C DO 70 I=1,IN                                               J 460
70 R(I)=V(I)                                                  J 470
C K=0                                                           J 480
C DO 90 I=1,J                                                 J 490
C C=-RV(I+1)/RV(I)                                           J 500
C DO 80 II=1,IN                                               J 510
C CV(II)=C*R(II)                                              J 520
C NN=K+II                                                       J 530
C I2=I2+1                                                      J 540
80 V(NN)=CV(II)+V(I2)                                         J 550
C K=NN+1                                                        J 560
C I2=I2+1                                                      J 570
90 V(K)=C                                                       J 580
C IF (J.EQ.NCFLG) GO TO 100                                    J 590
C IN=IN+1                                                       J 600

```

APPENDIX A - Continued

100	GO TO 20	J 610
	K=1-NT	J 620
	KK=0	J 630
	DO 110 J=1,NCFLG	J 640
	K=K+NT	J 650
	KK=KK+NT	J 660
110	CONTINUE	J 670
	DO 120 J=1,NT	J 680
120	ANS(J)=-V(J)	J 690
	RETURN	J 700
	END	J 710-

APPENDIX A – Continued

	OVERLAY(RING,3,0)	K 10
	PROGRAM PRESURE	K 20
C		K 30
C	THIS OVERLAY COMPUTES NACELLE AND CENTER BODY SURFACE PRESSURES	K 40
C		K 50
	COMMON /CORD/ X(170),R(170),C,RAVG,NN,N,DMIN,T(170),RB(170),XBN	K 60
	COMMON /ONE/ ROUT(170),RIN(170),M,DMAX,XI(170),XIO(170),ALPHO(170)	K 70
	1,ALPHOO(170,1),XBL(170),ALPT(170),ALPTH(170),DRDX(170),DRDXH(170),	K 80
	2LAM,IT,ITMAX	K 90
	COMMON /TWO/ IP,CAM,GAM(170),GQ(170),ALPOO(170,1)	K 100
	COMMON /THREE/ VOUT(170),VIN(170)	K 110
	COMMON /FIVE/ CPO(170),MCR	K 120
	DIMENSION RHOO(170), CPI(170)	K 130
	REAL KSQ,LAM,M	K 140
	IF (IT.LE.ITMAX) GO TO 10	K 150
	PRINT 190	K 160
	PRINT 130	K 170
	PRINT 140	K 180
	PRINT 170	K 190
10	CONTINUE	K 200
	XXX=(C/N)*.75	K 210
	DO 120 J=1,N	K 220
	XOJ=XIO(J)*RAVG/C	K 230
	RHOO(J)=1.	K 240
	XX=(C/N)*.25	K 250
C		K 260
C	COMPUTE VELOCITIES ON NACELLE SURFACE - DO 20	K 270
C		K 280
	WX1JUO=0.	K 290
	WR1JUO=0.	K 300
	WX1QJU=0.	K 310
	WR1QJU=0.	K 320
	WXQJU=0.	K 330
	WRQJU=0.	K 340
	WXBQJU=0.	K 350
	WRBQJU=0.	K 360
	DO 20 I=1,N	K 370
	DELXI=XI(I)-XIO(J)	K 380
	KSQ=4./(DELXI**2+4.)	K 390
	EK=EKA(KSQ)	K 400
	SK=SKK(KSQ)	K 410
	CALL MTLUP (XX,RBXI,2,NN,170,1,IP,X,RB)	K 420
	IF (XX.LE.XBN) RBXI=0.	K 430
	TEMP1=(1./(2.*SQRT(DELXI**2+4.)))*(((2.-KSQ)/(1.-KSQ))*EKA(KSQ))-	K 440
	1(2.*SKK(KSQ))-((KSQ/(1.-KSQ))*EKA(KSQ))	K 450
	TEMP2=((-1.)*DELXI*SQRT(KSQ))/4.)*(((2.-KSQ)/(1.-KSQ))*EKA(KSQ))	K 460
	1-(2.*SKK(KSQ))	K 470
	TEMP7=(4.*EK)/((SQRT(4.+DELXI**2))*DELXI)	K 480
	TEMP8=2.*TEMP1	K 490
	TEMP11=RHOO(J)/(2.*((DELXI**2+RHOO(J)**2)**1.5))	K 500
	TEMP12=(DELXI)/(2.*((DELXI**2+RHOO(J)**2)**1.5))	K 510
	WX1JUO=WX1JUO+TEMP1*ALPHO(I)*GAM(I)*(1./(2.*3.14159))	K 520
	WR1JUO=WR1JUO+TEMP2*ALPHO(I)*GAM(I)*(1./(2.*3.14159))	K 530
	WX1QJU=WX1QJU+(TEMP1*GQ(I)*(XI(1)-XI(2)))/(2.*3.14159))	K 540
	WR1QJU=WR1QJU+(TEMP2*GQ(I)*(XI(1)-XI(2)))/(2.*3.14159))	K 550
	WXQJU=WXQJU-(TEMP7*ALPT(I)*(XI(1)-XI(2)))/(2.*3.14159))	K 560
	WRQJU=WRQJU+(TEMP8*ALPT(I)*(XI(1)-XI(2)))/(2.*3.14159))	K 570
	WXBQJU=WXBQJU+TEMP12*(RBXI/RAVG)*DRDX(I)*(XI(1)-XI(2))	K 580
	WRBQJU=WRBQJU+TEMP11*(RBXI/RAVG)*DRDX(I)*(XI(1)-XI(2))	K 590
	XX=XX+(C/N)	K 600

APPENDIX A - Continued

```

20  CONTINUE                                     K 610
    IF (J.EQ.N) GO TO 30                       K 620
    TEMP3=(ALPHO(J)*GAM(J)+ALPHO(J+1)*GAM(J+1))*0.25*(1./(XI(1)-XI(2))) K 630
    TEMP31=.25*(GQ(J)+GQ(J+1))                 K 640
    GO TO 40                                    K 650
30  TEMP3=ALPHO(J)*GAM(J)*.50*(1./(XI(1)-XI(2)))*.3333333333           K 660
    TEMP31=.50*(GQ(J)*.3333333333)            K 670
40  CONTINUE                                     K 680
    WX1JU00=WX1JU0+TEMP3                       K 690
    WX1JU0I=WX1JU0-TEMP3                       K 700
    WX1QJU0I=WX1QJU0-TEMP3                     K 710
    WX1QJU0=WX1QJU0+TEMP3                     K 720
    WRQJU0I=WRQJU0+ALPH(J)                     K 730
    WRQJU0=WRQJU0-ALPH(J)                     K 740
C                                         K 750
C  CALCULATE TOTAL VELOCITY SQUARED AND APPLY COMPRESSIBILITY FACTOR      K 760
C                                         K 770
    VTO=(1.+(WX1JU00+WX1QJU0+WXQJU+WBQJU)/(1.-M**2))**2                 K 780
    VTI=(1.+(WX1JU0I+WX1QJU0I+WXQJU+WBQJU)/(1.-M**2))**2                 K 790
C                                         K 800
C  APPLY RIEGELS FACTOR                                                       K 810
C                                         K 820
    VTO=VTO/(1.+(TAN((ALPOO(J,1)+ALPH(J))/SQRT(1.-M**2)))**2)           K 830
    VTI=VTI/(1.+(TAN((ALPOO(J,1)-ALPH(J))/SQRT(1.-M**2)))**2)           K 840
    VOUT(J)=SQRT(VTO)                                                         K 850
    VIN(J)=SQRT(VTI)                                                         K 860
C                                         K 870
C  COMPUTE CPO AND CPI                                                         K 880
C                                         K 890
    IF (M.EQ.0.) GO TO 50                                                     K 900
    CPO(J)=(2./(1.4*(M**2)))*((1.+(.2*(M**2)*(1.-VTO)))**(.4/.4)-1.)      K 910
    CPI(J)=(2./(1.4*(M**2)))*((1.+(.2*(M**2)*(1.-VTI)))**(.4/.4)-1.)      K 920
    GO TO 60                                                                    K 930
50  CPO(J)=(1.-VTO)                                                            K 940
    CPI(J)=(1.-VTI)                                                            K 950
60  CONTINUE                                                                    K 960
C                                         K 970
C  COMPUTE CENTER BODY SURFACE VELOCITIES - DO 70                            K 980
C                                         K 990
    WX1J=0.                                                                      K1000
    WR1J=0.                                                                      K1010
    WX1QJ=0.                                                                      K1020
    WR1QJ=0.                                                                      K1030
    WXQJ=0.                                                                      K1040
    WRQJ=0.                                                                      K1050
    WBQJ=0.                                                                      K1060
    WRBQJ=0.                                                                      K1070
    XX=(C/N)*.25                                                                  K1080
    CALL MTLUP (XXX,RBXJ,2,NN,170,1,IP,X,RB)                                    K1090
    IF (XXX.LE.XBN) RBXJ=0.                                                       K1100
    RH00(J)=RBXJ/RAVG                                                             K1110
    IF (RH00(J).LE.0.) GO TO 80                                                  K1120
    DO 70 I=1,N                                                                    K1130
    DELXI=XI(I)-XIO(J)                                                            K1140
    CALL MTLUP (XX,RBXI,2,NN,170,1,IP,X,RB)                                    K1150
    IF (XX.LE.XBN) RBXI=0.                                                       K1160
    KSQ=(4.*RH00(J))/((DELXI**2)+((1.+RH00(J))**2))                             K1170
    EK=EKA(KSQ)                                                                    K1180
    SK=SKK(KSQ)                                                                    K1190
    TEMP1=(1./(2.*SQRT((DELXI**2)+((1.+RH00(J))**2))))*(((2.-KSQ)/(1.

```

APPENDIX A - Continued

```

1-KSQ))*EK)-(2.*SK)-((1./RHOO(J))*(KSQ/(1.-KSQ))*EK)      K1210
TEMP2=(((-1.)*DELXI)/(2.*RHOO(J)*SQRT((DELXI**2)+(1.+RHOO(J)**2) K1220
1)))*(((2.-KSQ)/(1.-KSQ))*EK)-(2.*SK))                    K1230
TEMP7=(4.*DELXI*EK)/((SQRT((DELXI**2)+(1.+RHOO(J)**2)))*((DELXI* K1240
1**2)+(1.-RHOO(J)**2)))
TEMP8=(2./(RHOO(J)*SQRT((DELXI**2)+(1.+RHOO(J)**2)))*((1.-((2. K1260
1*RHOO(J)*(RHOO(J)-1.))/((DELXI**2)+(1.-RHOO(J)**2))))*EK)-SK) K1270
TEMP11=RHOO(J)/(2.*((DELXI**2+RHOO(J)**2)**1.5))           K1280
TEMP12=(DELXI)/(2.*((DELXI**2+RHOO(J)**2)**1.5))           K1290
WX1J=WX1J+TEMP1*ALPHO(I)*GAM(I)*(1./(2.*3.14159))          K1300
WR1J=WR1J+TEMP2*ALPHO(I)*GAM(I)*(1./(2.*3.14159))          K1310
WX1QJ=WX1QJ+(TEMP1*GQ(I)*(XI(1)-XI(2)))/(2.*3.14159))     K1320
WR1QJ=WR1QJ+(TEMP2*GQ(I)*(XI(1)-XI(2)))/(2.*3.14159))     K1330
WXQJ=WXQJ-(TEMP7*ALPT(I)*(XI(1)-XI(2)))/(2.*3.14159))    K1340
WRQJ=WRQJ+(TEMP8*ALPT(I)*(XI(1)-XI(2)))/(2.*3.14159))    K1350
WXBQJ=WXBQJ+TEMP12*(RBXI/RAVG)*DRDX(I)*(XI(1)-XI(2))      K1360
WRBQJ=WRBQJ+TEMP11*(RBXI/RAVG)*DRDX(I)*(XI(1)-XI(2))      K1370
XX=XX+(C/N)                                                  K1380
70  CONTINUE                                                  K1390
80  VBA=(1.+(WX1J+WX1QJ+WXQJ+WXBQJ)/(1.-M**2))**2+((WR1J+WR1QJ+WRQJ+WR K1400
1BQJ)/SQRT(1.-M**2))**2
VBI=(1.+WXBQJ/(1.-M**2))**2+(WRBQJ/SQRT(1.-M**2))**2      K1420
C   K1430
C   COMPUTE CENTER BODY PRESSURES                            K1440
C   K1450
IF (M.EQ.0.) GO TO 90
CPBA=(2./(1.4*(M**2)))*((1.+(.2*(M**2)*(1.-VBA))**(.4/.4)-1.) K1470
CPBI=(2./(1.4*(M**2)))*((1.+(.2*(M**2)*(1.-VBI))**(.4/.4)-1.) K1480
GO TO 100
90  CPBA=(1.-VBA)                                            K1500
CPBI=(1.-VBI)                                              K1510
100 CONTINUE                                                K1520
IF (IT.LE.ITMAX) GO TO 110
WRITE (6,150) J,XOJ,CPO(J),CPI(J),VTO,VTI,WX1JU00,WX1JU0I,WX1JU0,W K1540
1R1JU0
WRITE (6,160) WX1QJU0,WX1QJUI,WX1QJU,WR1QJU,WXQJU,WRQJU0,WRQJUI,WR K1560
1QJU
WRITE (6,180) CPBA,CPBI,WXBQJU,WRBQJU,RHOO(J)              K1580
110 CONTINUE                                                K1590
XXX=XXX+(C/N)                                              K1600
120 CONTINUE                                                K1610
RETURN                                                      K1620
C   K1630
C   K1640
130 FORMAT (1X,1HJ,7X,5HXOJ/C,8X,3HCP0,9X,3HCPI,8X,3HVT0,10X,3HVTI,6X, K1650
17HWX1JU00,6X,7HWX1JU0I,7X,6HWX1JU0,7X,6HWR1JU0)           K1660
140 FORMAT (19X,7HWX1QJU0,6X,7HWX1QJUI,7X,6HWX1QJU,7X,6HWR1QJU,8X,5HWX K1670
1QJU,7X,6HWRQJU0,7X,6HWRQJUI,8X,5HWRQJU)                  K1680
150 FORMAT (1X,I3,3(2X,F10.5),6(2X,E11.4))                  K1690
160 FORMAT (13X,8(2X,E11.4))                                 K1700
170 FORMAT (19X,4HCPBA,9X,4HCPBI,7X,6HWXBQJU,7X,6HWRBQJU,4X,9HRH00-80D K1710
1Y/)                                                         K1720
180 FORMAT (10X,2(2X,F11.5),3X,2(2X,E11.4),F10.4/)         K1730
190 FORMAT (1H1,20HNACELLE SURFACE SOLN,10X,48HALL PERTURB VEL ARE ON K1740
1EQUIV INCOMP NACELLE SURF,10X,26HCENTER BODY RHOO AND PRESS//) K1750
END                                                         K1760-

```

APPENDIX A – Continued

```

OVERLAY(RING,4,0) L 10
PROGRAM BNDLYR L 20
C L 30
C THIS OVERLAY EXTRAPOLATES THE VELOCITIES IN THE TRAILING EDGE L 40
C REGION OF THE NACELLE AND COMPUTES THE BOUNDARY LAYER ON THE L 41
C NACELLE. THEN THE NACELLE COORDINATES ARE MODIFIED FOR THE L 42
C DISPLACEMENT THICKNESS. L 43
C L 50
COMMON /CORD/ X(170),R(170),C,RAVG,NN,N,DMIN,T(170),RB(170),XBN L 60
COMMON /ONE/ ROUT(170),RIN(170),M,DMAX,XI(170),XIO(170),ALPHO(170) L 70
1,ALPHOO(170,1),XBL(170),ALPT(170),ALPTH(170),DRDX(170),DRDXH(170), L 80
2LAM,IT,ITMAX L 90
COMMON /TWO/ IP,CAM,GAM(170),GQ(170),ALPOO(170,1) L 100
COMMON /THREE/ VOUT(170),VIN(170) L 110
COMMON /FOUR/ XOVC(170),RO(170),RI(170),DELO(170),DELI(170),WLS(40 L 120
1),DOLDO(170),DOLDI(170),UNRREF,SAM,XFOR,XAFT L 130
DIMENSION UOURO(170),UOURI(170),THE(170),H(170),DELST(170),XL L 140
1S(40),YLS(40,1),RESID(40,1),SUM(1),ALS(3,3),BLS(3,1),CLS0(40 L 150
2,2),CLSI(40,3),DDEL(170) L 160
REAL JOHN,LAM,M L 170
C L 180
C EXTRAPOLATE OUTER SURFACE VELOCITIES FROM XFOR PERCENT CHORD TO L 190
C TRAILING EDGE BY LINEAR LEAST SQUARE FIT OF VELOCITIES L 200
C BETWEEN XFOR AND XAFT PERCENT CHORD L 210
C L 220
L=0 L 230
DO 10 J=1,N L 240
JOHN=XBL(J)/C L 250
IF (JOHN.LT.XFOR) GO TO 10 L 260
IF (JOHN.GT.XAFT) GO TO 10 L 270
L=L+1 L 280
XLS(L)=XBL(J) L 290
YLS(L,1)=VOUT(J) L 300
10 CONTINUE L 310
CALL LSQPOL (XLS,YLS,WLS,RESID,L,SUM,1,ALS,BLS,2,CLS0,40,3) L 320
DO 20 J=1,N L 330
JOHN=XBL(J)/C L 340
IF (JOHN.LT.XFOR) GO TO 20 L 350
VOUT(J)=BLS(1,1)+BLS(2,1)*XBL(J) L 360
20 CONTINUE L 370
C L 380
C EXTRAPOLATE INNER SURFACE VELOCITIES FROM XFOR PERCENT CHORD TO L 390
C TRAILING EDGE BY PARABOLIC LEAST SQUARE FIT OF VELOCITIES L 400
C BETWEEN XFOR AND XAFT PERCENT CHORD AND LAST OUTER SURFACE L 410
C VELOCITY FROM ABOVE L 420
C L 430
L=0 L 440
DO 30 J=1,N L 450
JOHN=XBL(J)/C L 460
IF (JOHN.LT.XFOR) GO TO 30 L 470
IF (JOHN.GT.XAFT) GO TO 30 L 480
L=L+1 L 490
XLS(L)=XBL(J) L 500
YLS(L,1)=VIN(J) L 510
30 CONTINUE L 520
L=L+1 L 530
XLS(L)=XBL(N) L 540
YLS(L,1)=VOUT(N) L 550
CALL LSQPOL (XLS,YLS,WLS,RESID,L,SUM,1,ALS,BLS,3,CLSI,40,3) L 560
DO 40 J=1,N L 570

```

APPENDIX A - Continued

```

JOHN=XBL(J)/C                                L 580
IF (JOHN.LT.XFOR) GO TO 40                    L 590
VIN(J)=BLS(1,1)+(BLS(2,1)*XBL(J))+(BLS(3,1)*(XBL(J)**2)) L 600
CONTINUE                                      L 610
40 C                                           L 620
C INTERPOLATE FOR VELI AT INPUT X             L 630
C                                             L 640
LUG=NN-1                                      L 650
DO 50 I=2,LUG                                L 660
BLAIR=X(I)                                    L 670
CALL MTLUP (BLAIR,GLOSS,2,N,170,1,IP,XBL,VOUT) L 680
CALL MTLUP (BLAIR,TIM,2,N,170,1,IP,XBL,VIN)   L 690
UOURO(I)=GLOSS                                L 700
UOURI(I)=TIM                                   L 710
50 CONTINUE                                    L 720
UOURO(1)=VOUT(1)                              L 730
UOURI(1)=VIN(1)                                L 740
UOURO(NN)=VOUT(NN)                            L 750
UOURI(NN)=VIN(NN)                             L 760
DO 60 I=1,NN                                  L 770
JOHN=X(I)/C                                    L 780
IF (JOHN.LT..02) UOURI(I)=UOURO(I)           L 790
60 CONTINUE                                    L 800
C                                             L 810
C COMPUTE OUTER BOUNDARY LAYER AND MODIFY OUTER WING COORDINATES FOR L 820
C DISPLACEMENT THICKNESS                     L 830
C                                             L 840
CALL BLYR (X,RO,NN,UOURO,UNRREF,THE,H,DELST) L 850
DO 100 I=1,NN                                 L 860
DELO(I)=((DELO(I)*SAM)+(IT*DELST(I)))/(SAM+IT) L 870
IF (IT.EQ.1) 70,80                            L 880
70 ROUT(I)=RO(I)+(DELO(I)/2.)                 L 890
GO TO 90                                       L 900
80 ROUT(I)=RO(I)+DELO(I)                       L 910
90 DDEL(I)=DELST(I)-DOLDO(I)                  L 920
DOLDO(I)=DELST(I)                             L 930
100 CONTINUE                                   L 940
C                                             L 950
C FIND NEW DMAX                               L 960
C                                             L 970
DO 140 I=1,NN                                 L 980
IF (I.EQ.1) 110,120                            L 990
110 ELIZ=ROUT(I)                               L1000
GO TO 140                                       L1010
120 IF (ROUT(I).GT.ELIZ) 130,140              L1020
130 ELIZ=ROUT(I)                               L1030
140 CONTINUE                                   L1040
DMAX=2.*ELIZ                                    L1050
WRITE (6,230) IT,DMAX,(XOVC(I),X(I),UOURO(I),DELST(I),DDEL(I),DELO L1060
I(I),ROUT(I),THE(I),H(I),I=1,NN)              L1070
C                                             L1080
C COMPUTE INNER BOUNDARY LAYER AND MODIFY INNER WING COORDINATES FOR L1090
C DISPLACEMENT THICKNESS                     L1100
C                                             L1110
CALL BLYR (X,RI,NN,UOURI,UNRREF,THE,H,DELST) L1120
DO 180 I=1,NN                                 L1130
DELI(I)=((DELI(I)*SAM)+(IT*DELST(I)))/(SAM+IT) L1140
IF (IT.EQ.1) 150,160                          L1150
150 RIN(I)=RI(I)-(DELI(I)/2.)                 L1160
GO TO 170                                       L1170

```

APPENDIX A - Continued

160	RIN(I)=RI(I)-DELI(I)	L1180
170	DDEL(I)=DELST(I)-DOLDI(I)	L1190
	DOLDI(I)=DELST(I)	L1200
180	CONTINUE	L1210
C		L1220
C	FIND NEW DMIN	L1230
C		L1240
	DO 220 I=1,NN	L1250
	IF (I.EQ.1) 190,200	L1260
190	ELIZ=RIN(I)	L1270
	GO TO 220	L1280
200	IF (RIN(I).LT.ELIZ) 210,220	L1290
210	ELIZ=RIN(I)	L1300
220	CONTINUE	L1310
	DMIN=2.*ELIZ	L1320
	WRITE (6,240) IT,DMIN,(XOVC(I),X(I),UOURI(I),DELST(I),DDEL(I),DELI	L1330
	I(I),RIN(I),THE(I),H(I),I=1,NN)	L1340
	SAM=SAM+IT	L1350
	IT=IT+1	L1360
	RETURN	L1370
C		L1380
C		L1390
230	FORMAT (1H1,4X,44HOUTER WING SHAPE MODIFIED BY BOUNDARY LAYER./4X,	L1400
	150HVELOCITIES ARE ONES USED TO COMPUTE BOUNDARY LAYER//4X,3HIT=,I3	L1410
	2,4X,5HDMAX=,F9.4//7X,3HX/C,9X,1HX,5X,5HUOURI,5X,5HDELST,6X,4HDEL,	L1420
	36X,4HDELO,6X,4HROUT,7X,3HTHE,9X,1HH//(9F10.4))	L1430
240	FORMAT (1H1,4X,44HINNER WING SHAPE MODIFIED BY BOUNDARY LAYER./4X,	L1440
	150HVELOCITIES ARE ONES USED TO COMPUTE BOUNDARY LAYER//4X,3HIT=,I3	L1450
	2,4X,5HDMIN=,F9.4//7X,3HX/C,9X,1HX,5X,5HUOURI,5X,5HDELST,6X,4HDEL,	L1460
	36X,4HDELI,7X,3HRIN,7X,3HTHE,9X,1HH//(9F10.4))	L1470
	END	L1480

APPENDIX A - Continued

```

SUBROUTINE BLYR (S,R,NX,UOUR,UNRREF,THE,H,DELST)
C
C THIS SUBROUTINE COMPUTES THE INCOMPRESSIBLE TURBULENT AXISYMMETRIC
C BOUNDARY LAYER USING A SLIGHT MODIFICATION OF TRUCKENBRODT'S METHOD
C PAGE 584 - 585 OF BOUNDARY LAYER THEORY BY SCHLICHTING,4TH EDITION
C
C TRANSITION IS ASSUMED AT THE LEADING EDGE.
C
REAL IARG,IARGL,IUOUR,L
DIMENSION R(200), S(200), UOUR(200), IUOUR(200), UAOUR(200), REY(2
100), CF(200), ARG(200), IARG(200), THE(200), RTHE(200), B(200), AR
2GL(200), IARGL(200), L(200), TL(13), TH(13), H(200), DELST(200), S
3QRTXI(200)
DO 10 I=1,NX
IF (UOUR(I).LT..00001) UOUR(I)=0.00001
CONTINUE
10
C
C U AVE OVER U REF
C
CALL INT (S,UOUR,NX,IUOUR)
UAOUR(1)=UOUR(1)
DO 20 I=2,NX
UAOUR(I)=IUOUR(I)/S(I)
20
C
C CF
C
REY(1)=0.
CF(1)=1.
DO 30 I=2,NX
REY(I)=UNRREF*UAOUR(I)*S(I)
IF (REY(I).LE.1.) REY(I)=1.
CF(I)=.0745/(REY(I)**.218)+.00072
30
CONTINUE
C
C THETA
C
DO 40 I=1,NX
ARG(I)=UOUR(I)**(10./3.)*R(I)**(7./6.)
CALL INT (S,ARG,NX,IARG)
THE(1)=0.
DO 50 I=2,NX
IF (IARG(I).LE.0.) IARG(I)=0.
THE(I)=(UAOUR(I)*S(I))**(1./7.)*CF(I)/2.*IARG(I)**(6./7.)/(UOUR(I)
1**3*R(I))
40
C
C SHAPE FACTOR
C
C XI
C
SQRTXI(1)=0.
DO 60 I=1,NX
SQRTXI(I)=(IARG(I))**2
60
CONTINUE
C
C L
C
DO 70 I=1,NX
RTHE(I)=UNRREF*UOUR(I)*THE(I)
IF (RTHE(I).LT.1.) RTHE(I)=1.
B(I)=.07*ALOG10(RTHE(I))-.23
70

```

APPENDIX A - Continued

	IF (B(I).LT.0.) B(I)=0.	M 610
70	ARGL(I)=(B(I)-ALOG(UOUR(I)))*2.*SQRTXI(I)	M 620
	CALL INT (SQRTXI,ARGL,NX,IARGL)	M 630
	L(I)=0.	M 640
	DO 100 I=2,NX	M 650
	IF (SQRTXI(I).EQ.0.) GO TO 80	M 660
	L(I)=ALOG(UOUR(I))+IARGL(I)/SQRTXI(I)**2	M 670
	GO TO 90	M 680
80	L(I)=0.	M 690
90	IF (L(I).GT.1.) L(I)=1.	M 700
100	IF (L(I).LT.-.19) L(I)=-.19	M 710
C		M 720
C	H AND DELTA STAR	M 730
C		M 740
	DATA TL/-.183,-.172,-.157,-.131,-.1,-.05,.0,.05,.1,.3,.5,.7,1./,TH	M 750
	1/2.4,2.2,2.0,1.8,1.645,1.495,1.4,1.335,1.295,1.2,1.15,1.12,1.07/,N	M 760
	2TL/13/	M 770
	IP=-1	M 780
	DO 110 I=1,NX	M 790
	TEP1=L(I)	M 800
	CALL MTLUP (TEP1,TEP2,2,NTL,13,1,IP,TL,TH)	M 810
	H(I)=TEP2	M 820
	DELST(I)=THE(I)*H(I)	M 830
110	CONTINUE	M 840
	RETURN	M 850
	END	M 860-

APPENDIX A - Continued

	SUBROUTINE INT (X,Y,N,ANS)	N 10
C		N 20
C	THIS SUBROUTINE IS USED BY SUBROUTINE BLYR TO INTEGRATE Y DX FROM	N 30
C	X(1) TO X(I). RESULT EQUALS ANS(I). I RUNS FROM 1 TO N.	N 40
C		N 50
	DIMENSION X(100), Y(100), ANS(100)	N 60
	SUM=0.0	N 70
	ANS(1)=0.	N 80
	IF (N.EQ.2) GO TO 90	N 90
	I=1	N 100
	GO TO 40	N 110
10	XA=X(I)-X(I-1)	N 120
	XB=X(I+1)-X(I)	N 130
	YA=Y(I)-Y(I-1)	N 140
	YB=Y(I+1)-Y(I)	N 150
	IF (XA.EQ.0..OR.XB.EQ.0.) GO TO 20	N 160
	IF (YA/XA.GE.2.*YB/XB.AND.YA/XA.GE.0.) GO TO 20	N 170
	IF (YA/XA.LE.2.*YB/XB.AND.YA/XA.LE.0.) GO TO 20	N 180
	SUMFW=XB*(Y(I)+Y(I+1)/3.+(XA**2*YB+XB**2*YA)/(6.*XA*(XA+XB)))	N 190
	GO TO 30	N 200
20	SUMFW=XB*((Y(I)+Y(I+1))/2.)	N 210
30	IF (I.EQ.N-1) GO TO 80	N 220
40	I=I+1	N 230
	XA=X(I)-X(I-1)	N 240
	XB=X(I+1)-X(I)	N 250
	YA=Y(I)-Y(I-1)	N 260
	YB=Y(I+1)-Y(I)	N 270
	IF (XA.EQ.0..OR.XB.EQ.0.) GO TO 50	N 280
	IF (YB/XB.GE.2.*YA/XA.AND.YB/XB.GE.0.) GO TO 50	N 290
	IF (YB/XB.LE.2.*YA/XA.AND.YB/XB.LE.0.) GO TO 50	N 300
	SUMBK=XA*(Y(I)-YA/3.-(XB**2*YA+XA**2*YB)/(6.*XB*(XA+XB)))	N 310
	GO TO 60	N 320
50	SUMBK=XA*((Y(I)+Y(I-1))/2.)	N 330
60	IF (I.EQ.2) GO TO 70	N 340
	SUM=SUM+(SUMFW+SUMBK)/2.	N 350
	ANS(I)=SUM	N 360
	GO TO 10	N 370
70	SUM=SUMBK	N 380
	ANS(2)=SUM	N 390
	GO TO 10	N 400
80	SUM=SUM+SUMFW	N 410
	ANS(N)=SUM	N 420
	GO TO 100	N 430
90	ANS(2)=((Y(1)+Y(2))/2.)*(X(2)-X(1))	N 440
100	CONTINUE	N 450
	RETURN	N 460
	END	N 470-

APPENDIX A - Continued

```

SUBROUTINE LSQPOL (X,Y,W,RESID,N,SUM,L,A,B,M,C,NMAX,MMAX)      0 10
C                                                                0 20
C THIS SUBROUTINE IS A LEAST SQUARE POLYNOMIAL FIT. GIVEN A SET OF 0 30
C VALUES OF AN INDEPENDENT VARIABLE X WITH ASSOCIATED WEIGHTS W AND 0 40
C A SET OF CORRESPONDING VALUES OF Y. THE ROUTINE DETERMINES THE 0 50
C COEFFICIENTS OF THE POLYNOMIAL OF DEGREE M-1 WHICH GIVES THE BEST 0 60
C FIT IN THE LEAST SQUARES SENSE TO THE SET OF Y.              0 70
C                                                                0 80
DIMENSION X(NMAX), Y(NMAX,L), RESID(NMAX,L), A(MMAX,MMAX), B(MMAX, 0 90
1L), C(NMAX,M), SUM(L), W(NMAX)                                0 100
10 DO 20 I=1,N                                                  0 110
20 C(I,1)=1.0                                                  0 120
DO 30 J=2,M                                                    0 130
DO 30 I=1,N                                                    0 140
30 C(I,J)=C(I,J-1)*X(I)                                       0 150
DO 40 I=1,M                                                    0 160
DO 40 J=1,M                                                    0 170
A(I,J)=0.0                                                    0 180
DO 40 K=1,N                                                    0 190
40 A(I,J)=A(I,J)+C(K,I)*C(K,J)*W(K)                          0 200
DO 50 J=1,L                                                    0 210
DO 50 I=1,M                                                    0 220
B(I,J)=0.0                                                    0 230
DO 50 K=1,N                                                    0 240
50 B(I,J)=B(I,J)+C(K,I)*Y(K,J)*W(K)                          0 250
CALL MATINV (A,M,B,L,DETERM,RESID,C,MMAX,ISCALE)             0 260
DO 70 J=1,L                                                    0 270
SUM(J)=0.0                                                    0 280
KK=M                                                            0 290
DO 60 K=1,M                                                    0 300
C(K,1)=B(KK,J)                                               0 310
60 KK=KK-1                                                    0 320
DO 70 I=1,N                                                    0 330
RESID(I,J)=POLYE1(X(I),M,C)-Y(I,J)                          0 340
70 SUM(J)=SUM(J)+RESID(I,J)**2*W(I)                          0 350
RETURN                                                         0 360
END                                                            0 370-

```

APPENDIX A – Continued

C	SUBROUTINE MATINV (A,N,B,M,DETERM,IPIVOT,INDEX,NMAX,ISCALE)	P 10
C		P 20
C	THIS SUBROUTINE SOLVES THE MATRIX EQUATION AX=B WHERE A IS A	P 30
C	SQUARE COEFFICIENT MATRIX AND B IS A MATRIX OF CONSTANT VECTORS.	P 40
C		P 50
	DIMENSION IPIVOT(N), A(NMAX,N), B(NMAX,M), INDEX(NMAX,2)	P 80
	EQUIVALENCE (IROW,JROW), (ICOLUM,JCOLUM), (AMAX,T,SWAP)	P 90
C		P 100
C	INITIALIZATION	P 110
C		P 120
10	ISCALE=0	P 130
	R1=10.0**100	P 140
	R2=1.0/R1	P 150
	DETERM=1.0	P 160
	DO 20 J=1,N	P 170
20	IPIVOT(J)=0	P 180
	DO 360 I=1,N	P 190
C		P 200
C	SEARCH FOR PIVOT ELEMENT	P 210
C		P 220
	AMAX=0.0	P 230
	DO 70 J=1,N	P 240
	IF (IPIVOT(J)-1) 30,70,30	P 250
30	DO 60 K=1,N	P 260
	IF (IPIVOT(K)-1) 40,60,400	P 270
40	IF (ABS(AMAX)-ABS(A(J,K))) 50,60,60	P 280
50	IROW=J	P 290
	ICOLUM=K	P 300
	AMAX=A(J,K)	P 310
60	CONTINUE	P 320
70	CONTINUE	P 330
	IF (AMAX) 90,80,90	P 340
80	DETERM=0.0	P 350
	ISCALE=0	P 360
	GO TO 400	P 370
90	IPIVOT(ICOLUM)=IPIVOT(ICOLUM)+1	P 380
C		P 390
C	INTERCHANGE ROWS TO PUT PIVOT ELEMENT ON DIAGONAL	P 400
C		P 410
	IF (IROW-ICOLUM) 100,140,100	P 420
100	DETERM=-DETERM	P 430
	DO 110 L=1,N	P 440
	SWAP=A(IROW,L)	P 450
	A(IROW,L)=A(ICOLUM,L)	P 460
110	A(ICOLUM,L)=SWAP	P 470
	IF (M) 140,140,120	P 480
120	DO 130 L=1,M	P 490
	SWAP=B(IROW,L)	P 500
	B(IROW,L)=B(ICOLUM,L)	P 510
130	B(ICOLUM,L)=SWAP	P 520
140	INDEX(I,1)=IROW	P 530
	INDEX(I,2)=ICOLUM	P 540
	PIVOT=A(ICOLUM,ICOLUM)	P 550
	IF (PIVOT) 150,80,150	P 560
C		P 570
C	SCALE THE DETERMINANT	P 580
C		P 590
150	PIVOTI=PIVOT	P 600

APPENDIX A – Continued

	IF (ABS(DETERM)-R1) 180,160,160	P 610
160	DETERM=DETERM/R1	P 620
	ISCALE=ISCALE+1	P 630
	IF (ABS(DETERM)-R1) 210,170,170	P 640
170	DETERM=DETERM/R1	P 650
	ISCALE=ISCALE+1	P 660
	GO TO 210	P 670
180	IF (ABS(DETERM)-R2) 190,190,210	P 680
190	DETERM=DETERM*R1	P 690
	ISCALE=ISCALE-1	P 700
	IF (ABS(DETERM)-R2) 200,200,210	P 710
200	DETERM=DETERM*R1	P 720
	ISCALE=ISCALE-1	P 730
210	IF (ABS(PIVOTI)-R1) 240,220,220	P 740
220	PIVOTI=PIVOTI/R1	P 750
	ISCALE=ISCALE+1	P 760
	IF (ABS(PIVOTI)-R1) 270,230,230	P 770
230	PIVOTI=PIVOTI/R1	P 780
	ISCALE=ISCALE+1	P 790
	GO TO 270	P 800
240	IF (ABS(PIVOTI)-R2) 250,250,270	P 810
250	PIVOTI=PIVOTI*R1	P 820
	ISCALE=ISCALE-1	P 830
	IF (ABS(PIVOTI)-R2) 260,260,270	P 840
260	PIVOTI=PIVOTI*R1	P 850
	ISCALE=ISCALE-1	P 860
270	DETERM=DETERM*PIVOTI	P 870
C		P 880
C	DIVIDE PIVOT ROW BY PIVOT ELEMENT	P 890
C		P 900
	A(ICOLUM,ICOLUM)=1.0	P 910
	DO 280 L=1,N	P 920
280	A(ICOLUM,L)=A(ICOLUM,L)/PIVOT	P 930
	IF (M) 310,310,290	P 940
290	DO 300 L=1,M	P 950
300	B(ICOLUM,L)=B(ICOLUM,L)/PIVOT	P 960
C		P 970
C	REDUCE NON-PIVOT ROWS	P 980
C		P 990
310	DO 360 L1=1,N	P1000
	IF (L1-ICOLUM) 320,360,320	P1010
320	T=A(L1,ICOLUM)	P1020
	A(L1,ICOLUM)=0.0	P1030
	DO 330 L=1,N	P1040
330	A(L1,L)=A(L1,L)-A(ICOLUM,L)*T	P1050
	IF (M) 360,360,340	P1060
340	DO 350 L=1,M	P1070
350	B(L1,L)=B(L1,L)-B(ICOLUM,L)*T	P1080
360	CONTINUE	P1090
C		P1100
C	INTERCHANGE COLUMNS	P1110
C		P1120
	DO 390 I=1,N	P1130
	L=N+1-I	P1140
	IF (INDEX(L,1)-INDEX(L,2)) 370,390,370	P1150
370	JROW=INDEX(L,1)	P1160
	JCOLUM=INDEX(L,2)	P1170
	DO 380 K=1,N	P1180
	SWAP=A(K,JROW)	P1190
	A(K,JROW)=A(K,JCOLUM)	P1200

APPENDIX A - Continued

```
380 A(K,JCOLUM)=SWAP  
390 CONTINUE  
400 RETURN  
END
```

```
P1210  
P1220  
P1230  
P1240  
P1250-
```

APPENDIX A – Continued

	FUNCTION POLYE1 (X,M,C)	Q 10
C		Q 20
C	THIS IS A FUNCTION USED BY SUBROUTINE LSQPOL	Q 30
C		Q 40
	DATA BIG/0377777777777777/	Q 50
	DIMENSION C(M)	Q 60
	IF (M-1) 30,40,10	Q 70
10	N=M-1	Q 80
	POLYE1=C(1)	Q 90
	DO 20 I=1,N	Q 100
20	POLYE1=X*POLYE1+C(I+1)	Q 110
	RETURN	Q 120
30	POLYE1=BIG	Q 130
	RETURN	Q 140
40	POLYE1=C(1)	Q 150
	RETURN	Q 160
	END	Q 170-

APPENDIX A - Continued

	OVERLAY(RING,5,0)	R 10
	PROGRAM CRITM	R 20
C		R 30
C	THIS OVERLAY COMPUTES CRITICAL MACH NUMBER	R 40
C		R 50
	COMMON /CORD/ X(170),R(170),C,RAVG,NN,N,DMIN,T(170),RB(170),XBN	R 60
	COMMON /FIVE/ CPO(170),MCR	R 70
	REAL MCR	R 80
	CALL MCRIT (CPO,MCR)	R 90
	RETURN	R 100
	END	R 110-

APPENDIX A - Continued

	SUBROUTINE MCRIT (CPO,MCR)	S 10
C		S 20
C	THIS SUBROUTINE COMPUTES CRITICAL MACH NUMBER OF THE NACELLE BASED	S 30
C	ON THE OUTER SURFACE PRESSURE	S 40
C		S 50
	COMMON /CORD/ X(170),R(170),C,RAVG,NN,N	S 60
	DIMENSION CPO(170)	S 70
	REAL MCR	S 80
	A=0.	S 90
	DO 30 J=1,N	S 100
	IF (CPO(J)) 10,30,30	S 110
10	IF (A.EQ.0.) GO TO 20	S 120
	IF (CPO(J).LT.A) A=CPO(J)	S 130
	GO TO 30	S 140
20	A=CPO(J)	S 150
30	CONTINUE	S 160
	J=1	S 170
	MCR=.999	S 180
40	CP=(-2./MCR)*((1.-MCR)**1.5)*(SQRT(1.+MCR))	S 190
	IF (CP.LT.A) GO TO 50	S 200
	MCR=MCR-.001	S 210
	J=J+1	S 220
	IF (J.GE.999) GO TO 50	S 230
	GO TO 40	S 240
50	CONTINUE	S 250
	RETURN	S 260
	END	S 270-

APPENDIX A - Continued

```

OVERLAY(RING,6,0) T 10
PROGRAM MASFLOW T 20
C T 30
C THIS OVERLAY COMPUTES VI/VIN BY INTEGRATING THE INTERNAL MASS FLOW T 40
C AT SOME X STATION. THE X STATION IS PRESENTLY MIDCHORD BUT CAN T 41
C BE CHANGED BY CHANGING CARDS T 170, T 320, T 650, T 970. T 42
C T 50
COMMON /CORD/ X(170),R(170),C,RAVG,NN,N,DMIN,T(170),RB(170),XB T 60
COMMON /ONE/ ROUT(170),RIN(170),M,DMAX,XI(170),XIO(170),ALPHO(170) T 70
1,ALPHOO(170,1),XBL(170),ALPT(170),ALPTH(170),DRDX(170),DRDXH(170), T 80
2LAM,IT,ITMAX T 90
COMMON /TWO/ IP,CAM,GAM(170),GQ(170),ALPOO(170,1) T 100
COMMON /SIX/ NRHO,RAD(170),VIVIN,RXX,RBXI T 110
DIMENSION RHOO(170) T 120
REAL LAM,KSQ,M T 130
PRINT 150 T 140
PRINT 130 T 150
PRINT 140 T 160
XX=C/2. T 170
CALL MTLUP (XXX,RXX,2,NN,170,1,IP,X,R) T 180
CALL MTLUP (XXX,TXX,2,NN,170,1,IP,X,T) T 190
RXX=RXX-(TXX/2.) T 200
TEMP9=RXX/NRHO T 210
C T 220
C COMPUTE ALL RAD(J) T 230
C T 240
DO 20 J=1,NRHO T 250
IF (J.EQ.NRHO) GO TO 10 T 260
RAD(J)=RXX-(J*TEMP9) T 270
GO TO 20 T 280
10 RAD(J)=0. T 290
20 CONTINUE T 300
VIVIN=0. T 310
XX=C/2. T 320
CALL MTLUP (XX,RBXI,2,NN,170,1,IP,X,RB) T 330
IF (XX.LE.XBN) RBXI=0. T 340
TEST=RBXI/RAVG T 350
C T 360
C MASS FLOW - DO 90 T 370
C T 380
DO 90 J=1,NRHO T 390
C T 400
C COMPUTE THE RHOO(J) T 410
C T 420
IF (J.EQ.1) GO TO 30 T 430
IF (J.EQ.NRHO) GO TO 40 T 440
RHOO(J)=(RAD(J-1)+RAD(J))/(2.*RAVG) T 450
GO TO 50 T 460
30 RHOO(J)=(RXX+RAD(J))/(2.*RAVG) T 470
GO TO 50 T 480
40 RHOO(J)=RAD(J-1)/(2.*RAVG) T 490
50 CONTINUE T 500
IF (RHOO(J).LE.TEST) GO TO 100 T 510
C T 520
C VELOCITIES AT RHOO(J) - DO 60 T 530
C T 540
WX1JU0=0. T 550
WR1JU0=0. T 560
WX1QJU=0. T 570
WR1QJU=0. T 580

```

APPENDIX A - Continued

```

WXQJU=0. T 590
WRQJU=0. T 600
WXBQJU=0. T 610
WRBQJU=0. T 620
XX=(C/N)*.25 T 630
DO 60 I=1,N T 640
DELXI=XI(I) T 650
KSQ=(4.*RHOO(J))/((DELXI**2)+((1.+RHOO(J))**2)) T 660
EK=EKA(KSQ) T 670
SK=SKK(KSQ) T 680
CALL MTLUP (XX,RBXI,2,NN,170,1,IP,X,RB) T 690
IF (XX.LE.XBN) RBXI=0. T 700
TEMP1=(1./(2.*SQRT((DELXI**2)+((1.+RHOO(J))**2))))*(((2.-KSQ)/(1. T 710
1-KSQ))*EK)-(2.*SK)-((1./RHOO(J))*(KSQ/(1.-KSQ))*EK) T 720
TEMP2=((-1.)*DELXI)/(2.*RHOO(J)*SQRT((DELXI**2)+((1.+RHOO(J))**2) T 730
1))*(((2.-KSQ)/(1.-KSQ))*EK)-(2.*SK) T 740
TEMP7=(4.*DELXI*EK)/(SQRT((DELXI**2)+((1.+RHOO(J))**2)))*(DELXI* T 750
1**2)+((1.-RHOO(J))**2)) T 760
TEMP8=(2./(RHOO(J)*SQRT((DELXI**2)+((1.+RHOO(J))**2))))*(((1.-((2. T 770
1*RHOO(J)*(RHOO(J)-1.))/(DELXI**2)+((1.-RHOO(J))**2)))*EK)-SK) T 780
TEMP11=RHOO(J)/(2.*((DELXI**2+RHOO(J)**2)**1.5)) T 790
TEMP12=(DELXI)/(2.*((DELXI**2+RHOO(J)**2)**1.5)) T 800
WX1JUO=WX1JUO+TEMP1*ALPHO(I)*GAM(I)*(1./(2.*3.14159)) T 810
WR1JUO=WR1JUO+TEMP2*ALPHO(I)*GAM(I)*(1./(2.*3.14159)) T 820
WX1QJU=WX1QJU+(TEMP1*GQ(I)*(XI(1)-XI(2))/(2.*3.14159)) T 830
WR1QJU=WR1QJU+(TEMP2*GQ(I)*(XI(1)-XI(2))/(2.*3.14159)) T 840
WXQJU=WXQJU-(TEMP7*ALPT(I)*(XI(1)-XI(2))/(2.*3.14159)) T 850
WRQJU=WRQJU+(TEMP8*ALPT(I)*(XI(1)-XI(2))/(2.*3.14159)) T 860
WXBQJU=WXBQJU+TEMP12*(RBXI/RAVG)*DRDX(I)*(XI(1)-XI(2)) T 870
WRBQJU=WRBQJU+TEMP11*(RBXI/RAVG)*DRDX(I)*(XI(1)-XI(2)) T 880
XX=XX+(C/N) T 890
60 CONTINUE T 900
WX1JUOI=WX1JUO T 910
WX1QJUI=WX1QJU T 920
VTI=(1.+(WX1JUOI+WX1QJUI+WXQJU+WXBQJU)/(1.-M**2))**2 T 930
C T 940
C SUMMATION FOR MASS FLOW - ADD ONE TERM EACH TIME THRU DO 90 T 950
C T 960
XX=C/2. T 970
CALL MTLUP (XX,RBXI,2,NN,170,1,IP,X,RB) T 980
IF (XX.LE.XBN) RBXI=0. T 990
IF (J.EQ.1) GO TO 70 T1000
TEMP10=SQRT(VTI)*((RAD(J-1)**2-RAD(J)**2)/(RXX**2-RBXI**2)) T1010
GO TO 80 T1020
70 TEMP10=SQRT(VTI)*((RXX**2-RAD(J)**2)/(RXX**2-RBXI**2)) T1030
80 CONTINUE T1040
VIVIN=VIVIN+TEMP10 T1050
WRITE (6,120) J,RAD(J),RHOO(J),WX1JUO,WR1JUO,WX1QJU,WR1QJU,WXQJU,W T1060
1RQJU T1070
WRITE (6,110) VTI,VIVIN,TEMP10,WXBQJU,WRBQJU T1080
90 CONTINUE T1090
100 CONTINUE T1100
RETURN T1110
C T1120
C T1130
110 FORMAT (13X,5(2X,E11.4)/) T1140
120 FORMAT (1X,I3,3(2X,F10.5),6(2X,E11.4)) T1150
130 FORMAT (1X,1HJ,9X,3HRAD,8X,4HRHOO,6X,6HWX1JUO,7X,6HWR1JUO,7X,6HWX1 T1160
1QJU,7X,6HWR1QJU,8X,5HWXQJU,8X,5HWRQJU) T1170
140 FORMAT (23X,3HVTI,8X,5HVIVIN,7X,6HTEMP10,7X,6HWXBQJU,7X,6HWRBQJU/) T1180

```

APPENDIX A - Concluded

```
150  FORMAT (1H1,21HMASS FLOW COMPUTATION,10X,49HALL PERTURB VEL AND RA T1190
      1D ARE FOR EQUIV INCOMP GEOM//) T1200
      END T1210-
```

## APPENDIX B

### DERIVATION OF EQUATIONS (13) AND (23)

The velocity induced in the x-direction at  $\xi_0, \rho_0$  by a distribution of vortex rings on a cylinder of radius  $\rho = 1$  and of chord length  $c$  is found by use of equation (21). The result is

$$\frac{u_\gamma(\xi_0, \rho_0)}{V_\infty} = \frac{1}{2\pi} \int_{-1/\lambda}^{1/\lambda} \alpha_0(\xi) \gamma_0(\xi) \frac{k}{4\sqrt{\rho_0}} \left[ \frac{2-k^2}{1-k^2} - \frac{1}{\rho_0} \frac{k^2}{1-k^2} \right] E - 2K \, d\xi \quad (B1)$$

Replacing the modulus  $k$  by its definition in equation (11) and rearranging the result, equation (B1) becomes

$$\begin{aligned} \frac{u_\gamma(\xi_0, \rho_0)}{V_\infty} &= \frac{1}{2\pi} \int_{-1/\lambda}^{1/\lambda} \alpha_0(\xi) \gamma_0(\xi) \frac{E - K}{\sqrt{(\xi - \xi_0)^2 + (1 + \rho_0)^2}} \, d\xi \\ &+ \frac{1}{2\pi} \int_{-1/\lambda}^{1/\lambda} \frac{\alpha_0(\xi) \gamma_0(\xi)}{\sqrt{(\xi - \xi_0)^2 + (1 + \rho_0)^2}} \frac{2(\rho_0 - 1)E}{(\xi - \xi_0)^2 + (\rho_0 - 1)^2} \, d\xi \end{aligned} \quad (B2)$$

Equation (B2) must now be evaluated at  $\rho_0 = 1$  to obtain equation (13). Considering the first integral, at  $\rho_0 = 1$  and  $\xi = \xi_0$ , a singularity exists in the term containing the elliptic integral of the first kind  $K$ . To investigate this singularity, examine the integral in a small region extending  $\epsilon$  on each side of  $\xi_0$

$$\lim_{\epsilon \rightarrow 0} -\frac{1}{2\pi} \int_{\xi_0 - \epsilon}^{\xi_0 + \epsilon} \frac{\alpha_0(\xi) \gamma_0(\xi) K \, d\xi}{\sqrt{(\xi - \xi_0)^2 + 4}} \approx \frac{-\alpha_0(\xi_0) \gamma_0(\xi_0)}{2\pi} \lim_{\epsilon \rightarrow 0} \int_{\xi_0 - \epsilon}^0 K \, d\xi \quad (B3)$$

where the terms multiplying  $K$  are approximated by setting  $\xi = \xi_0$ . The elliptic integral  $K$  can be expanded in a series as a function of the complimentary modulus  $k'$  (ref. 23) in the following form

$$K = \sum_{m=0}^{\infty} \frac{\left(\frac{1}{2}\right)_m \left(\frac{1}{2}\right)_m}{m! m!} \left[ \ln\left(\frac{1}{k'}\right) - \psi\left(m + \frac{1}{2}\right) + \psi(m + 1) \right] k'^{2m} \quad \left( (k')^2 < 1 \right) \quad (B4)$$

APPENDIX B – Continued

where

$$k' = \sqrt{1 - k^2} = \sqrt{\frac{(\xi - \xi_0)^2}{(\xi - \xi_0)^2 + 4}}$$

and Pochhammer's symbol is defined by

$$\left(\frac{1}{2}\right)_m = \frac{1}{2} \left(\frac{1}{2} + 1\right) \left(\frac{1}{2} + 2\right) \dots \left(\frac{1}{2} + m - 1\right)$$

$$\left(\frac{1}{2}\right)_0 = 1$$

and  $\psi$  is the digamma function (ref. 24). By using equation (B4) and letting  $\epsilon \rightarrow 0$ , and therefore  $k' \rightarrow 0$ , it can be shown that the integral in equation (B3) goes to 0. Thus the principal value of the first integral in equation (B2) is found by treating it as an ordinary integral.

For  $\rho_0 = 1$ , the value of the second integral in equation (B2) can be determined as follows. For  $\xi \neq \xi_0$ , the integrand is 0 when  $\rho_0 = 1$ . Hence the limit must be found as  $\xi \rightarrow \xi_0$  simultaneously with  $\rho_0 \rightarrow 1$

$$\begin{aligned} \lim_{\rho_0 \rightarrow 1} \frac{1}{2\pi} \int_{-1/\lambda}^{1/\lambda} \frac{\alpha_0(\xi)\gamma_0(\xi)}{\sqrt{(\xi - \xi_0)^2 + (1 + \rho_0)^2}} \frac{2(\rho_0 - 1)E}{(\xi - \xi_0)^2 + (\rho_0 - 1)^2} d\xi \\ \approx \frac{\alpha_0(\xi_0)\gamma_0(\xi_0)}{2\pi} \lim_{\substack{\epsilon \rightarrow 0 \\ \rho_0 \rightarrow 1}} \int_{\xi_0 - \epsilon}^{\xi_0 + \epsilon} \frac{\rho_0 - 1}{(\xi - \xi_0)^2 + (\rho_0 - 1)^2} d\xi \end{aligned}$$

where  $E \approx 1$  because  $k \approx 1$ , and again the first term in the integrand is approximated by setting  $\xi = \xi_0$ . By defining a new variable

$$\xi' \equiv \frac{\xi - \xi_0}{\rho_0 - 1}$$

and requiring  $\rho_0 \rightarrow 1$  faster than  $\epsilon \rightarrow 0$  for a nontrivial solution, it is found that

APPENDIX B – Concluded

$$\lim_{\substack{\epsilon \rightarrow 0 \\ \rho_0 \rightarrow 1}} \int_{\xi_0 - \epsilon}^{\xi_0 + \epsilon} \frac{\rho_0 - 1}{(\xi - \xi_0)^2 + (\rho_0 - 1)^2} d\xi = \lim_{\substack{\epsilon \rightarrow 0 \\ \rho_0 \rightarrow 1}} \int_{-\frac{\epsilon}{\rho_0 - 1}}^{\frac{\epsilon}{\rho_0 - 1}} \frac{d\xi'}{(\xi')^2 + 1} = \pm \pi$$

so that

$$\lim_{\rho_0 \rightarrow 1} \frac{1}{2\pi} \int_{-1/\lambda}^{1/\lambda} \frac{\alpha_0(\xi) \gamma_0(\xi)}{\sqrt{(\xi - \xi_0)^2 + (1 + \rho_0)^2}} \frac{2(\rho_0 - 1)E}{(\xi - \xi_0)^2 + (\rho_0 - 1)^2} d\xi = \pm \frac{\alpha_0(\xi_0)}{2} \frac{\Gamma_0(\xi_0)}{\Delta\xi} \quad (\text{B5})$$

where  $\gamma_0(\xi_0) = \Gamma_0(\xi_0)/\Delta\xi$ . By substituting equation (B5) into equation (B2) and setting  $\rho_0 = 1$

$$\frac{u_\gamma(\xi_0, 1)}{V_\infty} = \int_{-1/\lambda}^{1/\lambda} \frac{\alpha_0(\xi) \gamma_0(\xi)}{2\pi} \frac{E - K}{\sqrt{(\xi - \xi_0)^2 + 4}} d\xi \pm \frac{\alpha_0(\xi_0)}{2} \frac{\Gamma_0(\xi_0)}{\Delta\xi} \quad (\text{B6})$$

Writing equation (B6) in summation form yields equation (13). Equation (23) is derived by a procedure analogous to the preceding derivation.

## REFERENCES

1. Hess, J. L.; and Smith, A. M. O.: Calculation of Potential Flow About Arbitrary Bodies. Progress in Aeronautical Sciences, Vol. 8, D. Küchemann, ed., Pergamon Press, Ltd., c.1967, pp. 1-138.
2. Trulin, Darryl J.; and Iversen, James D.: Pressure Distribution About a Finite Axisymmetric Nacelle. J. Aircraft, vol. 7, no. 1, Jan.-Feb. 1970, pp. 85-87.
3. Geissler, Wolfgang: Berechnung der Potentialströmung um rotationssymmetrische Rumpfe, Ringprofile und Triebwerkseinläufe. Z. Flugwiss., Jahrg. 20, Heft 12, Dec. 1972, pp. 457-462.
4. Young, C.: A Computer Program to Calculate the Pressure Distribution on an Annular Aerofoil. C.P. No. 1217, Brit. A.R.C., 1972.
5. Young, C.: An Investigation of Annular Aerofoils for Turbofan Engine Cowls. R. & M. No. 3688, Brit. A.R.C., 1972.
6. Mascitti, Vincent R.: A Rapid Numerical Solution to Subsonic Flow Over Planar and Axisymmetric Profiles at an Angle of Attack of  $0^{\circ}$ . NASA TN D-7410, 1974.
7. Belotserkovskii, Sergei Mikhailovich (Maurice Holt, transl. ed.): The Theory of Thin Wings in Subsonic Flow. Plenum Press, 1967, pp. 1-17, 91-104, 105-126.
8. Weissinger, Johannes: The Influence of Profile Thickness on Ring Airfoils in Steady Incompressible Flow. AFOSR TR 57-8, DDC No. AD 120 424, U.S. Air Force, Jan. 1957.
9. Hess, J. L.: Numerical Solution of the Integral Equation for the Neumann Problem With Application to Aircraft and Ships. Paper presented at Symposium on Numerical Solution of Integral Equations With Physical Applications, SIAM Fall Meeting (Univ. of Wisconsin), Oct. 1971.
10. Keith, J. S.; Ferguson, D. R.; Merkle, C. L.; Heck, P. H.; and Lahti, D. J.: Analytical Method for Predicting the Pressure Distribution About a Nacelle at Transonic Speeds. NASA CR-2217, 1973.
11. Grossman, Bernard; and Moretti, Gino: Development of Analytical Methods of Predicting the Pressure Distribution About a Nacelle at Transonic Speeds - Exact Solution. NASA CR-112271, 1973.
12. Küchemann, Dietrich; and Weber, Johanna: Aerodynamics of Propulsion. McGraw-Hill Book Co., Inc., 1953.
13. Ashley, Holt; and Landahl, Marten: Aerodynamics of Wings and Bodies. Addison-Wesley Pub. Co., Inc., c.1965.

14. Weber, J.: The Calculation of the Pressure Distribution Over the Surface of Two-Dimensional and Swept Wings With Symmetrical Aerofoil Sections. R. & M. No. 2918, Brit. A.R.C., 1956.
15. Schlichting, Hermann (J. Kestin, transl.): Boundary Layer Theory. Fourth ed., McGraw-Hill Book Co., Inc., c.1960.
16. Cebeci, Tuncer; Mosinskis, G. J.; and Smith, A. M. O.: Calculation of Viscous Drag of Two-Dimensional and Axisymmetric Bodies in Incompressible Flows. AIAA Paper No. 72-1, Jan. 1972, p. 5.
17. Stevens, W. A.; Goradia, S. H.; and Braden, J. A.: Mathematical Model for Two-Dimensional Multi-Component Airfoils in Viscous Flow. NASA CR-1843, 1971.
18. von Kármán, Th.: Compressibility Effects in Aerodynamics. J. Aeronaut. Sci., vol. 8, no. 9, July 1941, pp. 337-356.
19. Tulinius, J. R.: Theoretical Prediction of Thick Wing Aerodynamic Characteristics at Subsonic Speeds. NA-70-104, Los Angeles Div., North American Rockwell Corp., Oct. 9, 1970.
20. Re, Richard J.: An Investigation of Several NACA 1-Series Axisymmetric Inlets at Mach Numbers From 0.4 to 1.29. NASA TM X-2917, 1974.
21. Chudyk, D. W.: Transonic Wind Tunnel Tests of Several NASA Bodies of Revolution. Rep. No. AA-4018-W-5 (Contract No, NAS-1-10649), Cornell Aeronaut. Lab., Inc., Jan./Mar. 1971. (Available as NASA CR-112069.)
22. Shollenberger, Carl A.: An Investigation of a Two-Dimensional Propulsive Lifting System. Ph. D. Thesis, California Inst. Technol., 1971.
23. Byrd, Paul F.; and Friedman, Morris D.: Handbook of Elliptic Integrals for Engineers and Physicists. Lange, Maxwell & Springer, Ltd., 1954, p. 298.
24. Davis, Philip J.: Gamma Function and Related Functions. Handbook of Mathematical Functions, Milton Abramowitz and Irene A. Stegun, eds., Dover Publ., Inc., Fifth printing, pp. 253-293.



POSTMASTER : If Undeliverable (Section 158  
Postal Manual) Do Not Return

*"The aeronautical and space activities of the United States shall be conducted so as to contribute . . . to the expansion of human knowledge of phenomena in the atmosphere and space. The Administration shall provide for the widest practicable and appropriate dissemination of information concerning its activities and the results thereof."*

—NATIONAL AERONAUTICS AND SPACE ACT OF 1958

## NASA SCIENTIFIC AND TECHNICAL PUBLICATIONS

**TECHNICAL REPORTS:** Scientific and technical information considered important, complete, and a lasting contribution to existing knowledge.

**TECHNICAL NOTES:** Information less broad in scope but nevertheless of importance as a contribution to existing knowledge.

**TECHNICAL MEMORANDUMS:** Information receiving limited distribution because of preliminary data, security classification, or other reasons. Also includes conference proceedings with either limited or unlimited distribution.

**CONTRACTOR REPORTS:** Scientific and technical information generated under a NASA contract or grant and considered an important contribution to existing knowledge.

**TECHNICAL TRANSLATIONS:** Information published in a foreign language considered to merit NASA distribution in English.

**SPECIAL PUBLICATIONS:** Information derived from or of value to NASA activities. Publications include final reports of major projects, monographs, data compilations, handbooks, sourcebooks, and special bibliographies.

**TECHNOLOGY UTILIZATION PUBLICATIONS:** Information on technology used by NASA that may be of particular interest in commercial and other non-aerospace applications. Publications include Tech Briefs, Technology Utilization Reports and Technology Surveys.

*Details on the availability of these publications may be obtained from:*

**SCIENTIFIC AND TECHNICAL INFORMATION OFFICE**

**NATIONAL AERONAUTICS AND SPACE ADMINISTRATION**

**Washington, D.C. 20546**